

Stoichiometric and Catalytic C–H Activations

Kaeleigh Olsen

Sterling, VA

B.S. Chemistry, B.S. Mathematics, Randolph-Macon College, 2017

A Thesis presented to the Graduate Faculty
of the University of Virginia in Candidacy for the Degree of
Master of Science

Department of Chemistry

University of Virginia

March 2023

ABSTRACT

OLSEN, KAELEIGH E. Stoichiometric and Catalytic C–H Activations (Under the direction of T. Brent Gunnoe).

The primary focus of this Thesis is the study and development of photo-driven processes for the selective partial oxidation of methane. Light alkanes (*i.e.*, methane, ethane, propane) are the primary components of natural gas, which is an abundant resource accounting for approximately a quarter of global energy production. Complications exist regarding the storage of natural gas at these reserve sites and its transportation to other locations for its use due to its gaseous state. Additionally, current methods available for the conversion of natural gas to liquid products are not economically viable for at-wellhead implementation. Natural gas is often flared to carbon dioxide at these “stranded” locations, contributing several hundred million tons of carbon dioxide into the atmosphere annually. Thus, the development of an economically viable process for at-wellhead direct gas-to-liquid conversion of natural gas, with a particular focus on methane-to-methanol, is highly desired.

C–H activation is a platform for the functionalization of organic compounds, including alkanes, to more valuable products. Methods for C–H functionalization include transition metal catalysis and radical-based processes. The synergistic process described in Chapter Two combines the photoredox properties of a photocatalyst with halogen radical chemistry for the C–H functionalization of methane. With this process, we were able to achieve the selective partial oxidation of methane to functionalized product that is stable against over-oxidation with > 350 turnovers and ~60% yield based on methane.

We probe for the extension of our photo-driven process to use of simple transition metal salts in place of a photocatalyst in Chapter Three. Copper salts were found to be unsuccessful as oxidants under the conditions explored for photo-driven methane functionalization. Manganese oxides were found to facilitate photo-driven methane functionalization, albeit stoichiometrically.

In Chapter Four, the functionalization of carbon dioxide to carboxylic acids is discussed. Molecular, homogeneous bifunctional catalysis is proposed as a strategy to activate the C–H bonds of arenes for carboxylation to produce aromatic carboxylic acids. Herein, the activation of dihydrogen is chosen first as a model study. The hydrogenation of carbon dioxide and carbonyl-containing substrates (*i.e.*, aldehydes and ketones) is explored through a tandem approach using computational and experimental chemistry.

ACKNOWLEDGEMENTS

I wouldn't be where I am today, having completed this thesis, if it weren't for a long list of people and their support. First, I'd like to thank my PI, Professor Brent Gunnoe. Thank you for taking me on as a student in your research group. Thank you for time and time again going out of your way to support me in my interests, whether that be regarding research, professional development, or extracurriculars. Back before group selections were even made during my first year, I mentioned to you that I was interested in both synthetic chemistry and computational chemistry. You not only constructed a project where I could incorporate DFT, but you orchestrated a formal training by a collaborator and flew me out there. You've written countless recommendation letters for me over the years and supported my participation in the department Graduate Student Council and my involvement with local child advocacy work; thank you. Being a member of this group has undoubtedly made me a better scientist and professional, and has led me to discover my anticipated career path. I appreciate all of the skills I have learned being a part of this group and this program. Next, thank you to my candidacy committee, Professor Robert Gilliard, Professor Dean Harman, and Professor Charlie Machan, for continually supporting me over the years. A special thank you to Robert for including me in celebrations with your group since year one. I wish you the best of luck in your transition and getting your lab up and running at MIT.

There is no way I would have made it to graduate school if it weren't for my undergraduate advisor, Professor Serge Schreiner. Thank you for teaching me the basics of inorganic chemistry research, but more importantly, thank you for seeing the potential in me that you did. On your own time, you found ways to celebrate and showcase both my

coursework successes and my research successes. You nominated me for department, college, and national awards and supported me in research presentations at local, national, and international meetings and conferences. I am so thankful for every experience that you made possible. You taught me what it means to have strict work discipline, but also that without balance it won't make me feel fulfilled. You were the first chemistry professor I met when I toured Randolph-Macon College my senior year of high school. You were my first chemistry professor that following fall. You then became my academic advisor, research advisor, and the best mentor I've ever had. You were the one I turned to during the tough times throughout my college years and I thank you so much. I love that we have remained in touch and that I get to see you and Linda every now and then.

Thank you to the Office of Environmental Health & Safety at UVA for taking me on as a lab safety intern this spring and, specifically, to Clarissa Lynch and Tom Leonard for all of your work put into making it happen. Getting to know the group has been so enjoyable and I look forward to getting to know those who I haven't met yet. I really appreciate how willing everyone is to let me shadow and to answer my many questions. A special thank you to the Chemical & Lab Safety Team, Clarissa Lynch, Jim Reese, Evan Hall, and Bonnie Hockins, for welcoming me in to be a part of your team and to the Fire Safety & Prevention Team, Gerald Drumheller, Doug McGlothlin, and Britt Grimm, for working closely with me on my Fire Safety Day project. I can't express in words how thankful I am for this opportunity and how excited it has made me for a career in lab safety.

Thank you to my current lab mates Fanji Kong, Marc Bennett, Chris Webber, Chris Reid, and Jacob Dell. Fanji, you are the rock of this lab and we are so grateful to have you. Marc and Chris W., I admire the scientific curiosity that you both have. Chris R., thanks

for being an awesome office mate and training manual mentee. Jacob, I'm so excited you joined our lab. I left off two current lab mates from that list, Hannah Ketcham and Zoë Gehman, my lab mates turned close friends. I am so thankful that this department and this group has brought us together. I cherish our girls' nights, happy hours, coffee runs, midday walks through the cemetery, AFC swims/workouts, and countless other memories. You two have been there for me through a lot, and I cannot thank you enough for that. From dropping what you were doing to rush to my side and then spending all night with me in a time of crisis to routinely carving out time of your workdays so I can talk through my chemistry confusion or curiosities out to you, you two have always been there. To all of my current lab mates, you are amazing chemists and I cannot wait to see what each of your futures hold. Please stay in touch.

Thank you to my previous lab mates Nichole Liebov, Xiaofan Jia, Junqi Chen, Shunyan Gu, Ana Geer Ramos, Lauren Schmidt, and Ke Zhang. Nichole, you are the reason I joined this lab and I continue to look up to you. You were a phenomenal mentor and I have aspired, and continue to aspire, to emulate even just some of that. Xiaofan, thank you for being my training manual mentor and for helping me get acclimated in the lab. Thank you for being there for me on the scariest day I had in lab, even when I told you in the moment that I could handle it alone (Spoiler: I couldn't and you knew that). Junqi, you showed me how hard work pays off, but also the importance of checking in with yourself. Shunyan and Ana, thank you to the both of you for talking chemistry and life with me. I miss our days in Office 235 together. During Covid, I felt like we were in 24/7 texting communication with one another and it felt so reassuring to have that even though we were forced to be apart physically. Especially with such chaos going on in the world at the time,

it was comforting to process those things together. Lauren, thank you for being a rad undergrad mentee. You are a great scientist and a great musician. I had a blast watching you perform with the Charlottesville Symphony and for your Distinguished Major Violin Recital, and I wish you the best of luck in grad school. Ke, my OG CO₂ project mate, you have taught me how to be perseverant even when science is tough.

Nathan Coutard, I'm so thankful that I can call you not only a former postdoc in the lab, but a dear friend. I had no idea, at the time, when you got assigned to the desk next to mine in our old classroom office that we would become so close. You helped me a lot with science as my mentor on the DOE project and you helped me a lot with fixing things up around the house and property. Getting to know you and Page Allen was one of the best things that happened to me while I was here. Our dinner parties were the absolute best and I love that Pancake and Yarra got along (well the more accurate version is that Pancake tolerated Yarra, isn't it?). You two always have been just a phone call away, and continue to be, even though you're now on the other side of the globe. And who knows, I may try and stay your US mail keeper forever to give us an excuse to remain in regular contact. I miss you both lots.

Now onto department friends. Thank you to my first-year crew, Kelsie Wentz, Jacob Walley, Luke Freeman, Paul Miller, and Danai Agakidou, for your friendship and for all of the help with coursework. I can't believe how much our lives have changed over the past six years and it's so exciting to have seen, and continue to see, everyone's journey both professionally and personally. To Aditya Rane and AC Obi, my Dürty Nelly's and racquetball partners, you two keep life interesting and you know it. Thank you for all of the fun memories we've made together and thank you for being there for me through all

the not-so-great memories over the years. You two have taught me the importance of being kind to myself and of advocating for myself. AC, I am so happy for you and Tenzin having started your family, and I cannot wait to see your sweet little girl, Sonam, grow up (but I'm not rushing it!). Jacob Walley and Snigdha Das, I am so thankful that we got close, especially during our last year here together. I miss our board game nights. To our current girls' group, Hannah Ketcham, Zoë Gehman, Anna Davis, Kim Hollister, Emma Cook, Amelia Reid, and Megan Moberg, I thank you each for your friendship. Whether it's seeing a play, having a movie night, or doing something festive to celebrate a holiday, I always have a great time with y'all.

Kelsie Wentz, you were my very first friend here. I still think back to the first day of orientation when you walked through the door and I was so excited to see that you had decided to come to UVA, too. I wanted to be your friend so badly and when you sat down next to me that morning, that started us down a path of friendship that I couldn't have imagined. From studying for classes and candidacy together, to attending concerts at JPJ, to watching you marry the love of your life, we've had so many memories together. I look up to you so much, as an amazing chemist, a devoted friend and wife, and a passionate follower of Christ. People say they meet some of their best friends of all time in graduate school, and you are mine.

There's lots of other people I need to thank within the Department of Chemistry. I'm so thankful for all of the seasons of softball and volleyball intramurals with fellow grad students and postdocs. Shoutout to Josh Barker for organizing all of them. I am really thankful that my participation on the Graduate Student Council allowed for me to meet and develop relationships with such wonderful people. Annika Kraft, Abigail Graham, Anna

Davis, Viranga Wimalasiri, Eric Donarski, AC Obi, Levi Warring, and Haley Scolati, it was a pleasure working with you all and I thank you for your dedication and compassion towards your fellow graduate students. Cindy Knight, Seth Matula, Jerry Shifflett, Ed de Bary, thank you to each of you for all you've done for me. Cindy, you're a rockstar for starting the ChemPups program and thank you for including Yarra even though she's way shier than the other dogs. Seth Matula, thank you for taking time out of your day to talk life with me and for all of your advice. Jerry Shifflet and Ed de Bary, thank you both for responding to my plethora of pleas for help in the lab with all sorts of things, whether it was a simple ask to borrow a tool or an involved equipment fix for which you'd spend hours helping me with. It's been great getting to know you both.

There is no way I could have made it in this program without my community supports. Cherry Avenue Christian Church has become my home away from home. Through our Women's Ministry, Children's Ministry, and Thelma Carter Circle, I have gotten to know so many people who care for me and my well-being and I am beyond thankful. I'd like to thank my Sunday school teacher, Candace Wood, who welcomed me into her class with open arms on my very first Sunday there. I've learned so much from your teachings and from the rest of the Disciples class. I can't thank my pastors, Stan Martin and Lindsay Ellis, and their wives, Christi Martin and Wendy Ellis, enough for their constant support and guidance. Wendy, I love our coffee dates at Atlas and being a part of your bible study, and I thank you for being so invested in me, my achievements, and my happiness. You and Christi make me want to be the best version of myself I can be, as a girlfriend, daughter, sister, friend, and Christian. Boyd Knott, you are the closest thing I've ever had to a grandfather. Lastly, I'd like to thank my co-teacher, Thea Gibson, and my

preschool Sunday school class for filling me with so much joy. Piedmont Court Appointment Special Advocates became a significant part of my life while I've been here in Charlottesville and I have so much admiration for these child advocates, especially for my supervisor Kati Naess. The world would be a much better place if everyone was just a bit more like you, Kati. To my Spenga and Orange Theory families, especially to JB, thank you for being so much more than just places to work out at and for looking out for me. Thank you to Mirella Shaban for making our house on Woodland Drive feel like home. You're the most selfless person I know. I love that our relationship as roommates has developed into friendship, and I wish you the best of luck in your program.

Now onto my supports outside of Charlottesville. To my college friends who are like family, Kelsey Hahn, Nicole Nicholson, Sheridan Thornhill, and Maddie Tortora, thank you for being exactly who you each are. Even though we are spread across the country, we remain just a phone call away. I am so thankful for the relationships I have had with you and your parents. I hope to be able to visit with each of you more now. To my family, Janet, Paul, Aubrey, Hayden, and Mildred, I love you and I cannot thank you all enough. Mom and Dad, thank you for everything. I appreciate how you both always made sure I was doing alright while here at UVA, physically, mentally, emotionally, and financially, and never thought twice about stepping in to help when you thought I needed it, even when I was too hard-headed to admit it. Aubrey and Hayden, I'm so thankful for our relationships and I'm so incredibly proud of the two of you and the adults you have each become. I cherish the time that we get to spend together and I hope I can come visit you both more now. Nana, I know you won't be able to read this but I have so much to thank you for. You were fundamental in shaping who I grew up to be and you continue to

shape who I become. I look up to you, your values, and how you lived your life. I feel so incredibly blessed that you chose to move down to Virginia so that we could grow up with you being such a significant part of our childhoods. I miss you every day.

Yarra, my little lady, I wish I could articulate to you just how much you mean to me. Adopting you was the single best decision I made while in grad school and you've been my sidekick through it all. Neill Morris, thank you for being my absolute best friend. I never thought I would find someone like you. Thank you for including me in your life and for wanting to be a part of mine. Thank you for being there by my side, literally and figuratively, through the best and worst of times over the past two years. I cannot wait to do life with you and I'm so excited to see where it takes us together, you, me, Luke, and Yarra. I love you.

DEDICATION

In loving memory of Mildred “Mimi” Elsie Olsen

My Nana

(1928 – 2022)

TABLE OF CONTENTS

LIST OF SCHEMES.....	XVI
LIST OF FIGURES.....	XIX
LIST OF TABLES.....	XXII
1 Introduction.....	1
1.1 C–H Bond Activation.....	1
1.1.1 Hydrocarbons and Properties of C–H Bonds.....	1
1.1.2 Organometallic Mechanisms for C–H Activation.....	3
1.1.3 Electrophilic Processes for C–H Functionalization.....	6
1.1.4 Radical-Based Processes for C–H Functionalization.....	10
1.2 Thesis Aims.....	12
1.3 References.....	13
2 Photo-Catalytic, Selective Partial Oxidation of Methane using Decatungstate.....	18
2.1 Introduction.....	18
2.1.1 Motivations for Gas-To-Liquid Technologies for Natural Gas Use.....	18
2.1.2 Methods for Methane Functionalization.....	18
2.1.3 Oxy-Esterification (OxE) Process.....	20
2.1.4 Photo-Oxy-Esterification (Photo-OxE) Process.....	21
2.1.5 Photocatalysis using Decatungstate.....	21
2.1.6 Project Goals.....	22
2.2 Photo-OxE of Methane using Decatungstate.....	23
2.2.1 Reagent Screening and Optimization.....	23
2.2.2 MeTFA Stability, Kinetics of Methane Functionalization, and Decatungstate Re-Oxidation with Dioxygen.....	29
2.2.3 Screening of Non-Gaseous Oxidants for Decatungstate Re-Oxidation....	33
2.2.4 Mechanistic Studies based on Density Functional Theory (DFT).....	34
2.2.4.1 Global Mechanism.....	34

2.2.4.2	Chlorine-Based Radical Mechanism.....	36
2.2.4.3	Iodine-Free Radical Mechanism.....	37
2.2.4.4	Decatungstate Integration.....	38
2.2.4.5	Decatungstate Regeneration by Dioxygen.....	42
2.2.5	Reaction Tolerance to Water.....	44
2.3	Summary and Conclusions.....	45
2.4	Experimental Section.....	46
2.5	References.....	52
2.6	Chapter Appendix.....	68
2.6.1	Photochemical Methane Functionalization: Additional General Information.....	68
2.6.2	Re-Oxidation with Dioxygen.....	70
2.6.3	Screening of Solids as <i>In Situ</i> Co-Oxidants.....	71
2.6.4	Screening of Peroxides as <i>In Situ</i> Co-Oxidants.....	72
2.6.5	Reactions with Trifluoroacetic Anhydride.....	74
2.6.6	Background Reaction of Potassium Chloride and Iodine.....	75
2.6.7	Additional Calculations: Alternative Pathways.....	81
2.6.8	Chapter Appendix References.....	82
3	Extension of the Photo-OxE Process to Oxidants other than Decatungstate.....	83
3.1	Introduction.....	83
3.2	Attempted Extension of the Photo-OxE Process to Copper(II) Oxidants.....	84
3.3	Extension of the Photo-OxE Process to Manganese Oxidants.....	89
3.4	Conclusions and Future Directions.....	93
3.5	Experimental Section.....	95
3.6	References.....	101
4	A Tandem Experimental and Computational Study Using Hydrogenation as a Probe Reaction for New Methods of Carbon Dioxide Hydroarylation Using Bifunctional Catalysis.....	104

4.1	Introduction.....	104
4.1.1	C1 Incorporation Chemistry and Anthropogenic Carbon Dioxide (CO ₂).....	104
4.1.2	Chemical Properties and Reactivity of CO ₂	105
4.1.3	Industrial Processes for Synthesis of Carboxylic Acids.....	107
4.1.4	Desired Direct Carboxylation of Hydrocarbons and Arenes.....	108
4.1.5	Metal-Ligand Bifunctional Catalysis.....	109
4.1.6	Project Goals.....	110
4.1.7	Shvo Catalyst Background and Hydrogenation as Starting Point.....	111
4.2	Experimental Approach to Hydrogenation Chemistry.....	114
4.3	Computational Approach to Hydrogenation Chemistry.....	115
4.3.1	Density Functional Theory Details and Model System.....	115
4.3.2	Mechanisms of Shvo-Catalyzed Hydrogenation.....	116
4.3.3	Mechanistic Investigation of Formaldehyde and Carbon Dioxide Hydrogenation via Outer Sphere Concerted Mechanism.....	118
4.3.4	Solvent Effects on Formaldehyde and Carbon Dioxide Hydrogenation via Outer Sphere Concerted Mechanism.....	120
4.4	Exploration of Ligand Modifications.....	122
4.4.1	Selection of Shvo Analogues.....	122
4.4.2	Mechanistic Investigation of Formaldehyde and Carbon Dioxide Hydrogenation with Shvo Analogues via Outer Sphere Concerted Mechanism.....	123
4.4.3	Experimental Investigation of Carbon Dioxide Hydrogenation with Shvo Analogues.....	125
4.5	Conclusions and Future Directions.....	126
4.6	Experimental Section.....	127
4.7	References.....	136

LIST OF SCHEMES

CHAPTER 1

Scheme 1.1. Homolytic and heterolytic C–H bond cleavage of methane as a representative example.....	2
Scheme 1.2. General depiction of the pioneering example of transition metal-mediated C–H activation by Chatt and Davidson.....	4
Scheme 1.3. Traditional organometallic C–H activation pathways.....	4
Scheme 1.4. Proposed catalytic cycle of the Shilov process.....	6
Scheme 1.5. Proposed catalytic cycle of the Catalytica process.....	9
Scheme 1.6. Reactions of halogenation and oxyhalogenation using methane as the substrate. Step-wise mechanism for the halogenation of methane.....	11

CHAPTER 2

Scheme 2.1. Effect of differing concentrations of dioxygen on MeX (X = TFA, Cl) production reported as mmol of product, catalyst turnovers, and percent yield.....	32
Scheme 2.2. Comparison of high methane conversion aerobic methane to MeX (X = TFA, Cl) reaction with standard reagent loadings to preliminary re-oxidation reaction with standard reagent loadings and to optimal re-oxidation reaction with standard reagent loadings.....	33
Scheme 2.3. DFT Free energies at 298 K for the conversion of methane to MeTFA within the Cl/I system.....	36
Scheme 2.4. DFT Free energies at 298 K for the conversion of methane to MeTFA in the absence of I ₂	38
Scheme 2.5. DFT Free energies at 298 K for the generation of Cl• through ET of Cl ⁻ with DT•• and for the generation of CH ₃ • through HAT of CH ₄ with DT••.....	41
Scheme 2.6. DFT Free energies at 298 K for the conversion of dioxygen to H ₂ O and the regeneration of the DT ground state.....	43

Scheme 2.7. Modification of standard aerobic reaction conditions to include a mixture of HTFA and TFAA as reaction solvent, without and with added water	75
---	-----------

CHAPTER 3

Scheme 3.1. Reactions for which the addition of TFAA enables catalytic turnover using Mn sources for thermal methane oxidation in the presence of O₂.....	93
Scheme 3.2. Reactions for which the addition of TFAA enables catalytic turnover using Mn₂(HTFA)₄(μ-TFA)₂(TFA)₂ for photochemical methane oxidation in the presence of O₂.....	93

CHAPTER 4

Scheme 4.1. Common transformations of CO₂: nucleophilic attack and transition-metal mediated oxidative cycloaddition.....	106
Scheme 4.2. Current industrial methods for the synthesis of carboxylic acids.....	108
Scheme 4.3. Alternate, desired strategy for synthesis of carboxylic acids through direct carboxylation with CO₂.....	108
Scheme 4.4. Proposed catalytic cycle for a novel process combining aromatic C–H activation and CO₂ functionalization for the production of aromatic carboxylic acids using metal-ligand bifunctional catalysis.....	111
Scheme 4.5. Dimeric and monomeric forms of Shvo’s catalyst.....	112
Scheme 4.6. Conversion between the monomeric forms of Shvo’s catalyst.....	112
Scheme 4.7. Proposed catalytic cycle for Shvo-catalyzed arene carboxylation.....	114
Scheme 4.8. Hydrogenation of cyclohexanone and styrene by Shvo’s catalyst.....	115
Scheme 4.9. Proposed inner sphere concerted mechanism for Shvo-catalyzed ketone hydrogenation using formaldehyde as a model substrate.....	117
Scheme 4.10. Proposed outer sphere concerted mechanism for Shvo-catalyzed ketone hydrogenation using formaldehyde as a model substrate.....	118

Scheme 4.11. DFT calculated free energy profile diagrams for hydrogenation of formaldehyde and CO₂ using outer sphere concerted mechanism.....	119
Scheme 4.12. DFT calculated free energy profile diagrams for hydrogenation of formaldehyde and CO₂ using outer sphere concerted mechanism as a function of solvent.....	121
Scheme 4.13. DFT calculated free energy profile diagrams for hydrogenation of formaldehyde using Shvo analogues via outer sphere concerted mechanism as a function of solvent.....	124
Scheme 4.14. DFT calculated free energy profile diagrams for hydrogenation of CO₂ using Shvo analogues via outer sphere concerted mechanism as a function of solvent.....	125

LIST OF FIGURES

CHAPTER 2

Figure 2.1. Simplified scheme showing capability of photoexcited decatungstate for hydrogen atom abstraction from a generic alkane.....	23
Figure 2.2. Initial screening for the photochemical functionalization of methane by TBADT and KCl in HTFA.....	24
Figure 2.3. MeX (X = TFA, Cl) yield at various loadings of KCl, TBADT, and I ₂ ...	26
Figure 2.4. The effect of methane pressure on MeX yield and corresponding decatungstate TOs.....	29
Figure 2.5. Methane functionalization and MeTFA decay under standard aerobic reaction conditions with TBADT, KCl, and I ₂ as a function of time.....	31
Figure 2.6. Global mechanism for methane oxidation towards MeX.....	35
Figure 2.7. Spin-density diagram for the lowest-lying triplet decatungstate and hydrogen-binding energies for the 5 unique oxygen sites.....	40
Figure 2.8. Amount of MeX (X = TFA, Cl) produced under standard aerobic reaction conditions in which varying amounts of water were added to the start of the reaction.....	45
Figure 2.9. Labeled representative ¹ H NMR spectrum for photochemical methane functionalization.....	68
Figure 2.10. Photograph of a custom-built high pressure reaction vessel used for photolytic reactions.....	69
Figure 2.11. Labeled representative ¹ H NMR spectrum for re-oxidation experiments with dioxygen in which signal broadening prevents the ability to detect or measure MeCl formation.....	70
Figure 2.12. Comparison of the amount of MeX (X = TFA, Cl) produced as a method to screen substrates to serve as <i>in situ</i> oxidants for the re-oxidation of TBADT under standard aerobic reaction conditions.....	71
Figure 2.13. Photochemical methane functionalization under standard aerobic reaction conditions in the absence of TBADT as a function of time.....	77

Figure 2.14. Depiction of the set of experiments in Figure 2.13 as a scatter plot in which each data point represents an independent experiment.....78

CHAPTER 3

Figure 3.1. Screening of $\text{CuCl}_2 \cdot x\text{H}_2\text{O}$ with and without additives for the photochemical functionalization of methane in HTFA.....85

Figure 3.2. Comparison of reactions with and without $\text{CuCl}_2 \cdot x\text{H}_2\text{O}$ for the photochemical functionalization of methane using KCl in HTFA.....85

Figure 3.3. Screening of $\text{Cu}(\text{OAc})_2 \cdot x\text{H}_2\text{O}$ with and without additives for the photochemical functionalization of methane in HTFA.....86

Figure 3.4. Variation of KCl loading for the photochemical functionalization of methane using $\text{Cu}(\text{OAc})_2 \cdot x\text{H}_2\text{O}$ in HTFA.....87

Figure 3.5. Variation of I_2 loading for the photochemical functionalization of methane using $\text{Cu}(\text{OAc})_2 \cdot x\text{H}_2\text{O}$ and KCl in HTFA.....88

Figure 3.6. Screening of additives for the photochemical functionalization of methane using MnO_2 in HTFA.....90

Figure 3.7. Variation of iodine loading for the photochemical functionalization of methane using MnO and KCl in HTFA.....91

Figure 3.8. Structure of $\text{Mn}_2(\text{HTFA})_4(\mu\text{-TFA})_2(\text{TFA})_2$92

Figure 3.9. Labeled representative ^1H NMR spectrum for photochemical methane functionalization using Cu(II) salts.....98

Figure 3.10. Labeled representative ^1H NMR spectrum for photochemical methane functionalization using Mn oxides.....99

CHAPTER 4

Figure 4.1. Binding modes of CO_2 to transition metal complexes can be understood by the HOMO and LUMO of CO_2107

Figure 4.2. General structure of a metal-ligand bifunctional catalyst.....	110
Figure 4.3. Early examples of M/OH, M/NH, and M/CH metal-ligand bifunctional catalysts.....	110
Figure 4.4. Comparison of complex 3 to simplified model system used in DFT calculations.....	116
Figure 4.5. Shvo's catalyst and analogues depicted in their full chemical structures and in their simplified models utilized in DFT calculations.....	123
Figure 4.6. IR spectrum of tetraphenylcyclopentadienone.....	129
Figure 4.7. ¹H NMR spectrum of tetraphenylcyclopentadienone.....	129
Figure 4.8. IR spectrum of 1.....	131
Figure 4.9. ¹H NMR spectrum of 1.....	132
Figure 4.10. ORTEP plot of 1 as determined by single crystal X-ray crystallography.....	132

LIST OF TABLES

CHAPTER 1

Table 1.1. Bond dissociation energies and pK_a values for C–H bonds in select hydrocarbons.....	2
---	---

CHAPTER 2

Table 2.1. MeX (X = TFA, Cl) yields for the control reactions of remaining combinations of reagents.....	27
Table 2.2. Screening of peroxides to serve as <i>in situ</i> oxidants for the re-oxidation of TBADT.....	74
Table 2.3. Depiction of the set of experiments in Figure 2.13 as a table in which each line entry represents an independent experiment.....	78

CHAPTER 4

Table 4.1. Crystallographic data for 1.....	133
Table 4.2. Select bond lengths for 1.....	133

1 Introduction

1.1 C–H Bond Activation

1.1.1 Hydrocarbons and Properties of C–H Bonds

Hydrocarbons, a class of molecules comprised of only carbon and hydrogen, are the principal components of natural gas and petroleum.¹ They are used as precursors to fuels and lubricants and are used by the chemical industry for the production of higher-value chemicals.¹ Hydrocarbons can be saturated or unsaturated. Saturated hydrocarbons include alkanes (*e.g.*, paraffins) and cycloalkanes.¹ In these molecules, all four carbon atom valence electrons form bonds with unique carbon or hydrogen atoms (σ bonds). Unsaturated hydrocarbons include alkenes (*e.g.*, olefins), aromatic hydrocarbons (*e.g.*, arenes), and alkynes.¹ At the site of unsaturation, all four carbon atom valence electrons are not bound to unique carbon or hydrogen atoms. Alkenes contain at least one double bond (one σ bond plus one π bond) between carbon atoms. Aromatic hydrocarbons are cyclic structures with delocalized π electrons. Alkynes contain at least one triple bond (one σ bond plus two π bonds) between carbon atoms.

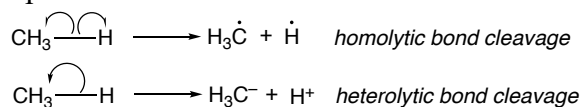
Hydrocarbon C–H bonds are non-polar and typically possess large kinetic and thermodynamic barriers for their cleavage.² The C–H bond dissociation energies (BDEs) and acidities (pK_{a} s) of select hydrocarbons are listed in Table 1.1. Often, these values can be used to understand trends in C–H bond cleavage. In general, there are two ways in which a C–H bond can be cleaved: homolytically and heterolytically (Scheme 1.1). Homolytic bond cleavage results in the two electrons of a σ bond being divided equally between the products to form two

radical species. BDE is defined as the standard enthalpy required to homolytically cleave a bond. Heterolytic bond cleavage results in both electrons of a σ bond being transferred to one of the products to produce an ion pair.

Table 1.1. Bond dissociation energies and pK_a values for C–H bonds in select hydrocarbons. Adapted from reference.²

Hydrocarbon	$\text{H}-\equiv\text{C}-\text{H}$		$\text{H}_2\text{C}=\overset{\text{H}}{\underset{\text{H}}{\text{C}}}$	$\text{H}_3\text{C}-\overset{\text{H}}{\underset{\text{H}}{\text{C}}}-\text{H}$	$\text{H}_3\text{C}-\overset{\text{H}}{\underset{\text{CH}_3}{\text{C}}}-\text{H}$	$\text{H}_3\text{C}-\overset{\text{H}}{\underset{\text{CH}_3}{\text{C}}}-\text{CH}_3$	
Type of C–H bond	C(sp)	C(sp ²) _{aromatic}	C(sp ²) _{vinyl}	C(sp ³) _{1°}	C(sp ³) _{2°}	C(sp ³) _{3°}	C(sp ³) _{allylic}
BDE (kcal/mol)	132	113	110	98	95	93	86
pK_a	~25	43	44	~50	~50	~50	43

Scheme 1.1. Homolytic and heterolytic C–H bond cleavage of methane as a representative example.



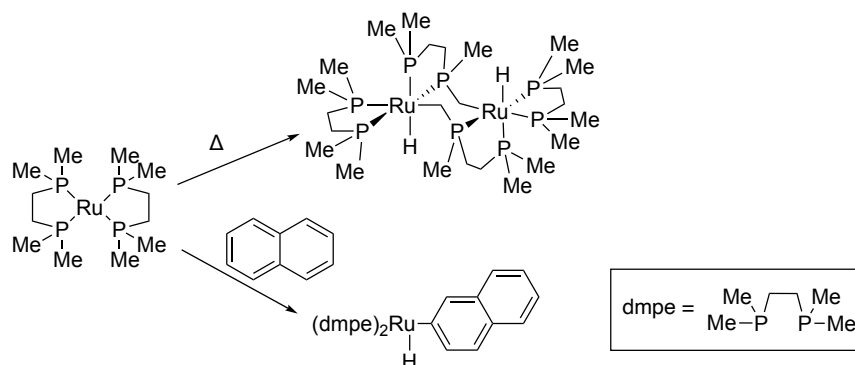
The following general trend exists regarding the magnitude of C–H BDEs: $\text{C}(\text{sp}) > \text{C}(\text{sp}^2)_{\text{aromatic}} > \text{C}(\text{sp}^2)_{\text{vinyl}} > \text{C}(\text{sp}^3)_{1^\circ} > \text{C}(\text{sp}^3)_{2^\circ} > \text{C}(\text{sp}^3)_{3^\circ} > \text{C}(\text{sp}^3)_{\text{allylic}}$. Moving from sp to sp² to sp³ hybridization, the C–H BDE decreases. Within C–H bonds with sp³ hybridization, moving from primary to secondary to tertiary substituted carbons, the C–H BDE decreases. This trend can be explained by comparing the stabilities of the radical species resulting from homolytic C–H bond cleavage. As the stability of the carbon-centered radical species increases, the energy required for bond dissociation decreases. The following trend exists regarding the magnitude of C–H bond pK_a s: $\text{C}(\text{sp}) < \text{C}(\text{sp}^2) < \text{C}(\text{sp}^3)$. Moving from sp to sp² to sp³ hybridization, the C–H pK_a value increases. This trend can be

explained by comparing the stabilities of the deprotonated species resulting from heterolytic C–H bond cleavage. As C–H bond acidity increases, and pK_a decreases, the stability of the deprotonated species increases.²

1.1.2 Organometallic Mechanisms for C–H Activation

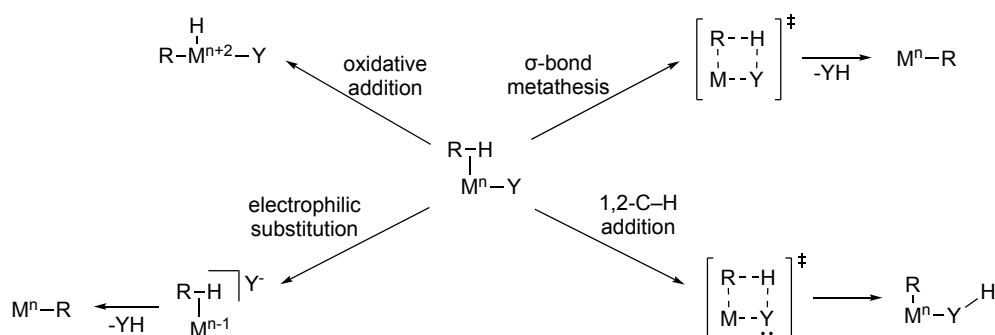
An organometallic species is defined as a complex containing a metal-carbon bond. In one definition, an organometallic C–H activation reaction results in the formation of a complex in which the activated substrate is bound to the metal center through a new metal-carbon bond. The seminal discovery of metal-mediated C–H activation is often credited to Chatt and Davidson and their 1965 report of a Ru(0) complex capable of naphthalene C–H bond activation.³ The Ru(0) bisdiphosphine complex $\text{Ru}(\text{dmpe})_2$ (dmpe = 1,2-bis(dimethylphosphino)ethane) was found to be capable of intramolecular C–H activation of its phosphine methyl group in the absence of naphthalene (Scheme 1.2 top), but in the presence of naphthalene, $\text{Ru}(\text{dmpe})_2$ is capable of intermolecular C–H activation of naphthalene to form $(\text{dmpe})_2\text{Ru}(\text{H})(\text{naphthalene})$ (Scheme 1.2 bottom). This work represented some of the first examples of well-defined C–H bond cleavage mediated by a transition metal complex.⁴

Scheme 1.2. General depiction of the pioneering example of transition metal-mediated C–H activation by Chatt and Davidson. Intramolecular activation of 1,2-bis(dimethylphosphino)ethane (dmpe) shown at top and intermolecular activation of naphthalene shown at bottom. Adapted from reference.⁵



Mechanisms of transition metal-mediated C–H activation reactions have been studied extensively.^{4,6} Herein, four classifications of transition metal-mediated C–H activation are discussed whereby an organometallic species is generated: oxidative addition, σ -bond metathesis, electrophilic substitution, and 1,2-C–H addition. Scheme 1.3 shows reaction pathways for these four classifications of C–H activation.⁴

Scheme 1.3. Traditional organometallic C–H activation pathways. For 1,2-C–H addition, Y = OR, NR, or NHR. Adapted from reference.⁴



Oxidative addition typically occurs with low-valent, electron-rich, middle-to-late transition metals. The active transition metal species for oxidative addition is generally coordinatively unsaturated, which often renders it unstable and reactive. Thus, the active species for oxidative addition is typically generated *in situ* from a more stable precursor. Oxidative addition generating two new metal-ligand bonds at a single metal results in the formal oxidation of the metal center by two electrons.

Electrophilic substitution generally occurs with late or post-transition metals. In this reaction, metal-carbon bond formation is coupled with the loss of a proton, often through protonation of a base that is not coordinated to the metal center, in the C–H bond breaking step. In most cases of electrophilic substitution, the metal center's formal oxidation state remains unchanged.

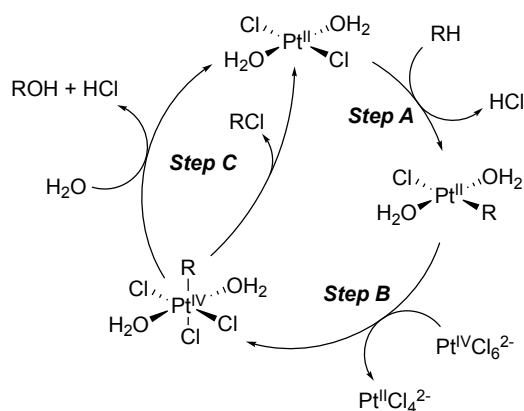
σ -Bond metathesis mechanisms typically involve metal centers that are not easily oxidized (*e.g.*, electron-deficient, early-to-mid transition metal complexes). In this mechanism, there is no formal change in the metal center oxidation state. This reaction operates through a four-centered metallocyclic transition state. The 1,2-C–H addition reaction is similar to σ -bond metathesis in that it operates through a four-centered metallocyclic transition state. Here, a lone pair on the ligand heteroatom is involved in the C–H bond breaking process, leading to a six-electron transition state, which contrasts with the four-electron transition state for σ -bond metathesis. Traditionally, 1,2-C–H addition reactions have involved early (*e.g.*, d^0) transition metal-imido complexes.⁷⁻⁹ Reports of 1,2-C–H addition with Ru^{II} and Ir^{III} complexes bearing hydroxy and methoxy ligands, respectively, suggest that late

transition metal complexes in high oxidation states can operate through this mechanism.¹⁰⁻¹²

1.1.3 Electrophilic Processes for C–H Functionalization

Electrophilic complexes have been shown to be effective for catalytic C–H bond functionalization. In the mid 20th century, Shilov reported a process using Pt(II) as an electrophilic catalyst for methane to MeX (X = Cl or OH) conversion in aqueous solvent.^{13,14} Scheme 1.4 outlines the proposed mechanism for the Shilov process.⁶ The alkane (RH) is rendered susceptible to C–H bond activation by the electrophilic Pt(II), d⁸, 16-electron complex (Step A). The subsequent Pt(II)-alkyl complex is oxidized forming a Pt(IV), d⁶, 18-electron complex (Step B). The metal-bound electrophilic alkyl group then reacts with water or chloride via a reductive nucleophilic functionalization step forming an equivalent of MeX product along with hydrochloric acid (Step C).

Scheme 1.4. Proposed catalytic cycle of the Shilov process. Adapted from reference.⁶



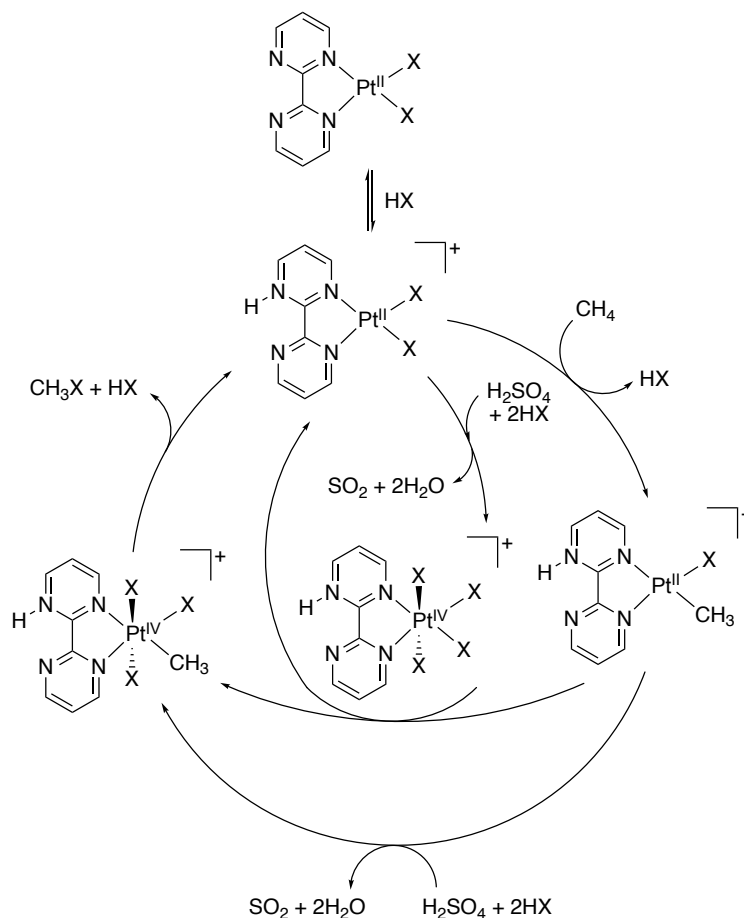
Although the Shilov process was a groundbreaking achievement as an early example of a catalytic, direct methane-to-methanol (MTM) process, it suffered from limitations precluding it from commercialization.⁶ While the process is catalytic in Pt(II), Pt(IV) is needed as a stoichiometric oxidant. Also, the platinum catalyst is not overly stable and metallic platinum precipitates from solution.

Following the report of the Shilov process, Periana and coworkers built upon this framework and extended electrophilic mediated C–H activation to a variety of late transition metal complexes.¹⁵⁻¹⁷ Most well-known is the development of the Catalytica process in 1998 in which (bpym)PtCl₂ (bpym = 2,2'-bipyrimidine) was found to catalyze methane to methyl bisulfate conversion in oleum (fuming sulfuric acid).¹⁸ This process, shown in Scheme 1.5, uses a Pt(II) electrophilic catalyst, but, here, oleum serves as an air-recyclable oxidant rather than stoichiometric Pt(IV). In fact, oleum serves three roles in this process: as solvent, as oxidant, and as protecting group for the functionalized product.¹⁹ The reaction achieves > 90% selectivity at < 70% conversion. Methyl bisulfate, a derivative of methanol, was found to be ~100 times less reactive than methane under the reaction conditions.²⁰

Although the Catalytica process provides marked improvements to the Shilov process (no stoichiometric precious metal-based oxidant needed, bisulfate group serving as protecting group against over-oxidation, high methane conversion achieved), the requirements of superacidic solvent coupled with challenges regarding reaction rate, product separation, and water inhibition similarly limited the commercial application of the Catalytica process.²¹

The Schüth group found that substitution of the Catalytica catalyst, (bpym)PtCl₂, with simple platinum salts (*e.g.*, K₂PtCl₄) led to turnover frequencies (TOFs) ~20 times higher than (bpym)PtCl₂ for methane to methyl bisulfate conversion in oleum.²² Impressively, the reaction achieves 99% selectivity for methyl bisulfate at conversions < 30%. Regarding the challenges associated with product separation in the Catalytica process, it was found that the addition of organic solvent (*e.g.*, CHCl₃, C₂H₄Cl₂) simplifies hydrolysis and separation of methyl bisulfate from oleum.²³ Regarding reaction inhibition by water, due to intolerance of the Pt(II) complexes, it was found that addition of ionic liquids as co-solvents improved the solubility of the Pt(II) complexes and higher yields of methyl bisulfate were achieved.^{24, 25}

Periana and coworkers found that metal-based electrophilic processes could be extended from transition metal to main group elements. Tl(TFA)₃ and Pb(TFA)₄ are capable of light alkane (*i.e.*, methane, ethane, propane) functionalization in trifluoroacetic acid (HTFA), a non-superacid, to the corresponding alkyl esters with moderate-to-high yields and selectivities.²⁶ This report presented experimental and computational support for a mechanism involving electrophilic C–H bond activation to form metal alkyl intermediates. It was proposed that the absence of ligand field stabilization and the increased lability of ligands in main group complexes with filled d-orbitals allows more facile alkane coordination relative to transition metal complexes.



Scheme 1.5. Proposed catalytic cycle of the Catalytica process. X = Cl⁻ or SO₃OH⁻. Each complex contains an outer-sphere, anionic X, omitted for clarity. Adapted from reference.²⁰

Molecular iodine (I₂) was found to be active for methane to methyl bisulfate conversion in oleum in the presence of sulfur trioxide.²⁷ This reaction was also proposed to operate via electrophilic C–H activation. Support for an electrophilic process, and against a radical-based process, includes no change in the reaction rate or selectivity upon the addition of dioxygen or potassium persulfate. In addition to I₂, Gang and coworkers achieved methane to methyl bisulfate conversion in oleum using KI, NaI, I₂O₅, KIO₃, and KIO₄.²⁸ This may indicate that all of these iodine-containing species funnel to the same active species for electrophilic C–H activation.

1.1.4 Radical-Based Processes for C–H Functionalization

Radical-based methods offer an alternative route for C–H functionalization. Biology has developed enzymes, methane monooxygenases (MMOs), that operate via radical-based methods for MTM reactions.²⁹ However, biological and biomimetic processes will not be discussed herein.

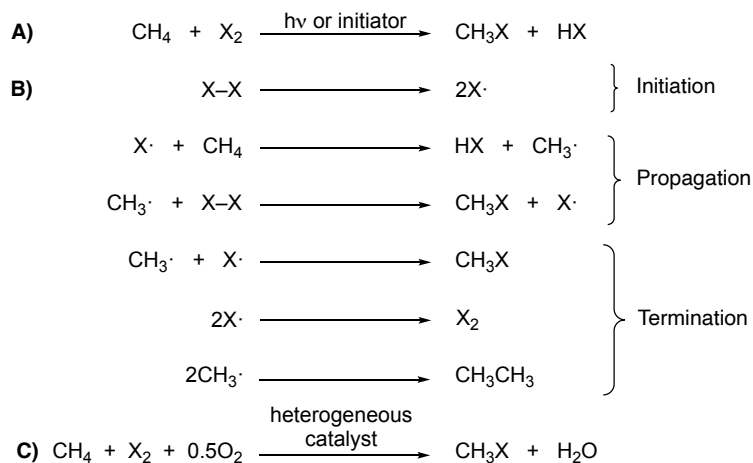
C–H bonds do not necessarily need to interact with a metal center for C–H bond breaking to occur via a radical-based mechanism. In hydrogen atom abstraction, also referred to as hydrogen atom transfer (HAT), a hydrocarbon C–H bond is homolytically broken to form a hydrocarbyl radical. This process requires the formation of a reactive species that is capable of abstracting the hydrogen atom.

Halogenation of C–H bonds to form C–X bonds is an example of a radical-based C–H functionalization (Scheme 1.6A).³⁰ This process involves the production of halogen radicals capable of hydrogen atom abstraction, which is typically achieved by irradiation or with a radical initiator. Halogenation reactions generally suffer from over-functionalization to produce poly-halogenated species since free radical-based homolytic C–H bond cleavage favors weaker bonds, and the C–H bonds of the mono-halogenated species are weaker than the C–H bonds of the starting species.³¹

Scheme 1.6B shows a stepwise mechanism for the radical halogenation of methane as a representative example.^{30, 32} During initiation, a dihalogen bond is homolytically cleaved in an endothermic step. Then in propagation, a halogen radical abstracts a hydrogen atom from methane. The resulting methyl radical reacts with an additional equivalent of X–X forming a methyl halide. In termination, the

free radicals undergo radical coupling reactions with one another forming equivalents of methyl halide, dihalogen, and ethane.

Scheme 1.6. Reactions of halogenation (A) and oxyhalogenation (C) using methane as the substrate. B) Step-wise mechanism for the halogenation of methane. Adapted from reference.³²



Halogenation of alkanes was first reported in 1840 by Dumas who demonstrated chlorine and marsh gas react to form carbon tetrachloride.³³ It was found later that methyl chloride was obtained as a product of this chlorination chemistry. In the early 1900s, the Hoechst process was developed for the commercial production of chloromethanes from methane and chlorine gas. With refinements and improvements, this process continues to serve as a commercial method for the production of chloromethanes.³⁴ Around this time, it was recognized that methyl chloride was a valuable chemical for the production of methanol, ethers, and other higher-value chemicals. However, because the mechanism of the Hoechst process disfavors the mono-halogenated product and each substitution of a chlorine

atom generates an equivalent of hydrochloric acid, an alternate process for more selective methyl chloride production was desired.^{34, 35}

The stability of halogen radicals increase as follows: $F\cdot < Cl\cdot < Br\cdot < I\cdot$. Methane fluorination (Scheme 1.6A, X = F) is extremely exothermic and can be explosive ($\Delta H_r^\circ = -103$ kcal/mol). Methane iodination (Scheme 1.6A, X = I) is endothermic ($\Delta H_r^\circ = 13$ kcal/mol). Methane chlorination (Scheme 1.6A, X = Cl) and bromination (Scheme 1.6A, X = Br) are both mildly exothermic, chlorination ($\Delta H_r^\circ = -25$ kcal/mol) more than bromination ($\Delta H_r^\circ = -7.2$ kcal/mol).³⁴ Thus, both chlorine and bromine are poised for use in halogenation chemistry. Although bromination has been studied for halogenation chemistry, interest in bromine is largely outweighed by chlorine due to the lower cost and higher abundance of chlorine.

Alkane oxyhalogenation uses HX (X = Cl, Br) and dioxygen with heterogeneous metal catalysts for production of halogenated species (Scheme 1.6C).³⁶ An appealing attribute to these reactions when compared to halogenation is that halogens are used with higher atom economy. Similar to halogenation chemistry, however, oxyhalogenation suffers from over-oxidation to poly-halogenated species.³⁶

1.2 Thesis Aims

This Thesis is comprised of projects related to C–H bond activation. In Chapter 2, a process for the partial oxidation of methane catalyzed by a photocatalyst will be described, for which we propose a HAT mechanism for the C–H activation of methane. Chapter 3 details efforts to extend the photo-driven

process to use simple metal salts and oxides in place of a photocatalyst. Chapter 4 contains the utilization of a bifunctional, molecular catalyst for hydrogenation of carbon dioxide as a model study for analogous hydroarylation chemistry of carbon dioxide.

1.3 References

1. Olah, G. A.; Molnar, A., *Hydrocarbon Chemistry, 2nd Edition*. John Wiley & Sons: 2003.
2. Roudesly, F.; Oble, J.; Poli, G., Metal-catalyzed C---H activation/functionalization: The fundamentals. *J. Mol. Catal. A: Chem.* **2017**, *426* (Part B), 275-296.
3. Chatt, J. D., J. M., The Tautomerism of Arene and Ditertiary Phosphine Complexes of Ruthenium(0), and the Preparation of New Types of Hydrido-complexes of Ruthenium(II). *J. Am. Chem. Soc.* **1965**, 843-845.
4. Gunnoe, T. B., Metal-Mediated Carbon-Hydrogen Bond Activation. In *Physical Inorganic Chemistry*, 2010; pp 495-549.
5. Goldman, A. S.; Goldberg, K. I., Organometallic C-H Bond Activation: An Introduction. In *Activation and Functionalization of C-H Bonds*, American Chemical Society: 2004; Vol. 885, pp 1-43.
6. Labinger, J. A.; Bercaw, J. E., Understanding and exploiting C-H bond activation. *Nature* **2002**, *417* (6888), 507-514.
7. Walsh, P. J.; Hollander, F. J.; Bergman, R. G., Generation, alkyne cycloaddition, arene carbon-hydrogen activation, nitrogen-hydrogen activation and dative ligand trapping reactions of the first monomeric

- imidozirconocene ($\text{Cp}_2\text{Zr:NR}$) complexes. *J. Am. Chem. Soc.* **1988**, *110* (26), 8729-8731.
8. Cummins, C. C.; Baxter, S. M.; Wolczanski, P. T., Methane and benzene activation via transient $(t\text{-Bu}_3\text{SiNH})_2\text{Zr}=\text{NSi-}t\text{-Bu}_3$. *J. Am. Chem. Soc.* **1988**, *110* (26), 8731-8733.
9. Arndtsen, B. A.; Bergman, R. G.; Mobley, T. A.; Peterson, T. H., Selective Intermolecular Carbon-Hydrogen Bond Activation by Synthetic Metal Complexes in Homogeneous Solution. *Acc. Chem. Res.* **1995**, *28* (3), 154-162.
10. Feng, Y.; Lail, M.; Barakat, K. A.; Cundari, T. R.; Gunnoe, T. B.; Petersen, J. L., Evidence for the Net Addition of Arene C–H Bonds across a Ru(II)–Hydroxide Bond. *J. Am. Chem. Soc.* **2005**, *127* (41), 14174-14175.
11. Tenn, W. J.; Young, K. J. H.; Bhalla, G.; Oxgaard, J.; Goddard, W. A.; Periana, R. A., CH Activation with an O-Donor Iridium–Methoxo Complex. *J. Am. Chem. Soc.* **2005**, *127* (41), 14172-14173.
12. Webb, J. R.; Burgess, S. A.; Cundari, T. R.; Gunnoe, T. B., Activation of carbon–hydrogen bonds and dihydrogen by 1,2-CH-addition across metal–heteroatom bonds. *Dalton Trans.* **2013**, *42* (48), 16646-16665.
13. Shilov, A. E.; Shul'pin, G. B., Activation of C–H Bonds by Metal Complexes. *Chem. Rev.* **1997**, *97* (8), 2879-2932.
14. Gol'dshleger, N. F.; Es'kova, V. V.; Shilov, A. E.; Shteinman, A. A., Reactions of alkanes in solutions of platinum chloride complexes. *Zh. Fiz. Khim.* **1972**, *46* (5), 1353-1354.

15. Periana, R. A.; Taube, D. J.; Evitt, E. R.; Löffler, D. G.; Wentreck, P. R.; Voss, G.; Masuda, T., A mercury-catalyzed, high-yield system for the oxidation of methane to methanol. *Science* **1993**, *259* (5093), 340-343.
16. Periana, R. A.; Mironov, O.; Taube, D.; Bhalla, G.; Jones, C. J., Catalytic, oxidative condensation of CH₄ to CH₃COOH in one step via CH activation. *Science* **2003**, *301* (5634), 814-818.
17. Jones, C.; Taube, D.; Ziatdinov, V. R.; Periana, R. A.; Nielsen, R. J.; Oxgaard, J.; Goddard III, W. A., Selective Oxidation of Methane to Methanol Catalyzed, with C–H Activation, by Homogeneous, Cationic Gold. *Angew. Chem. Int. Ed.* **2004**, *43* (35), 4626-4629.
18. Periana, R. A.; Taube, D. J.; Gamble, S.; Taube, H.; Satoh, T.; Fujii, H., Platinum Catalysts for the High-Yield Oxidation of Methane to a Methanol Derivative. *Science* **1998**, *280* (5363), 560-564.
19. Ahlquist, M.; Nielsen, R. J.; Periana, R. A.; Goddard Iii, W. A., Product Protection, the Key to Developing High Performance Methane Selective Oxidation Catalysts. *J. Am. Chem. Soc.* **2009**, *131* (47), 17110-17115.
20. Gunsalus, N. J.; Koppaka, A.; Park, S. H.; Bischof, S. M.; Hashiguchi, B. G.; Periana, R. A., Homogeneous Functionalization of Methane. *Chem. Rev.* **2017**, *117* (13), 8521-8573.
21. Conley, B. L.; Tenn, W. J.; Young, K. J. H.; Ganesh, S. K.; Meier, S. K.; Ziatdinov, V. R.; Mironov, O.; Oxgaard, J.; Gonzales, J.; Goddard, W. A.; Periana, R. A., Design and study of homogeneous catalysts for the selective,

- low temperature oxidation of hydrocarbons. *J. Mol. Catal. A: Chem.* **2006**, *251* (1), 8-23.
22. Zimmermann, T.; Soorholtz, M.; Bilke, M.; Schüth, F., Selective Methane Oxidation Catalyzed by Platinum Salts in Oleum at Turnover Frequencies of Large-Scale Industrial Processes. *J. Am. Chem. Soc.* **2016**, *138* (38), 12395-12400.
23. Mukhopadhyay, S.; Zerella, M.; Bell, A. T., A High-Yield, Liquid-Phase Approach for the Partial Oxidation of Methane to Methanol using SO₃ as the Oxidant. *Adv. Synth. Catal.* **2005**, *347* (9), 1203-1206.
24. Cheng, J.; Li, Z.; Haught, M.; Tang, Y., Direct methane conversion to methanol by ionic liquid-dissolved platinum catalysts. *Chem. Commun.* **2006**, (44), 4617-4619.
25. Xu, Z.; Oxgaard, J.; Goddard, W., The Mechanism by Which Ionic Liquids Enable Shilov-Type CH Activation in an Oxidizing Medium. *Organometallics* **2008**, *27* (15), 3770-3773.
26. Hashiguchi, B. G.; Konnick, M. M.; Bischof, S. M.; Gustafson, S. J.; Devarajan, D.; Gunsalus, N.; Ess, D. H.; Periana, R. A., Main-Group Compounds Selectively Oxidize Mixtures of Methane, Ethane, and Propane to Alcohol Esters. *Science* **2014**, *343* (6176), 1232-1237.
27. Periana, R. A.; Mirinov, O.; Taube, D. J.; Gamble, S., High yield conversion of methane to methyl bisulfate catalyzed by iodine cations. *Chem. Commun.* **2002**, 2376-2377.

28. Gang, X.; Zhu, Y.; Birch, H.; Hjuler, H. A.; Bjerrum, N. J., Iodine as catalyst for the direct oxidation of methane to methyl sulfates in oleum. *Appl. Catal., A* **2004**, *261* (1), 91-98.
29. Sirajuddin, S.; Rosenzweig, A. C., Enzymatic Oxidation of Methane. *Biochemistry* **2015**, *54* (14), 2283-2294.
30. Bruckner, R., *Advanced Organic Chemistry Reaction Mechanisms*. 1 ed.; Elsevier: 2001.
31. Crabtree, R. H., Aspects of Methane Chemistry. *Chem. Rev.* **1995**, *95* (4), 987-1007.
32. Liebov, N. S. Hydrocarbon Functionalization. University of Virginia, 2019.
33. Liebig, J., Ueber die Zusammensetzung der Talg-, Oel und Margarin-Säure. *Justus Liebigs Ann. Chem.* **1840**, *33* (1), 1-29.
34. Paunović, V.; Pérez-Ramírez, J., Catalytic halogenation of methane: a dream reaction with practical scope? *Catal. Sci. Technol.* **2019**, *9* (17), 4515-4530.
35. Rossberg, M. L., W.; Pfeleiderer, G.; Tögel, A.; Dreher, E.-L.; Langer, E.;; Rassaerts, H. K., P.; Strack, H.; Cook, R.; Beck, U.; Lipper, K.-A.; Torkelson, T. R.; Löser, E.; Beutel, K. K.; Mann, T., Chlorinated Hydrocarbons. In *Ullmann's Encyclopedia of Industrial Chemistry*, Wiley-VCH: Weinheim, 2000.
36. Lin, R.; Amrute, A. P.; Pérez-Ramírez, J., Halogen-Mediated Conversion of Hydrocarbons to Commodities. *Chem. Rev.* **2017**, *117* (5), 4182-4247.

2 Photo-Catalytic, Selective Partial Oxidation of Methane using Decatungstate

This chapter is adapted from the manuscript “Partial Oxidation of Methane Enabled by Decatungstate Photocatalysis Coupled to Free Radical Chemistry” by Charles B. Musgrave III,[#] Kaeleigh Olsen,[#] Nichole S. Liebov, John T. Groves, William A. Goddard III, T. Brent Gunnoe, which has been submitted.

[#]These authors contributed approximately equally.

2.1 Introduction

2.1.1 Motivations for Gas-To-Liquid Technologies for Natural Gas Use

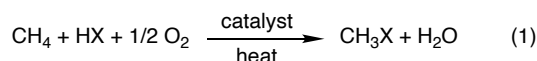
Conversion of light alkanes from natural gas into value-added chemicals is a cornerstone of the chemical industry. The development of new catalytic processes for the direct conversion of methane (and other light alkanes) to higher-value liquid products is important for increased use of stranded natural gas and for other sources (e.g., biogas) of methane and light alkanes.¹⁻³ Highly desired processes include the direct partial oxidation of methane, ethane, and propane to liquid products, so called direct gas-to-liquid (GTL) conversions, with a particular focus on methane-to-methanol. Given the substantial global natural gas reserves, which account for ~25% of global energy,⁴ there is enormous potential for direct GTL technologies. Additionally, these reserves are often in stranded locations, where at-wellhead GTL conversion is most desirable.

2.1.2 Methods for Methane Functionalization

Current commercial methods for indirect methane-to-methanol conversion involve the highly energy- and capital-intensive methane reforming reaction ($\text{H}_2\text{O} + \text{CH}_4 \rightarrow \text{CO} + 3 \text{H}_2$) followed by Fischer-Tropsch chemistry to produce methanol

or longer chain hydrocarbons.^{5, 6} A more desirable alternative is the direct mono-oxygenation of methane by $\frac{1}{2}$ O₂ to produce methanol. While methane partial oxidation using $\frac{1}{2}$ O₂ is thermodynamically favorable, challenges include (1) overcoming the large activation barrier required to break a non-polar C–H bond of methane (bond dissociation energy ~105 kcal/mol), and (2) evading over-oxidation of methanol, due to the weaker C–H bond of methanol (96 kcal/mol) compared to methane.^{7, 8}

Radical-based chemistry, such as catalytic oxychlorination, offers a route for C–H functionalization of light alkanes to produce functionalized products (eq. 1).⁹⁻¹³ Unfortunately, such processes often suffer from the over-oxidation dilemma, again due to weaker C–H bonds in the product (*e.g.*, 101 kcal/mol for CH₃Cl).¹⁴ In fact, methane conversion using catalytic oxychlorination is often limited to < 10% in order to achieve adequately high selectivity.¹⁵



Electrophilic Pt(II) catalysis introduced by Shilov and coworkers was an early example of catalytic methane mono-functionalization, but this process suffered from the requirement of stoichiometric Pt(IV) oxidant.¹⁶ The Catalytica process pioneered by Periana and coworkers achieved methane to methyl bisulfate conversion with > 70% yield and > 90% selectivity, using the key strategy of protecting of the mono-functionalized product toward over oxidation by the electron-withdrawing bisulfate group. However, the energy requirements for the separation of product from oleum and reconcentration of sulfuric acid was a challenge for potential commercialization.^{17, 18} Molecular iodine has been shown to

functionalize light alkanes in oleum, but this approach could not be extended to non-superacidic media.^{19, 20} Main group compounds, such as $\text{Tl}(\text{TFA})_3$, $\text{Pb}(\text{TFA})_4$, and hypervalent iodine, namely $(\text{C}_6\text{F}_5)\text{I}^{\text{III}}(\text{TFA})_2$, have been shown to functionalize light alkanes in non-superacidic solvent, albeit stoichiometrically.²¹

Metal-exchanged zeolites (*e.g.*, copper) are capable of methane oxidation to methanol.²²⁻²⁹ However, these catalysts typically do not yield high methane conversion with high selectivity. Also, methanol extraction requires significant dilution for separation, which typically destroys the active site, requiring subsequent high-temperature oxidation for catalyst restoration.³⁰

2.1.3 Oxy-Esterification (OxE) Process

To improve product yields, we and other groups have pursued a strategy to circumvent over-oxidation through installation of a protecting group in the functionalized alkyl product.^{31, 32} For example, we reported the thermal (100-235 °C) partial oxidation of light alkanes (methane, ethane, propane) in trifluoroacetic acid (HTFA) by chloride-iodate and chloride-periodate systems via a method termed oxyesterification (OxE). OxE produced the corresponding alkyl esters (RTFA) with > 20% yield relative to the alkanes and > 80% selectivity towards mono-oxidized products.^{33, 34} We discovered that the ester moiety protects the products from subsequent oxidation, thus permitting production of the corresponding alcohol, along with regeneration of HTFA through hydrolysis.^{35, 36} Oxygen-recyclable cobalt and manganese catalysts have also been shown to effectively oxidize methane in HTFA.³⁷⁻³⁹ Recently, we reported the use of

molecular Mn oxides and Mn salts for methane partial oxidation along with a mechanistic study.⁴⁰

2.1.4 Photo-Oxy-Esterification (Photo-OxE) Process

Several groups have reported photo-driven C–H functionalization for which the generation of chlorine radical from chloride appears to be a key step. Germane here, several examples of such reactions that are successful for unactivated hydrocarbons (*e.g.*, cyclohexane) have been reported.⁴¹⁻⁴⁵ Using the strategy of generating chlorine from chloride, we recently pursued photo-driven light alkane functionalization in a process we refer to as photo-oxy-esterification (photo-OxE).^{46, 47} Higher yields were obtained for the chloride-iodate process by photo-OxE (~50% yield was achieved for methane) compared to yields for the analogous thermally driven reaction.⁴⁷ We also reported that Fe(TFA)₃ mediates photo-driven hydrocarbon functionalization.⁴⁶ The Schelter and Goldberg groups recently reported photo-driven, aerobic alkane iodination in acetonitrile using catalytic [ⁿBu₄N]Cl.⁴⁸

2.1.5 Photocatalysis using Decatungstate

Polyoxometalates (POMs) have emerged as a widely successful class of photocatalysts for organic transformations due to their ability to perform both electron transfer (ET) and hydrogen atom transfer (HAT) reactions.⁴⁹⁻⁵² The decatungstate anion ([W₁₀O₃₂]⁴⁻ or DT) is currently employed as a HAT photocatalyst because of its ready availability and the array of C–H bonds it can cleave.⁵³⁻⁵⁸ Furthermore, DT has been used for a variety of C(sp³)–H functionalizations, including C–C bond formations and oxidation reactions.⁵⁹⁻⁷³

Laudadio and coworkers reported the functionalization of light alkanes (*e.g.*, methane, ethane, propane, isobutane) to C–C coupled products using DT in a photocatalytic flow system.⁷⁴ In a separate report, Laudadio and coworkers reported DT-mediated selective oxidation of aliphatic substrates to ketone-containing products.⁶³ Figure 2.1 depicts the structure of the DT salt, TBADT [TBA = (*n*Bu₄N)₄ (*n*Bu = *n*-butyl)], and its ability to perform HAT in its photoexcited state; here DT•• denotes the suspected excited triplet state (referred to in previous publications as wO or DT*)⁷⁰ and HDT• denotes the reduced species after HAT.

2.1.6 Project Goals

Because our previously reported thermal and photo-initiated OxE processes for light alkane functionalization are proposed to rely on HAT,^{35, 36, 47} we hypothesized that the addition of DT as a photo-driven HAT reagent may accelerate the mono-oxidation of light alkanes to alkyl esters in a chloride-iodine system.

Of particular interest was the possibility that photo-excited DT could also generate chlorine atoms, Cl•, under these reaction conditions due to the very high reduction potential of DT••.⁵⁶ There have been a number of recent advances in the photogeneration of Cl•, including photoreduction of metal chlorides^{42, 43, 45, 46, 75-78} and photoredox oxidation of chloride ion (Cl⁻).^{41, 79-81} As noted above, photogeneration of chlorine has been used to functionalize unactivated hydrocarbons.⁴¹⁻⁴⁵ DT is robust under acidic conditions and has a high quantum yield for photoexcitation, but it has not been employed for the generation of Cl• as a C–H activation mediator. Herein, we study DT as a photocatalyst for methane partial oxidation in the presence of chloride and iodine to form methyl

trifluoroacetate (MeTFA) and methyl chloride (MeCl or CH₃Cl) and use Density Functional Theory (DFT) calculations to investigate the mechanism.

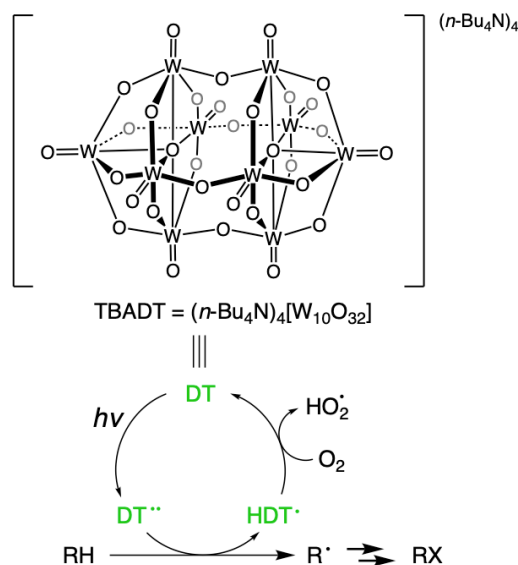


Figure 2.1. Simplified scheme showing capability of photoexcited decatungstate (DT^{••}) for hydrogen atom abstraction from a generic alkane (RH). HDT[•] denotes the reduced radical species following hydrogen atom abstraction.

2.2 Photo-OxE of Methane using Decatungstate

2.2.1 Reagent Screening and Optimization

An initial screening of the photochemical reactivity of an aerobic mixture of TBADT (0.014 mmol) and KCl (0.67 mmol) in HTFA (8 mL) pressurized with 100 psig of methane (~24 mmol) resulted in the formation of 0.043 ± 0.015 mmol of MeX (X = TFA, Cl) after 24 h of mercury arc lamp irradiation. This corresponds to a yield of $0.18 \pm 0.071\%$ and a 42:1 ratio of MeTFA to MeCl. Herein, percent yields are reported with respect to methane, and all data are the result of a minimum of three separate experiments with standard deviations. Product formation was determined by ¹H NMR spectroscopy and referenced against a known amount of

either HOAc or CH_3NO_2 as an internal standard. When TBADT was ground using a mortar and pestle before addition to the reactor (with all other conditions unchanged), 0.10 ± 0.008 mmol of MeX was produced in $0.43 \pm 0.027\%$ yield with a 33:1 ratio of MeTFA to MeCl (Figure 2.2). The corresponding turnovers (TOs) of TBADT were 3.1 ± 1.1 and 7.3 ± 0.58 when TBADT was unground and ground, respectively. The increased product formation and the decreased standard deviation using the ground TBADT suggests that smaller particle size increased TBADT's solubility in HTFA.

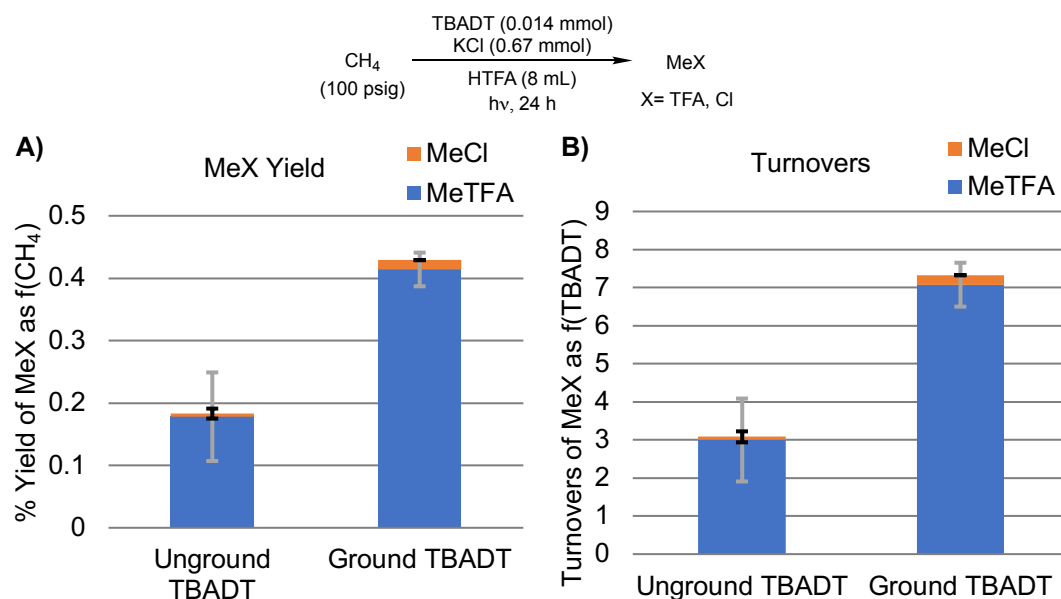


Figure 2.2. Initial screening for the photochemical functionalization of methane by TBADT (0.014 mmol) and KCl (0.67 mmol) in HTFA after 24 h of mercury arc lamp irradiation. TBADT was either used directly or ground before addition to the reactor. MeX (X = TFA, Cl) is plotted as methane conversion (A) and catalytic turnovers based on TBADT (B). Each bar graph represents the average of a minimum of three independent experiments with error bars depicting the standard deviation of the three experiments.

The analogous reaction to that shown in Figure 2.1 but in the absence of KCl produced no MeTFA; this is likely because no radical traps are present to

quench $\text{CH}_3\cdot$ (see below for mechanism discussion). Various loadings of KCl were tested, and it was observed that doubling the KCl loading from 0.67 mmol to 1.34 mmol had a positive effect on MeX yield; however, increasing the KCl loading to 2.68 mmol had minimal effect, within deviation, on MeX yield (Figure 2.3A). Using 1.34 mmol of KCl, various loadings of TBADT were tested, with the optimal amount of TBADT being 0.007 mmol, as this maximized MeX yield (Figure 2.3B).

In our previous reports of light alkane partial oxidation using iodate as the oxidant, mechanistic studies indicated that I_2 is likely generated *in situ* from iodate and serves to trap alkyl radicals in solution.³⁵ Thus, I_2 was explored as a reaction additive in our TBADT photochemistry. We found 0.025 mmol of I_2 to be optimal, as this loading maximized MeX yield (Figure 2.3C). The addition of TBADT, KCl, and I_2 in their optimized loadings in 8 mL HTFA led to the formation of 0.45 ± 0.030 mmol of MeX in $1.9 \pm 0.078\%$ yield with a 4.2:1 ratio of MeTFA to MeCl after 24 h of mercury arc lamp irradiation. This MeX formation as a function of TBADT corresponds to 64 ± 4.3 TOs. These optimized reagent loadings in 8 mL HTFA and 100 psig CH_4 will be referred to as the standard aerobic reaction conditions throughout the remainder of this chapter.

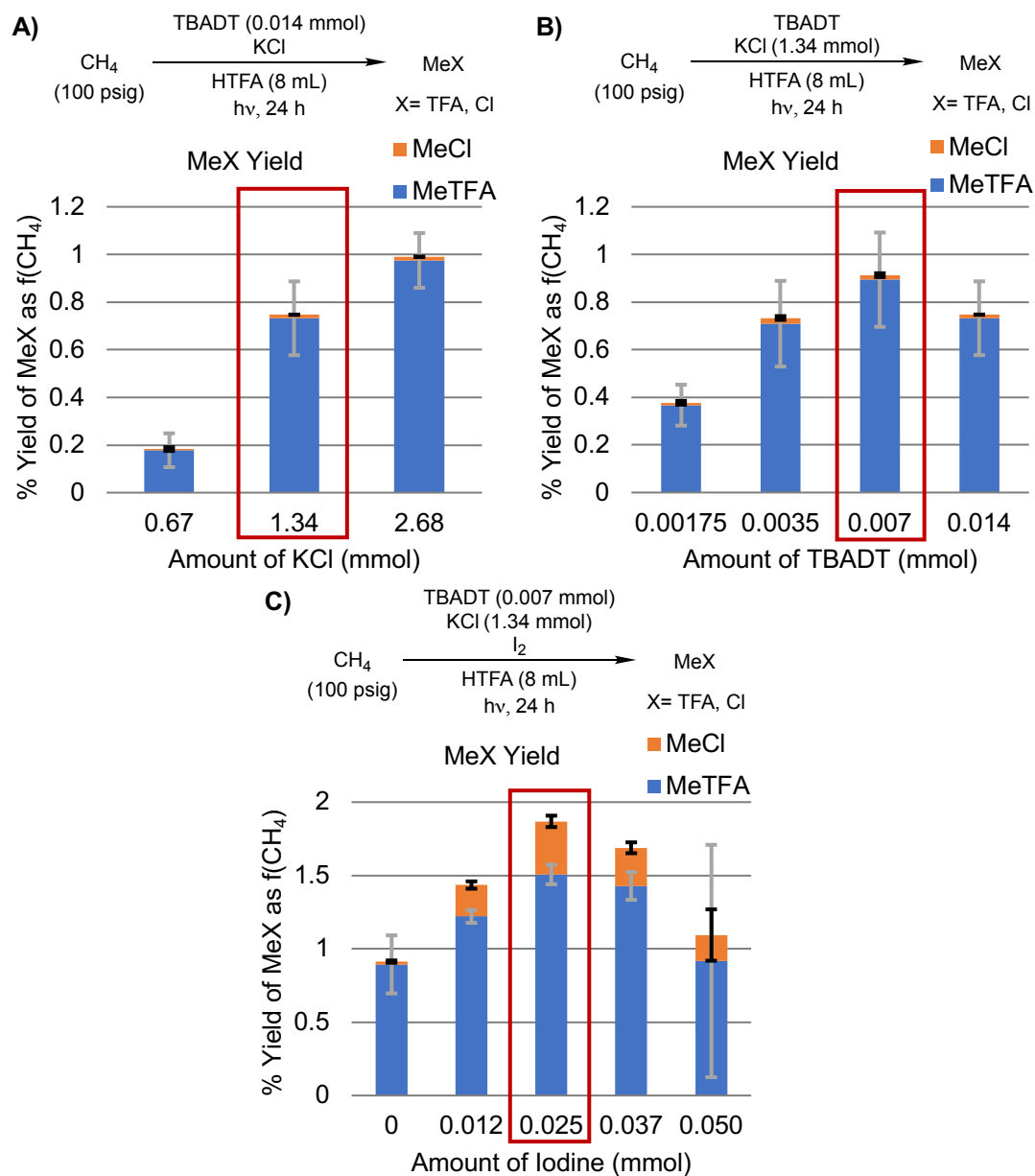


Figure 2.3. MeX (X = TFA, Cl) yield at various loadings of KCl (A), TBADT (B), and I₂ (C). Red boxes indicate optimal reagent loadings in the standard aerobic reaction conditions. Each bar graph represents the average of at least three independent experiments with error bars depicting the standard deviations.

Other combinations of TBADT, KCl and/or I₂ in HTFA led to decreased CH₄ functionalization (Table 2.1). For the reaction of KCl and I₂, it was found that iodine loading is crucial for MeX production. Specifically, increasing the loading

of I₂ to 0.050 mmol with 1.34 mmol of KCl led to no MeX production within standard deviation (Table 2.1, Entry 4). However, halving the amount of I₂ to 0.025 mmol with 1.34 mmol KCl (corresponding to standard aerobic reaction conditions) led to substantial MeX formation (Table 2.1, Entry 5). The investigation of the background reaction of 1.34 mmol of KCl and 0.025 mmol of I₂ for methane functionalization in HTFA is described in the Appendix. The bimodal nature of MeX production as a function of time for this background reaction can be seen in Figure 2.13. The bifurcated results hint that radical chain processes for MeX formation are possible, but the initiation of such reactions is highly dependent on factors that we could not identify nor control.

Table 2.1. MeX (X = TFA, Cl) yields for the control reactions of remaining combinations of reagents.^a

Entry	Reagents	% Yield of MeTFA	% Yield of MeCl
1	TBADT (0.007 mmol), I ₂ (0.025 mmol)	0.13 ± 0.069	0
2	KCl (1.34 mmol)	0.36 ± 0.069	0.010 ± 0.0088
3	I ₂ (0.025 mmol)	0.50 ± 0.16	0
4	KCl (1.34 mmol), I ₂ (0.050 mmol)	0.010 ± 0.010	0
5	KCl (1.34 mmol), I ₂ (0.025 mmol)	1.7 ± 0.26	0.42 ± 0.063

^a The reagents were added to 8 mL HTFA, pressurized with 100 psig CH₄, and irradiated with a mercury arc lamp for 24 h. Each entry line represents the average of at least three independent experiments reported with their standard deviations.

Additional control reactions were performed. When heated (180 °C for 3 h) without irradiation, TBADT (0.014 mmol) and KCl (1.34 mmol) in HTFA (8 mL) with 100 psig CH₄ resulted in no MeX formation. When the standard aerobic reaction conditions were pressurized with 100 psig Ar instead of CH₄ and subjected

to a mercury arc lamp for 24 h, MeX production was not observed. Minimal methane functionalization ($< 0.03\%$ yield) occurred when KBr was used in place of KCl under the standard aerobic reaction conditions. When the standard aerobic reaction conditions were instead subjected to fume hood LED lighting or a 370 nm LED lamp, CH₄ functionalization occurred, albeit at much slower rates and with lower yields. Acetic acid (HOAc) was explored as a solvent alternative to HTFA. With pure HOAc as solvent, MeX formation was not observed. Using HOAc and HTFA solvent mixtures, the chemistry was not clean enough to extract meaningful results.

Using standard aerobic reaction conditions, CH₄ pressure was varied (Figure 2.4). At lower methane pressures, MeX yield based on methane was improved in the TBADT–KCl–I₂ system. For example, reacting TBADT (0.007 mmol), KCl (1.34 mmol), and I₂ (0.025 mmol) with 15 psig of methane (~4 mmol) afforded 0.35 ± 0.0057 mmol of MeX in $8.9 \pm 0.58\%$ yield with a 6.4:1 ratio of MeTFA to MeCl after 24 h of reaction. This MeX formation as a function of TBADT corresponds to 50 ± 0.82 TOs. This is the highest conversion achieved with this system under aerobic conditions (without the inclusion of additional dioxygen).

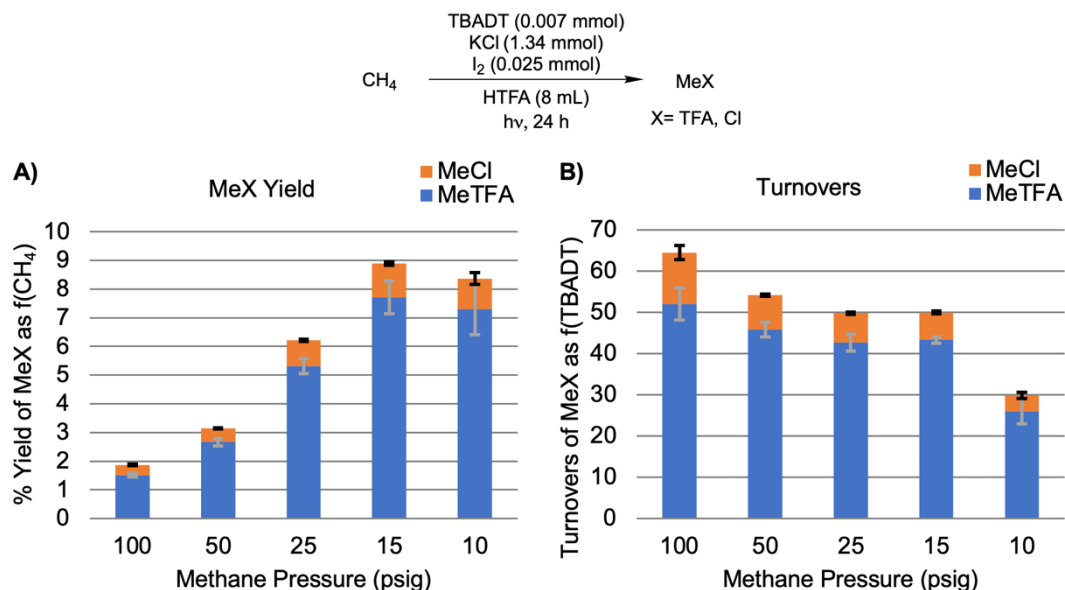


Figure 2.4. The effect of methane pressure on MeX yield (A) and corresponding decatungstate TOs (B). Each bar graph represents the average of at least three independent experiments with error bars depicting the standard deviations.

2.2.2 MeTFA Stability, Kinetics of Methane Functionalization, and Decatungstate Re-Oxidation with Dioxygen

Product stability was explored under standard aerobic reaction conditions with the addition of 0.35 mmol MeTFA at time $t = 0$ h and pressurization with 100 psig Ar in place of CH_4 . MeTFA was found to be stable under these conditions with $> 94\%$ MeTFA remaining after 41 h (Figure 2.5).

Using standard aerobic reaction conditions, the time of mercury arc lamp irradiation was varied to explore CH_4 oxidation as a function of time (Figure 2.5). According to product formation versus time, it appears that MeX formation halts at $t \cong 21$ h. However, the exact time is difficult to discern due to the large deviations inherent to the photoreactions. The lack of further product formation after $t \cong 21$ h could indicate depletion of the limiting reagent. At $t \cong 21$ h, 0.44 ± 0.010 mmol of

MeX was present. This corresponds to $\sim 62 \pm 1.5$ TOs of TBADT and consumption of $\sim 32\%$ of starting KCl.

Using the standard aerobic reaction conditions, the reagents were added to the reactor in air and then sealed. It was speculated that the dioxygen present in the headspace of the reactor was fully consumed at $t \cong 21$ h, thus preventing photocatalyst re-oxidation. The amount of dioxygen estimated to be in the headspace was calculated to be ~ 0.75 mmol. Thus, at $t \cong 21$ h, the concentration of dioxygen likely becomes too low to re-oxidize TBADT. This speculation is further supported by the blue color of the post-reaction solutions, indicative of spent decatungstate in its reduced form.

We began our studies on dioxygen dependence by varying the amount of dioxygen present in the reactor headspace before the start of the reaction. It has been shown that dioxygen is incapable of quenching $DT^{\bullet\bullet}$, such that catalyst deactivation by dioxygen is very unlikely.⁸² We studied the impact of dioxygen by purging the reaction solution with either dinitrogen or dioxygen. Purging was performed by bubbling the respective gas into the reaction solution for 1 minute after charging the reactor with TBADT, KCl, I_2 , and HTFA and before pressurizing with CH_4 . When the solution was purged with dinitrogen, no MeX was produced (Scheme 2.1B). When the solution was purged with dioxygen, 0.90 ± 0.30 mmol MeX was produced after 24 h of irradiation (Scheme 2.1C). Scheme 2.1 details a comparison of these solution-purged reactions to the standard aerobic reaction. These results provide support for dioxygen as the limiting reagent, in which dioxygen re-oxidizes spent TBADT back to its active form.

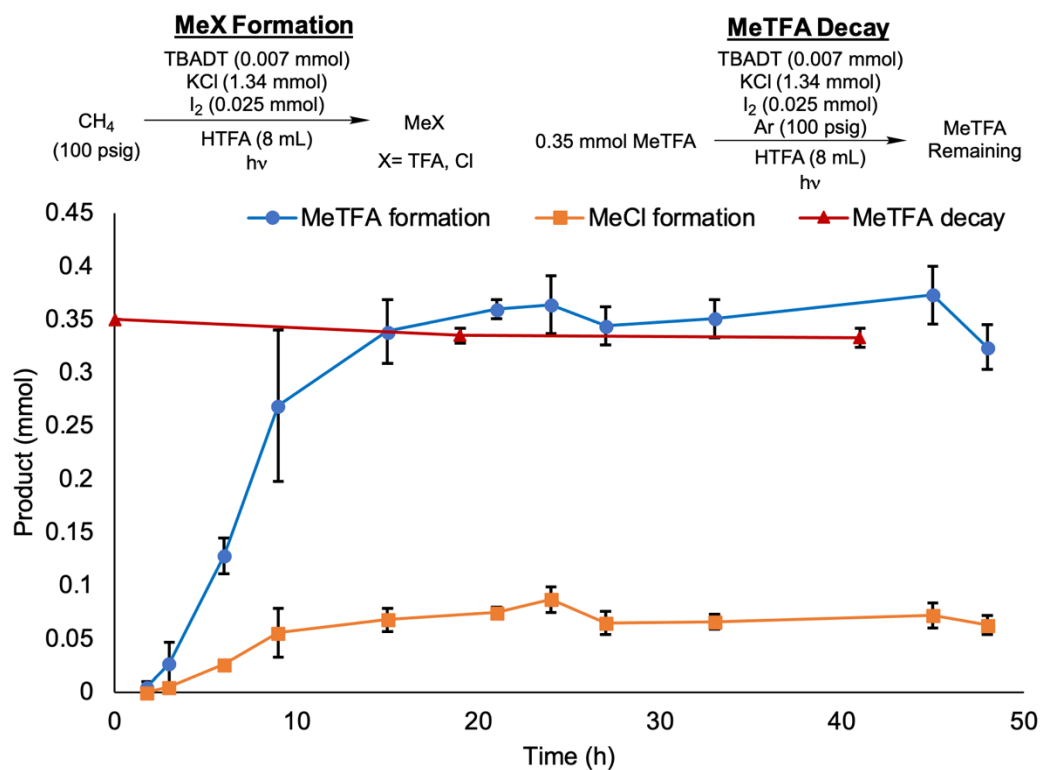
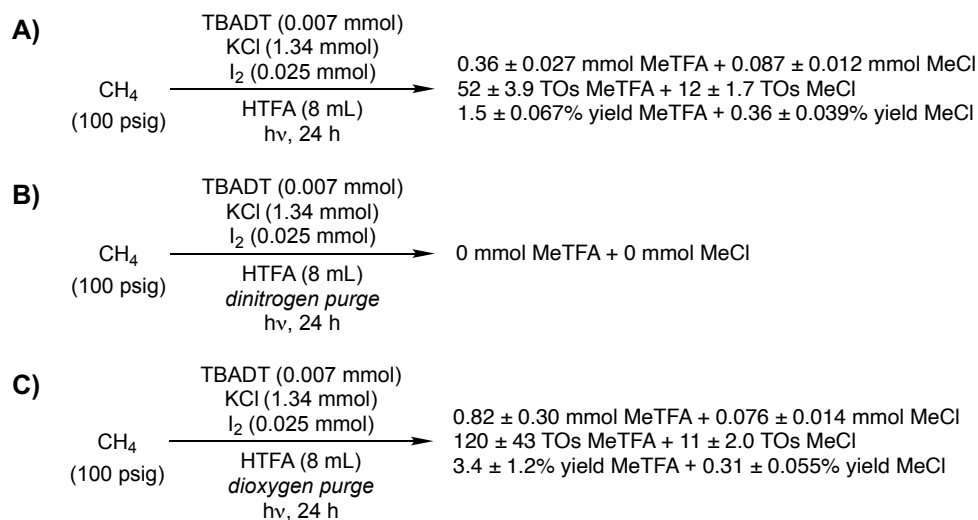


Figure 2.5. Methane functionalization and MeTFA decay under standard aerobic reaction conditions with TBADT, KCl, and I_2 as a function of time. Each data point represents the average of at least three independent experiments with error bars depicting the standard deviations.

Additional experiments were performed to further probe the re-oxidation of TBADT by dioxygen. After irradiation of the high methane conversion aerobic reaction conditions (15 psig CH_4) for 24 h, dioxygen top pressure was added to the reactors, followed by further irradiation. A series of experiments were performed in which we modulated the amount of dioxygen added, the number of dioxygen pressurizations, and the amount of irradiation time between dioxygen top pressure additions. In many of these experiments, the formation of MeCl could not be accurately quantified due to signal broadening in the ^1H NMR spectra (see Figure 2.11 for representative ^1H NMR spectrum). A preliminary re-oxidation reaction as

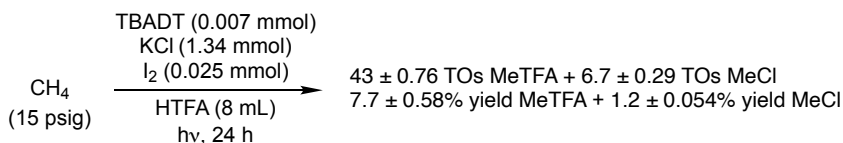
well as the optimal re-oxidation reaction are displayed in Scheme 2.2, along with the high methane conversion aerobic reaction for comparison. We note that the optimal re-oxidation experiment reached the pressure limitations of the reaction vessel. Because dioxygen is our limiting reagent under these conditions, it is feasible that MeX formation will continue with additional dioxygen if a reactor with a higher-pressure limit or continuous-flow of dioxygen is used.

Scheme 2.1. Effect of differing concentrations of dioxygen on MeX (X = TFA, Cl) production reported as mmol of product, catalyst turnovers, and percent yield. A = standard aerobic reaction conditions; B = dinitrogen-purged reaction solution; C = dioxygen-purged reaction solution. Each reaction scheme represents the average of at least three independent experiments reported with their standard deviation.

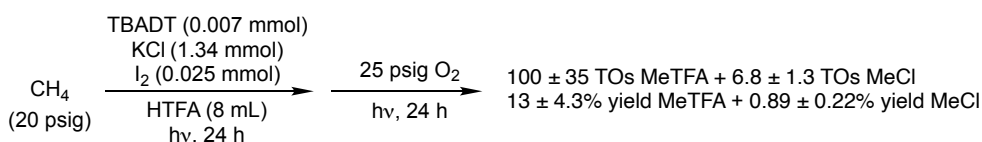


Scheme 2.2. Comparison of high methane conversion aerobic methane to MeX (X = TFA, Cl) reaction with standard reagent loadings (A) to preliminary re-oxidation reaction with standard reagent loadings (B) and to optimal re-oxidation reaction with standard reagent loadings (C). Results are reported as catalyst TOs and percent yields based on methane. Each reaction scheme represents the average of at least three independent experiments reported with their standard deviation.

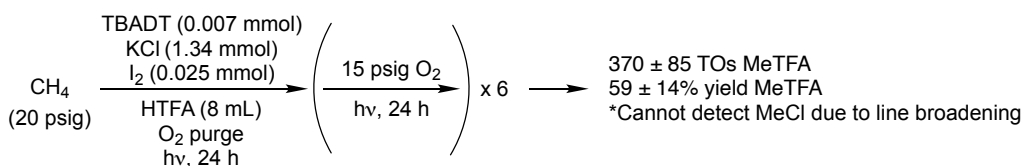
A) High Methane Conversion Aerobic Reaction



B) Preliminary Re-oxidation Reaction



C) Optimal Re-oxidation Reaction



2.2.3 Screening of Non-Gaseous Oxidants for Decatungstate Re-Oxidation

In an effort to circumvent the pressure limitations of the reactors described above with dioxygen, non-gaseous additives were explored as potential co-oxidants, such as copper salts and peroxides. None of the copper salts explored ($\text{CuCl}_2 \cdot x\text{H}_2\text{O}$, $\text{Cu}(\text{OAc})_2 \cdot x\text{H}_2\text{O}$ {OAc = $\text{C}_2\text{H}_3\text{O}_2^-$ }, $\text{Cu}(\text{TFA})_2 \cdot x\text{H}_2\text{O}$) nor $\text{K}_2\text{S}_2\text{O}_8$ had any beneficial effect on product formation (Figure 2.12). Alkyl peroxides (tert-butyl hydroperoxide, di-tert-butyl peroxide) were then explored as potential co-oxidants, resulting in > 100% yield of MeX (Table 2.2). However, this > 100% MeX yield was due to peroxide decomposition for which photo-induced cleavage of the peroxide O–O bond followed by decomposition leads to the production of methyl radicals and acetone (see Appendix for details).^{83, 84} When hydrogen

peroxide (which is unable to generate methyl radicals) was used, no improvement of MeX yield (within deviation) was observed relative to the high methane conversion aerobic reaction. The large deviations for these reactions can be explained by photodecomposition. UV irradiation initiates O–O bond cleavage to hydroxyl radicals which form water and dioxygen through a radical chain mechanism, leading to differing concentrations of these three compounds in reaction solution.⁸⁵ Overall, no solids or liquids were identified as effective co-oxidants.

2.2.4 Mechanistic Studies based on Density Functional Theory (DFT)

Section 2.2.4 describes the computational studies carried out by Charles Musgrave.

2.2.4.1 Global Mechanism

DT's involvement in the chemistry is not trivial. DT is primarily known for its ability to perform HAT on alkanes to generate alkyl radicals. In the present case, this could be HAT to convert methane to $\text{CH}_3\bullet$, which has been previously observed.⁷⁴ We initially considered that DT also abstracts H from HTFA to form $\text{TFA}\bullet$. However, HTFA's polarity mismatch with DT⁵⁵ and strong O–H BDE (113.7 kcal/mol) would make HAT of the HTFA O–H bond by DT unlikely.⁸⁶ If we assume that HCl is generated through HAT from methane by $\text{Cl}\bullet$, it is plausible that DT undergoes a HAT with HCl to regenerate the $\text{Cl}\bullet$. However, the difference in $\text{p}K_{\text{a}}$ between H-TFA and H-Cl is > 6 units, such that HCl would likely deprotonate to form Cl^- . An alternative path for Cl^- would be to undergo electron transfer (ET) with $\text{DT}\bullet\bullet$ to again form $\text{Cl}\bullet$ and reduce $\text{DT}\bullet\bullet$ to $\text{DT}\bullet^-$.^{80,87} We propose a two-fold involvement of DT in the methane oxidation chemistry. First, active

DT•• abstracts hydrogen from CH₄ to form CH₃•. Second, DT•• oxidizes Cl⁻ to Cl•; Cl• can either directly react with CH₄ via HAT, or associate with a Cl⁻ to form a Cl₂•⁻ radical trap. With these considerations in mind, we propose the mechanism depicted in Figure 2.6.

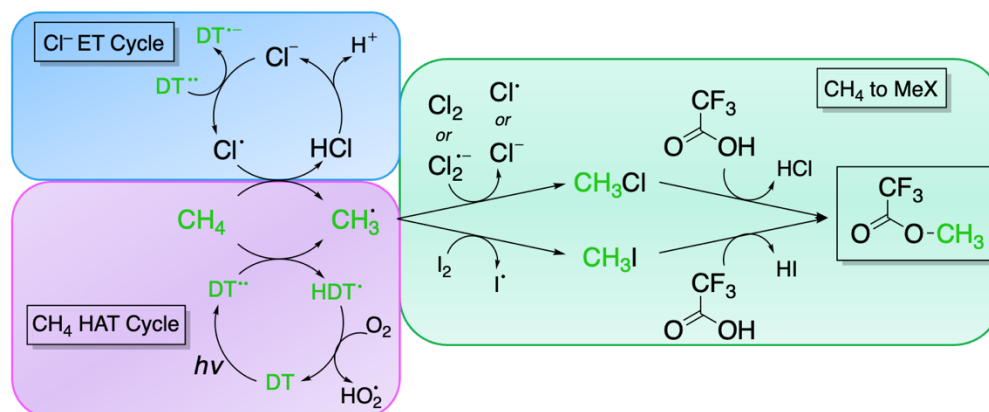


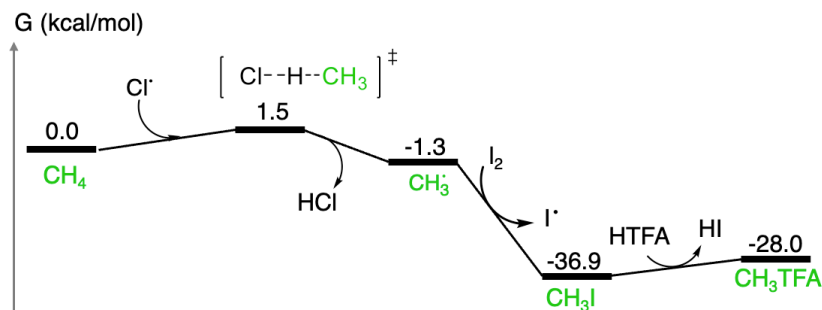
Figure 2.6. Global mechanism for methane oxidation towards MeX. The mechanism can be partitioned into 3 sub-mechanisms working synergistically. The first sub-mechanism (green, labeled CH₄ to MeX) is the Cl/I radical-based pathway in which methane (or CH₃• after HAT) is converted to MeTFA and MeCl (CH₃Cl in figure). The second sub-mechanism (blue, labelled Cl⁻ ET Cycle) is the DT•• + Cl⁻ ET to generate Cl•. The third sub-mechanism (purple, labelled CH₄ HAT Cycle) is the HAT of CH₄ with DT•• or Cl• to generate CH₃•.

We probed the mechanism for CH₄ conversion to MeTFA hypothesized in Figure 6 using quantum mechanics (QM) calculations at the DFT level. We begin with the first sub-mechanism, which involves the actual conversion of CH₄ to MeTFA. With Cl• as the HAT agent and I₂ as the radical trap, the sub-mechanism occurs as:

- CH₄ reacts with Cl• to generate CH₃• and HCl
- CH₃• is then trapped by I₂ to form CH₃I and I•
- CH₃I reacts with HTFA to form MeTFA and HI

The free energy surface for this pathway is detailed in Scheme 2.3.

Scheme 2.3. DFT Free energies at 298 K for the conversion of methane to MeTFA within the Cl/I system.



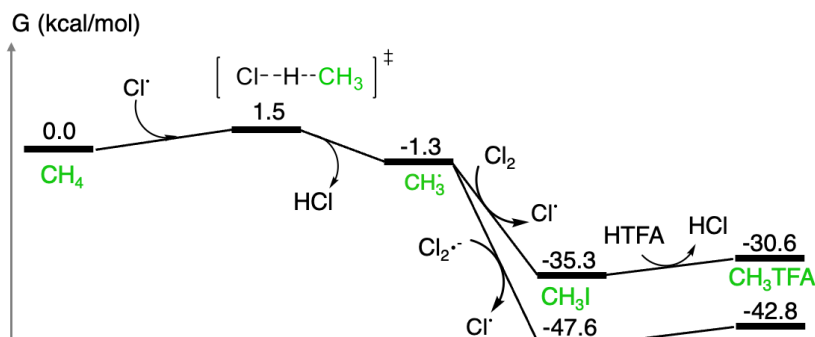
2.2.4.2 Chlorine-Based Radical Mechanism

The barrier required for HAT between CH_4 and Cl^\bullet to produce CH_3^\bullet and HCl is calculated to be 1.5 kcal/mol above the methane starting state, while the reaction step is overall downhill by -1.3 kcal/mol. Following formation of CH_3^\bullet , molecular I_2 reacts to form CH_3I and I^\bullet . DFT predicts this step to be barrierless and exergonic by -35.6 kcal/mol, which places CH_3I at -36.9 kcal/mol below the methane starting state. Following the formation of CH_3I , MeTFA can now form by an $\text{S}_{\text{N}}2$ solvolysis reaction with HTFA. In this reaction step, the divalent O of HTFA acts as a nucleophile to attack the C of CH_3I , forming $\text{HTFA}^+\text{-CH}_3$ and I^- . The now trivalent O of $\text{HTFA}^+\text{-CH}_3$ gives up H^+ to I^- , forming HI and the desired MeTFA product. DFT predicts that this conversion of HTFA and MeI to MeTFA and HI is uphill 8.9 kcal/mol. The acidity of HI, which should protonate water, would drive the conversion of MeI and HTFA to MeTFA and HI to completion. In this sub-mechanism, the overall conversion of CH_4 to MeTFA is -28.0 kcal/mol when Cl^\bullet is the HAT agent with I_2 as the radical trap.

2.2.4.3 Iodine-Free Radical Mechanism

It is important that we also consider the chemistry in the absence of iodine, since this is the condition of some experiments. In the absence of iodine, we observe that oxidation of CH₄ to MeTFA still occurs, however with decreased turnovers. This is likely because without iodine, Cl₂ or Cl₂^{•-} (which forms when Cl[•] and Cl⁻ associate)⁸⁸ serve as the radical trapping agent, in which CH₃Cl is formed instead of CH₃I.³⁵ Because Cl⁻ is a poorer leaving group than I⁻, CH₃Cl + HTFA solvolysis to form HCl and MeTFA is likely retarded. However, HAT between CH₄ and Cl[•] is not affected by the absence of iodine. The free-energy pathway is depicted in Scheme 2.4. As noted, HAT between CH₄ and Cl[•] remains unchanged with a barrier of 1.5 kcal/mol, resulting in the alkyl radical and HCl at -1.3 kcal/mol. Trapping of the alkyl radical with Cl₂ is downhill -34.0 kcal/mol, resulting in formation of CH₃Cl at -35.3 kcal/mol. With Cl₂^{•-} radical trapping is downhill -46.3 kcal/mol, resulting in CH₃Cl and Cl⁻ at -47.6 kcal/mol. Like the case with CH₃I, we propose CH₃Cl follows an S_N2 solvolysis pathway with HTFA to generate MeTFA and HCl. Solvolysis between CH₃Cl and HTFA is uphill 4.7 kcal/mol, resulting in HCl and the desired MeTFA at -30.6 kcal/mol (-42.8 when Cl₂^{•-} is the radical trap). While solvolysis with MeCl (4.7 kcal/mol) is thermodynamically more accessible than MeI (8.9 kcal/mol), the actual kinetics for MeCl solvolysis will be slower because the HTFA⁺-CH₃ + Cl⁻ ion pair is less stable than the iodine analog, on account of Cl⁻ being a worse leaving group than I⁻.

Scheme 2.4. DFT Free energies at 298 K for the conversion of methane to MeTFA in the absence of I₂.



2.2.4.4 Decatungstate Integration

Previous reports have shown that ground state DT, specifically NaDT and TBADT, can be photoexcited by 365-390 nm light to a highly active HAT reagent.^{56, 67, 89, 90} The absorption spectrum for DT anion shows a large peak at 324 nm, corresponding to a HOMO-LUMO transition, also marked by ligand to metal charge transfer (LMCT).^{91, 92} This photoexcitation is likely a closed-shell singlet to open-shell singlet transition of DT in which the SOMOs reside on the oxygens. The open-shell singlet relaxes from the Franck-Condon point to the open-shell singlet minima in < 1 ps.⁵⁶ This excited singlet reportedly decays via an intersystem crossing to the active triplet state, which is stabilized by the exchange interaction. This active triplet state is formed with a quantum yield of 0.5-0.6 and exists for 55 ± 20 ns in acetonitrile.^{56, 93-98} The triplet state (DT••) has radical character on the electrophilic oxygens, such that it can readily pull H atoms off neighboring molecules (like CH₄ and HCl) to generate radicals when the substrate oxidation potential is above +2.44 V vs. saturated calomel electrode (SCE).⁵⁶ When the

oxidation potential is below +2.44 V vs. SCE, the complex is expected to perform ET; this is the regime in which DT oxidizes Cl^- to $\text{Cl}\cdot$.⁸⁸ Following ET, protonation of $\text{DT}\cdot$ from the medium would result in $\text{HDT}\cdot$ with an overall doublet spin. Previously published experimental evidence shows that after reacting, the solution containing DT turns dark blue with strong absorption bands in the 600-800 nm range; which we interpret as the formal reduction of W in DT.^{82, 87, 90, 92, 99-101} The species responsible for the blue color occurs after relatively long periods of time and is not active in catalysis. For our purposes, we focus on the singlet ground state DT, the lowest-lying triplet $\text{DT}\cdot\cdot$ and the reduced $\text{HDT}\cdot$.

We calculate that the initial excitation of DT to the lowest-lying triplet $\text{DT}\cdot\cdot$ requires 43.5 kcal/mol; experimentally this excitation arises through irradiation by 365-390 nm light. For simplicity, we set $\text{DT}\cdot\cdot$ as the reference state of 0.0 kcal/mol in Scheme 2.5. Spin density analysis reveals significant unpaired spin on the bridging oxygens in $\text{DT}\cdot\cdot$. Oddly, the terminal oxo ligands exhibit little spin density, contrary to previous beliefs that the terminal oxos are responsible for HAT.⁵⁶ To confirm this finding, we analyzed the hydrogen binding (HB) energies for the 5 unique oxygens of $\text{DT}\cdot\cdot$ (Figure 2.7).

DT Site	H-binding Energy (kcal/mol)
1	-29.0
2	-47.3
3	-35.0
4	-47.7
5	-41.4

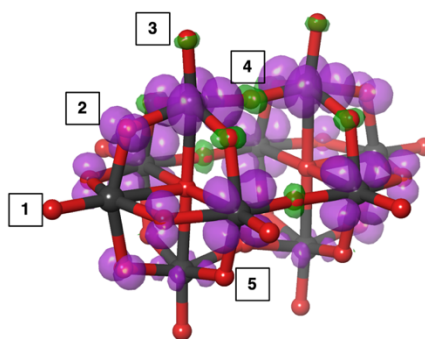
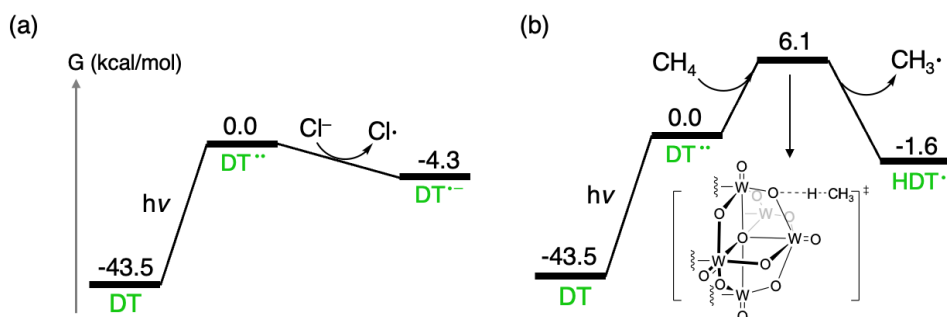


Figure 2.7. Spin-density diagram for the lowest-lying triplet decatungstate (purple= α , green= β) and hydrogen-binding energies (kcal/mol) for the 5 unique oxygen sites. The oxygen and tungsten atoms are red and grey, respectively.

We define the HB energy as the free energy of the reaction $\text{H}\cdot + \text{DT}\cdot\cdot \rightarrow \text{HDT}\cdot$. Sites 2, 4, and 5 are bridging oxygens and sites 1 and 3 are terminal oxo ligands. As the spin density analysis suggests, binding $\text{H}\cdot$ to the bridging oxygen sites was most favorable. The HB energy to sites 2, 4, and 5 are -47.3, -47.7, and -41.4 kcal/mol respectively. In contrast, the HB energy to sites 1 and 3 are -29.0 and -35.0 kcal/mol respectively, indicating that binding H to the terminal oxo ligands is significantly less favorable. Overall, site 4 provides the best HB energy while site 1 is the worst. Thus site 4 would appear responsible for the HAT since it binds H the strongest, but we note that site 4 is not easily accessible due to the two adjacent oxo groups. For example, CH_4 does not readily undergo HAT with site 4 because the adjacent oxo ligands would repel the CH_4 due to Pauli Repulsion. Instead, we propose that HAT occurs through site 2. Site 2 is easily accessible for HAT and

provides the second-best HB energy, only 0.4 kcal/mol less than site 4. Ravelli and coworkers also proposed that site 4 is shielded and therefore not active for HAT.⁵⁶ Site 1 was previously believed to be the active HAT site because it contributes more to the shape of the HOMO-1 orbital compared to site 2 (HOMO-1 is where the unpaired spin resides), and because its geometric parameters match that of HAT with a triplet carbonyl in which the process occurs in-plane with the C=O bond. We claim that the difference between sites 1 and 2 for HOMO-1 contribution is small and that both sites provide geometric parameters suitable for HAT with a carbonyl. This combined with site 2's more favorable HB energy leads us to propose that site 2 is responsible for HAT.

Scheme 2.5. DFT Free energies at 298 K for (a) the generation of $\text{Cl}\cdot$ through ET of Cl^- with $\text{DT}\cdot\cdot$ and (b) for the generation of $\text{CH}_3\cdot$ through HAT of CH_4 with $\text{DT}\cdot\cdot$.



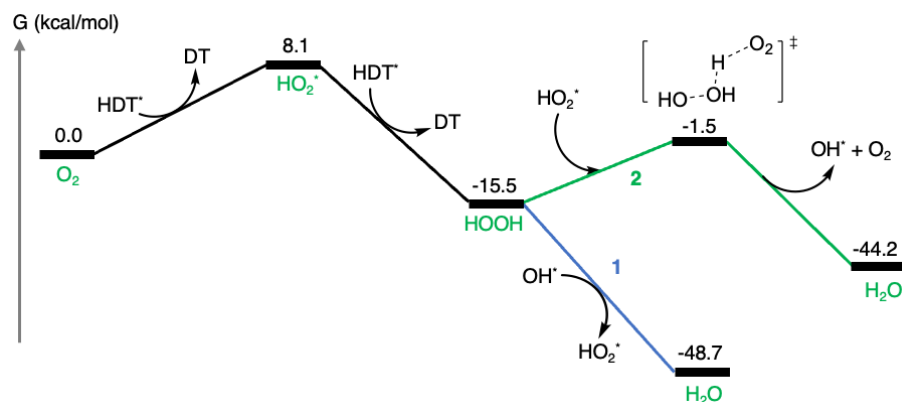
Scheme 2.5 shows ET to $\text{DT}\cdot\cdot$ from Cl^- to form $\text{Cl}\cdot$ and HAT to $\text{DT}\cdot\cdot$ from CH_4 to form $\text{CH}_3\cdot$; preceding these steps is the photoexcitation of DT to $\text{DT}\cdot\cdot$, which DFT predicts requires 43.5 kcal/mol. For simplicity, we choose $\text{DT}\cdot\cdot$ to be the reference state at 0.0 kcal/mol. DFT predicts ET to $\text{DT}\cdot\cdot$ from Cl^- is downhill - 4.3 kcal/mol.^{87, 102} Following ET, $\text{DT}\cdot^-$ would protonate to form $\text{HDT}\cdot$ (not shown).

We find that HAT from CH₄ to DT•• is -1.6 kcal/mol downhill with a transition state barrier of 6.1 kcal/mol above the DT•• reference state. Subsequent regeneration of DT from HDT• is achieved through oxidation by dioxygen.

2.2.4.5 Decatungstate Regeneration by Dioxygen

HAT leads to the HDT• species which can undergo further re-oxidation to regenerate the DT catalyst and funnel H towards H₂O. Given the presence of dioxygen (O₂) in the reaction vessel, the first step is likely a HAT in which triplet O₂ pulls H off HDT• to generate HO₂• and a ground state singlet DT. The HO₂• can then pull another H off an additional equivalent of HDT• to generate HOOH. We envision that during catalysis, there exists a pool of O–H containing species such as OH•, HOOH, HO₂•, etc. These species can react in numerous ways, making it difficult to predict exactly how O₂ and HOOH may funnel towards a thermodynamic sink. However, our previous study on peroxide radical chemistry revealed that in a large ensemble of O–H-containing species, the reactions that occur most are (1) HOOH + OH• → HO₂• + H₂O and (2) HOOH + HO₂• → OH• + O₂ + H₂O.¹⁰³ Both reactions consume an HOOH and produce an H₂O. We hypothesize that upon formation of HOOH from HO₂•, either of these two reactions can consume the HOOH to form H₂O. This H₂O formation mechanism is depicted in Scheme 2.6.

Scheme 2.6. DFT Free energies at 298 K for the conversion of dioxygen to H₂O and the regeneration of the DT ground state.



Starting with triplet O₂, HAT to pull H off the doublet HDT• to regenerate ground state singlet DT while forming HO₂• is uphill 8.1 kcal/mol. HO₂• can now perform a secondary HAT on an additional HDT• to form HOOH plus another singlet DT; this step is downhill to -15.5 kcal/mol. Formation of HOOH opens numerous avenues for a plethora of possible reaction steps. However, we believe the most likely reactions that can occur are either (1) HOOH + OH• → HO₂• + H₂O or (2) HOOH + HO₂• → OH• + O₂ + H₂O. Reaction 1 is barrierless to form HO₂• and H₂O at -48.7 kcal/mol. Reaction 2 requires a barrier of -1.5 kcal/mol (or 14.0 kcal/mol relative to preceding HOOH intermediate) and is downhill to form OH•, O₂, and H₂O at -44.2 kcal/mol. Overall, this sub-mechanism converts O₂ to H₂O and regenerates 2 ground-state DT from 2 HDT•. We note that this mechanism does not account for DT's reduced -5 or -6 states that are observed in experiment. We believe these states are formed via non-catalytic electron transfer side reactions that do not contribute to the catalytic methane oxidation chemistry. Indeed, previous experimental studies claim that these -5 and -6 states are formed over long time periods and are not catalytic.⁵⁶

2.2.5 Reaction Tolerance to Water

The DFT-predicted reaction mechanism suggests $\text{HO}_2\cdot$ formation from the re-oxidation of $\text{HDT}\cdot$ by O_2 , which eventually funnels to the formation of H_2O . Thus, we experimentally probed the reaction tolerance to water. Varying equivalents of water were added at the start of the reaction under our standard aerobic reaction conditions to quantify the effect on the amount of MeX produced. The formation of MeX is plotted against equivalents of added water relative to TBADT in Figure 2.8. At 1,000 equivalents of water relative to TBADT (7.0 mmol H_2O), there is no effect on MeX production. At 10,000 equivalents of water relative to TBADT (70 mmol H_2O), MeX production is shut down. At this concentration of water, the impact on reaction rate is likely due to a solvent effect (*e.g.*, reduced acidity) rather than a specific kinetic impact (Figure 2.8).

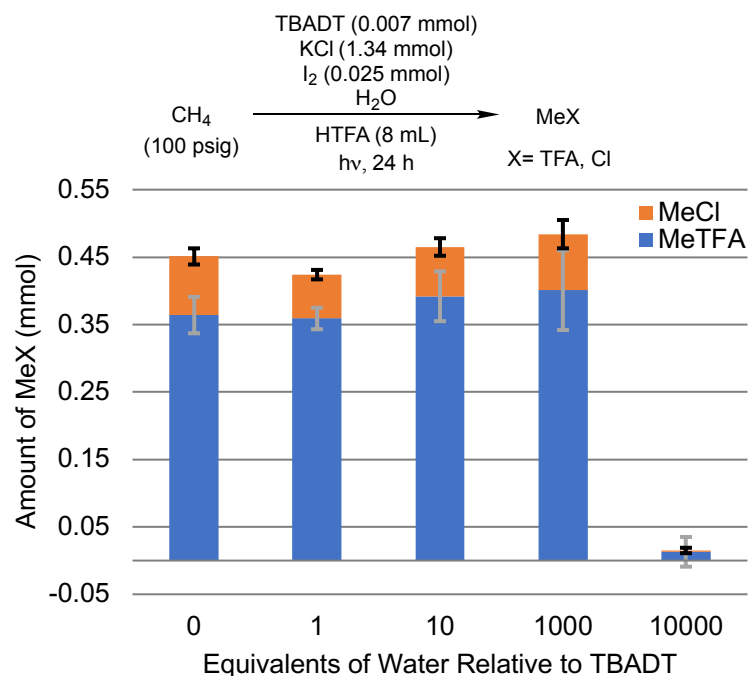


Figure 2.8. Amount of MeX (X = TFA, Cl) produced under standard aerobic reaction conditions in which varying amounts of water were added to the start of the reaction. Equivalents of water are reported with respect to TBADT. Each bar graph represents the average of at least three independent experiments with error bars depicting the standard deviation of the three experiments.

2.3 Summary and Conclusions

We have demonstrated the partial oxidation of methane using a photochemically driven process comprised of catalytic TBADT, chloride, and iodine in HTFA. Under aerobic conditions, MeX yield reached ~9%. Our kinetic studies revealed a dependence on dioxygen concentration. Re-oxidation experiments with dioxygen led us to achieve methane to MeTFA conversion with > 350 TOs based on TBADT and ~60% yield based on methane when optimized. MeTFA was shown to be stable under standard reaction conditions, with > 94% remaining after 41 h.

Density Functional Theory calculations were used to determine the reaction mechanism, which validates our proposal that photo and radical chemistry synergistically perform methane functionalization. Based on the DFT calculations and experiments, we propose a radical pathway in which a hydrogen atom is abstracted from methane by a chlorine atom or by triplet DT•• to generate a methyl radical, which is then trapped by some chlorine or iodine species (Cl_2 , $\text{Cl}_2^{\bullet-}$, I_2) to generate a methyl halide.³⁵ From there, HTFA undergoes $\text{S}_{\text{N}}2$ solvolysis with the methyl halide to form the desired ester product, MeTFA. The chlorine radicals in this mechanism are generated through electron transfer from chloride anion to DT••. We propose that after ET by DT•• and subsequent protonation, dioxygen re-oxidizes HDT• and subsequently forms water.

The addition of DT to the chloride-iodine system presents a novel strategy for the photo-driven partial oxidation of methane towards MeTFA. DT's remarkable quantum efficiency and HAT reactivity provides synergy with the free radical chemistry of chloride and iodine, affording the desired MeTFA product which maintains excellent stability.

2.4 Experimental Section

CAUTION. Many of the reagents and conditions described herein are particularly hazardous. Appropriate safety measures should be taken and appropriate personal protective equipment should be worn when handling strong acids, especially in large volumes. Broadband mercury arc lamps are dangerous to the skin and eyes, and even a brief exposure can result in permanent damage. The lamps must only be turned on while encased in an enclosure that precludes exposure

to the naked eye. Cool to room temperature water must always be recirculated around the lamp to prevent uncontrolled overheating; this is especially important when conducting reactions containing mixtures of methane and air or dioxygen.

NOTE: Mixtures of methane and dioxygen are potentially explosive.¹⁰⁴

General Comments and Materials. All reactions were carried out under ambient atmosphere unless indicated otherwise. Methane, oxygen, nitrogen, and argon were purchased from GTS-Welco and used as received. Potassium chloride, potassium bromide, iodine, trifluoroacetic acid (> 99.9%), glacial acetic acid, nitromethane, copper(II) acetate hydrate, copper(II) chloride hydrate, copper(II) trifluoroacetate hydrate, potassium persulfate, di-tert-butyl peroxide, tert-butyl hydroperoxide, hydrogen peroxide, and trifluoroacetic anhydride were purchased commercially and used as received. Tetrabutylammonium decatungstate (TBADT) was synthesized and characterized according to literature procedure, for which the reagents were purchased commercially and used as received.¹⁰⁵ High pressure reaction vessels were constructed from Fisher-Porter tubes, purchased from Andrews Glass, and custom-built reactor tops were constructed from Swagelok stainless steel fittings (see Figure 2.10). These reaction vessels can be safely pressurized to 250 psig at room temperature. The photolysis enclosure was constructed with a power supply feeding a broadband mercury arc lamp. The mercury arc lamp was nested in a quartz immersion well in which cool to room temperature DI water (15-40 °C) was recirculated through at all times the lamp was powered on. The power supply (450-watt, product #7830-60), Hanovia mercury arc lamp (medium pressure, 450 watt, 121.92 mm arc length, 244.35 mm overall

length, product #7825-34), and quartz immersion well (product #7854-27) were purchased from Ace Glass. The mercury arc lamp is quoted to irradiate ~ 40-48% in the ultraviolet spectral range, ~ 40-43% in the visible spectral range, and the remainder in the infrared spectral range. Mercury arc lamps were replaced every 1,000 hours. NMR analysis was performed using either a Varian Inova 500 or 600 MHz spectrometer. ^1H NMR data of reaction mixtures were obtained with a capillary of C_6D_6 as the internal lock reference. Chemical shifts are reported relative to the internal standards of either CH_3NO_2 (δ 4.18) or HOAc (δ 2.04). UV-vis spectral measurements of TBADT were collected on a Cary 60 UV-vis spectrometer. Samples were prepared in 1 cm square quartz cuvettes.

General Procedure for Photochemical Methane Functionalization.

Reactions were performed in triplicate. Each Fisher-Porter reactor was charged with a stir bar and solid reagents (TBADT, KCl , I_2) followed by 8 mL HTFA. Unless specified otherwise, TBADT was ground with a mortar and pestle prior to adding to the reactor. The reactors were sealed under air and weighed. The reactors were then pressurized with methane and weighed again. The amount of methane added was quantified by the difference in mass before and after methane addition. The reactors were then added to a photolysis enclosure, each positioned 16 cm from the mercury arc lamp with uniform stirring. Reaction time was started 15 minutes following lamp turn on to account for lamp warm up time to reach full intensity. After the reaction, the lamp was turned off and the photolysis chamber was kept closed for at least one minute to ensure the lamp was safely powered off. The reactors were removed, weighed to probe for leaks, and cooled in front of a fan for

at least 15 minutes. The reactors were then vented in a fume hood, 20 μL of internal standard (either CH_3NO_2 or HOAc) was added to each reaction, and the reaction mixtures were thoroughly stirred. An aliquot from each reaction mixture was removed and centrifuged, from which the supernatant of each was added to an NMR tube containing a sealed capillary containing C_6D_6 . The products were analyzed by ^1H NMR spectroscopy. See Figure 2.9 for a sample ^1H NMR spectrum.

MeTFA Stability Under Photochemical Conditions. Reactions were performed in triplicate. Each Fisher-Porter reactor was charged with 0.007 mmol TBADT, 1.34 mmol KCl, 0.025 mmol I_2 , and a stir bar followed by 8 mL HTFA and 0.35 mmol of MeTFA. The reactors were sealed under air, pressurized with 100 psig Ar, and weighed. The reactors were then added to a photolysis enclosure, each positioned 16 cm from the mercury arc lamp with uniform stirring. Reaction time was started 15 minutes following lamp turn on to account for lamp warm up time to reach full intensity. After the reaction, the lamp was turned off and the photolysis chamber was kept closed for at least one minute to ensure the lamp was safely powered off. The reactors were removed, weighed to probe for leaks, and cooled in front of a fan for at least 15 minutes. The reactors were then vented in a fume hood, 20 μL of internal standard (either CH_3NO_2 or HOAc) was added to each reaction, and the reaction mixtures were thoroughly stirred. An aliquot from each reaction mixture was removed and centrifuged, from which the supernatant of each was added to an NMR tube containing a sealed capillary containing C_6D_6 . The products were analyzed by ^1H NMR spectroscopy.

Experiments Involving Dinitrogen/Dioxygen Purges. Reactions were performed in triplicate. Each Fisher-Porter reactor was charged with 0.007 mmol TBADT, 1.34 mmol KCl, 0.025 mmol I₂, and a stir bar followed by 8 mL HTFA. The reactor tops were fitted to the reactors but not sealed. Using a long needle, the respective gas was bubbled through each reaction solution one at a time. Following one minute of bubbling, the needle was removed and the reactor valve was quickly sealed. The reactors were weighed, pressurized with 100 psig methane, and weighed again. The amount of methane added was quantified by the difference in mass before and after methane addition. The reactors were then added to a photolysis enclosure, each positioned 16 cm from the mercury arc lamp with uniform stirring. Reaction time was started 15 minutes following lamp turn on to account for lamp warm up time to reach full intensity. After 24 h of reaction, the lamp was turned off and the photolysis chamber was kept closed for at least one minute to ensure the lamp was safely powered off. The reactors were removed, weighed to probe for leaks, and cooled in front of a fan for at least 15 minutes. The reactors were then vented in a fume hood, 20 μ L of internal standard (either CH₃NO₂ or HOAc) was added to each reaction, and the reaction mixtures were thoroughly stirred. An aliquot from each reaction mixture was removed and centrifuged, from which the supernatant of each was added to an NMR tube containing a sealed capillary containing C₆D₆. The products were analyzed by ¹H NMR spectroscopy.

Re-oxidation Experiments with Dioxygen. Reactions were performed in triplicate. Each Fisher-Porter reactor was charged with 0.007 mmol TBADT, 1.34

mmol KCl, 0.025 mmol I₂, and a stir bar followed by 8 mL HTFA. Reactors were either sealed under air or purged with dioxygen. The reactors were weighed, pressurized with methane and weighed again. The amount of methane added was quantified by the difference in mass before and after methane addition. The reactors were then added to a photolysis enclosure, each positioned 16 cm from the mercury arc lamp with uniform stirring. Reaction time was started 15 minutes following lamp turn on to account for lamp warm up time to reach full intensity. After the reaction, the lamp was turned off and the photolysis chamber was kept closed for at least one minute to ensure the lamp was safely powered off. The reactors were removed, weighed to probe for leaks, and cooled in front of a fan for at least 15 minutes. The reactors were then pressurized with dioxygen to pressure and weighed again. The amount of dioxygen added was quantified by the difference in mass before and after dioxygen addition. The reactors were then subjected again to the mercury arc lamp. This process of adding additional dioxygen to pressure and re-subjecting to the mercury arc lamp was repeated as detailed in each set of reaction conditions. Following the last dioxygen addition and irradiation, the reactors were removed, weighed to probe for leaks, and cooled in front of a fan for at least 15 minutes. The reactors were then vented in a fume hood, 20 μL of internal standard (either CH₃NO₂ or HOAc) was added to each reaction, and the reaction mixtures were thoroughly stirred. An aliquot from each reaction mixture was removed and centrifuged, from which the supernatant of each was added to an NMR tube containing a sealed capillary containing C₆D₆. The products were analyzed by ¹H NMR spectroscopy.

Computational Details. All Density Functional Theory calculations were performed within the Jaguar software package version 10.9 from Schrodinger Inc. Structures were first optimized using the PBE flavor of DFT including the Grimme-Becke-Johnson (GBJ) D3 correction for London dispersion. W and I atoms were treated with the Los Alamos **large-core** triple-zeta pseudopotential augmented with polarization and diffuse functions (LAV3P*+ in Jaguar). All other atoms were treated with the 6-31+G(d) basis set. PBE-D3 geometry optimizations were followed by additional single-point energy (SPE) calculations with implicit solvent. SPEs were calculated with the M06-2X functional using the GBJ D3 dispersion correction. For the SPE, W and I were described with the Los Alamos **small-core** triple-zeta potential augmented with polarization and diffuse functions; all other atoms were described with the 6-311++G(d,p) basis set (LACV3P***++ in Jaguar). Solvent effects were included through the PBF Poisson Boltzmann continuum model with parameters matching trifluoroacetic acid. Frequency calculations were performed at the M06-2X-D3/LACV3P***++ level to predict thermochemical properties (zero-point energy, entropy, and temperature correction to enthalpy) at 298K and to confirm intermediate and transition states.

2.5 References

1. Olah, G. A.; Goepfert, A.; Prakash, G. K. S., *Beyond Oil and Gas: The Methanol Economy*. Wiley-VCH: Weinheim, Germany, 2009.
2. Gunsalus, N. J.; Koppaka, A.; Park, S. H.; Bischof, S. M.; Hashiguchi, B. G.; Periana, R. A., Homogeneous Functionalization of Methane. *Chem. Rev.* **2017**, *117* (13), 8521-8573.

3. Dummer, N. F.; Willock, D. J.; He, Q.; Howard, M. J.; Lewis, R. J.; Qi, G.; Taylor, S. H.; Xu, J.; Bethell, D.; Kiely, C. J.; Hutchings, G. J., Methane Oxidation to Methanol. *Chem. Rev.* **2022**.
4. *BP Statistical Review of World Energy 2022*. 71st ed.; BP: London, 2022.
5. Zakaria, Z.; Kamarudin, S. K., Direct conversion technologies of methane to methanol: An overview. *Renew. Sust. Energ. Rev.* **2016**, *65*, 250-261.
6. Schwach, P.; Pan, X.; Bao, X., Direct Conversion of Methane to Value-Added Chemicals over Heterogeneous Catalysts: Challenges and Prospects. *Chem. Rev.* **2017**, *117* (13), 8497-8520.
7. Tang, P.; Zhu, Q.; Wu, Z.; Ma, D., Methane activation: the past and future. *Energy Environ. Sci.* **2014**, *7* (8), 2580-2591.
8. Ravi, M.; Ranocchiari, M.; van Bokhoven, J. A., The Direct Catalytic Oxidation of Methane to Methanol—A Critical Assessment. *Angew. Chem. Int. Ed.* **2017**, *56* (52), 16464-16483.
9. Lin, R.; Amrute, A. P.; Pérez-Ramírez, J., Halogen-Mediated Conversion of Hydrocarbons to Commodities. *Chem. Rev.* **2017**, *117* (5), 4182-4247.
10. Zichittella, G.; Paunović, V.; Amrute, A. P.; Pérez-Ramírez, J., Catalytic Oxychlorination versus Oxybromination for Methane Functionalization. *ACS Catal.* **2017**, *7* (3), 1805-1817.
11. Podkolzin, S. G.; Stangland, E. E.; Jones, M. E.; Peringer, E.; Lercher, J. A., Methyl Chloride Production from Methane over Lanthanum-Based Catalysts. *J. Am. Chem. Soc.* **2007**, *129* (9), 2569-2576.

12. Wang, K. X.; Xu, H. F.; Li, W. S.; Zhou, X. P., Acetic acid synthesis from methane by non-synthesis gas process. *J. Mol. Catal. A: Chem.* **2005**, *225* (1), 65-69.
13. Paunović, V.; Zichittella, G.; Moser, M.; Amrute, A. P.; Pérez-Ramírez, J., Catalyst design for natural-gas upgrading through oxybromination chemistry. *Nat. Chem.* **2016**, *8* (8), 803-809.
14. Tschuikow-Roux, E.; Paddison, S., Bond dissociation energies and radical heats of formation in CH₃Cl, CH₂Cl₂, CH₃Br, CH₂Br₂, CH₂FCl, and CHFCl₂. *Int. J. Chem. Kinet.* **1987**, *19* (1), 15-24.
15. Breed, A.; Doherty, M. F.; Gadewar, S.; Grosso, P.; Lorkovic, I. M.; McFarland, E. W.; Weiss, M. J., Natural gas conversion to liquid fuels in a zone reactor. *Catal. Today* **2005**, *106* (1), 301-304.
16. Shilov, A. E.; Shul'pin, G. B., Activation of C–H Bonds by Metal Complexes. *Chem. Rev.* **1997**, *97* (8), 2879-2932.
17. Periana, R. A.; Taube, D. J.; Gamble, S.; Taube, H.; Satoh, T.; Fujii, H., Platinum Catalysts for the High-Yield Oxidation of Methane to a Methanol Derivative. *Science* **1998**, *280* (5363), 560-564.
18. Chen, S.-S.; Koppaka, A.; Periana, R. A.; Ess, D. H., Theory and Experiment Demonstrate that Sb(V)-Promoted Methane C–H Activation and Functionalization Outcompete Superacid Protonolysis in Sulfuric Acid. *J. Am. Chem. Soc.* **2021**, *143* (43), 18242-18250.

19. Periana, R. A.; Mirinov, O.; Taube, D. J.; Gamble, S., High yield conversion of methane to methyl bisulfate catalyzed by iodine cations. *Chem. Commun.* **2002**, 2376-2377.
20. Gang, X.; Zhu, Y.; Birch, H.; Hjuler, H. A.; Bjerrum, N. J., Iodine as catalyst for the direct oxidation of methane to methyl sulfates in oleum. *Appl. Catal., A* **2004**, *261* (1), 91-98.
21. Hashiguchi, B. G.; Konnick, M. M.; Bischof, S. M.; Gustafson, S. J.; Devarajan, D.; Gunsalus, N.; Ess, D. H.; Periana, R. A., Main-Group Compounds Selectively Oxidize Mixtures of Methane, Ethane, and Propane to Alcohol Esters. *Science* **2014**, *343* (6176), 1232-1237.
22. Groothaert, M. H.; Smeets, P. J.; Sels, B. F.; Jacobs, P. A.; Schoonheydt, R. A., Selective Oxidation of Methane by the Bis(μ -oxo)dicopper Core Stabilized on ZSM-5 and Mordenite Zeolites. *J. Am. Chem. Soc.* **2005**, *127* (5), 1394-1395.
23. Woertink, J. S.; Smeets, P. J.; Groothaert, M. H.; Vance, M. A.; Sels, B. F.; Schoonheydt, R. A.; Solomon, E. I., A $[\text{Cu}_2\text{O}]^{2+}$ core in Cu-ZSM-5, the active site in the oxidation of methane to methanol. *Proc. Natl. Acad. Sci. U.S.A.* **2009**, *106* (45), 18908-18913.
24. Alayon, E. M.; Nachtegaal, M.; Ranocchiari, M.; van Bokhoven, J. A., Catalytic conversion of methane to methanol over Cu–mordenite. *Chem. Commun.* **2012**, *48* (3), 404-406.
25. Vanelderden, P.; Snyder, B. E.; Tsai, M. L.; Hadt, R. G.; Vancauwenbergh, J.; Coussens, O.; Schoonheydt, R. A.; Sels, B. F.; Solomon, E. I.,

- Spectroscopic definition of the copper active sites in mordenite: selective methane oxidation. *J. Am. Chem. Soc.* **2015**, *137* (19), 6383-6392.
26. Grundner, S.; Markovits, M. A.; Li, G.; Tromp, M.; Pidko, E. A.; Hensen, E. J.; Jentys, A.; Sanchez-Sanchez, M.; Lercher, J. A., Single-site trinuclear copper oxygen clusters in mordenite for selective conversion of methane to methanol. *Nat. Commun.* **2015**, *6*, 7546.
27. Ipek, B.; Lobo, R. F., Catalytic conversion of methane to methanol on Cu-SSZ-13 using N₂O as oxidant. *Chem. Commun.* **2016**, *52* (91), 13401-13404.
28. Pappas, D. K.; Martini, A.; Dyballa, M.; Kvande, K.; Teketel, S.; Lomachenko, K. A.; Baran, R.; Glatzel, P.; Arstad, B.; Berlier, G.; Lamberti, C.; Bordiga, S.; Olsbye, U.; Svelle, S.; Beato, P.; Borfecchia, E., The Nuclearity of the Active Site for Methane to Methanol Conversion in Cu-Mordenite: A Quantitative Assessment. *J. Am. Chem. Soc.* **2018**, *140* (45), 15270-15278.
29. Brezicki, G.; Kammert, J. D.; Gunnoe, T. B.; Paolucci, C.; Davis, R. J., Insights into the Speciation of Cu in the Cu-H-Mordenite Catalyst for the Oxidation of Methane to Methanol. *ACS Catal.* **2019**, *9* (6), 5308-5319.
30. Kulkarni, A. R.; Zhao, Z.-J.; Siahrostami, S.; Nørskov, J. K.; Studt, F., Cation-exchanged zeolites for the selective oxidation of methane to methanol. *Catal. Sci. Technol.* **2018**, *8* (1), 114-123.
31. Walling, C.; Mayahi, M. F., Some Solvent and Structural Effects in Free Radical Chlorination. *J. Am. Chem. Soc.* **1959**, *81* (6), 1485-1489.

32. Tedder, J. M., Which Factors Determine the Reactivity and Regioselectivity of Free Radical Substitution and Addition Reactions? *Angew. Chem. Int. Ed.* **1982**, *21* (6), 401-410.
33. Fortman, G. C.; Boaz, N. C.; Munz, D.; Konnick, M. M.; Periana, R. A.; Groves, J. T.; Gunnoe, T. B., Selective monooxidation of light alkanes using chloride and iodate. *J. Am. Chem. Soc.* **2014**, *136* (23), 8393-8401.
34. Kalman, S. E.; Munz, D.; Fortman, G. C.; Boaz, N. C.; Groves, J. T.; Gunnoe, T. B., Partial oxidation of light alkanes by periodate and chloride salts. *Dalton Trans.* **2015**, *44* (12), 5294-5298.
35. Schwartz, N. A.; Boaz, N. C.; Kalman, S. E.; Zhuang, T.; Goldberg, J. M.; Fu, R.; Nielsen, R. J.; Goddard, W. A.; Groves, J. T.; Gunnoe, T. B., Mechanism of Hydrocarbon Functionalization by an Iodate/Chloride System: The Role of Ester Protection. *ACS Catal.* **2018**, *8* (4), 3138-3149.
36. Fu, R.; Nielsen, R. J.; Liebov, N. S.; Goddard, W. A., III; Gunnoe, T. B.; Groves, J. T., DFT Mechanistic Study of Methane Mono-Esterification by Hypervalent Iodine Alkane Oxidation Process. *J. Phys. Chem. C* **2019**, *123* (25), 15674-15684.
37. Vargaftik, M. N.; Stolarov, I. P.; Moiseev, I. I., Highly selective partial oxidation of methane to methyl trifluoroacetate. *J. Chem. Soc., Chem. Commun.* **1990**, 1049-1050.
38. Chen, W.; Kocal, J. A.; Brandvold, T. A.; Bricker, M. L.; Bare, S. R.; Broach, R. W.; Greenlay, N.; Popp, K.; Walenga, J. T.; Yang, S. S.; Low, J.

- J., Manganese oxide catalyzed methane partial oxidation in trifluoroacetic acid: Catalysis and kinetic analysis. *Catal. Today* **2009**, *140* (3), 157-161.
39. Tang, R.; Kochi, J. K., Cobalt(III) trifluoroacetate: An electron transfer oxidant. *J. Inorg. Nucl. Chem.* **1973**, *35* (11), 3845-3856.
40. Coutard, N.; Musgrave, C. B., III; Moon, J.; Liebov, N. S.; Nielsen, R. M.; Goldberg, J. M.; Li, M.; Jia, X.; Lee, S.; Dickie, D. A.; Schinski, W. L.; Wu, Z.; Groves, J. T.; Goddard, W. A., III; Gunnoe, T. B., Manganese Catalyzed Partial Oxidation of Light Alkanes. *ACS Catal.* **2022**, *12* (9), 5356-5370.
41. Deng, H. P.; Zhou, Q.; Wu, J., Microtubing-Reactor-Assisted Aliphatic C–H Functionalization with HCl as a Hydrogen-Atom-Transfer Catalyst Precursor in Conjunction with an Organic Photoredox Catalyst. *Angew. Chem. Int. Ed.* **2018**, *57* (39), 12661-12665.
42. Gonzalez, M. I.; Gygi, D.; Qin, Y.; Zhu, Q.; Johnson, E. J.; Chen, Y.-S.; Nocera, D. G., Taming the Chlorine Radical: Enforcing Steric Control over Chlorine-Radical-Mediated C–H Activation. *J. Am. Chem. Soc.* **2022**, *144* (3), 1464-1472.
43. Yang, Q. M.; Wang, Y. H.; Qiao, Y. S.; Gau, M.; Carroll, P. J.; Walsh, P. J.; Schelter, E. J., Photocatalytic C–H activation and the subtle role of chlorine radical complexation in reactivity. *Science* **2021**, *372* (6544), 847-852.
44. Li, Z.; Luo, L.; Li, M.; Chen, W.; Liu, Y.; Yang, J.; Xu, S.-M.; Zhou, H.; Ma, L.; Xu, M.; Kong, X.; Duan, H., Photoelectrocatalytic C–H halogenation

- over an oxygen vacancy-rich TiO₂ photoanode. *Nat. Commun.* **2021**, *12* (1), 6698.
45. Panetti, G. B.; Yang, Q.; Gau, M. R.; Carroll, P. J.; Walsh, P. J.; Schelter, E. J., Discovery and mechanistic investigation of photoinduced sp³ C–H activation of hydrocarbons by the simple anion hexachlorotitanate. *Chem Catal.* **2022**, *2* (4), 853-866.
46. Coutard, N.; Goldberg, J. M.; Valle, H. U.; Cao, Y.; Jia, X.; Jeffrey, P. D.; Gunnoe, T. B.; Groves, J. T., Aerobic Partial Oxidation of Alkanes Using Photodriven Iron Catalysis. *Inorg. Chem.* **2022**, *61* (2), 759-766.
47. Liebov, N. S.; Goldberg, J. M.; Boaz, N. C.; Coutard, N.; Kalman, S. E.; Zhuang, T.; Groves, J. T.; Gunnoe, T. B., Selective Photo-Oxygenation of Light Alkanes Using Iodine Oxides and Chloride. *ChemCatChem* **2019**, *11* (20), 5045-5054.
48. Hirscher, N. A.; Ohri, N.; Yang, Q.; Zhou, J.; Anna, J. M.; Schelter, E. J.; Goldberg, K. I., A Metal-Free, Photocatalytic Method for Aerobic Alkane Iodination. *J. Am. Chem. Soc.* **2021**, *143* (46), 19262-19267.
49. Gumerova, N. I.; Rompel, A., Synthesis, structures and applications of electron-rich polyoxometalates. *Nat. Rev. Chem.* **2018**, *2* (2), 112.
50. Pope, M. T.; Müller, A., Polyoxometalate Chemistry: An Old Field with New Dimensions in Several Disciplines. *Angew. Chem. Int. Ed.* **1991**, *30* (1), 34-48.

51. Long, D.-L.; Burkholder, E.; Cronin, L., Polyoxometalate clusters, nanostructures and materials: From self assembly to designer materials and devices. *Chem. Soc. Rev.* **2007**, *36* (1), 105-121.
52. Dupré, N.; Rémy, P.; Micoine, K.; Boglio, C.; Thorimbert, S.; Lacôte, E.; Hasenknopf, B.; Malacria, M., Chemoselective Catalysis with Organosoluble Lewis Acidic Polyoxotungstates. *Chem. Eur. J.* **2010**, *16* (24), 7256-7264.
53. Tzirakis, M. D.; Lykakis, I. N.; Orfanopoulos, M., Decatungstate as an efficient photocatalyst in organic chemistry. *Chem. Soc. Rev.* **2009**, *38* (9), 2609-2621.
54. Ravelli, D.; Protti, S.; Fagnoni, M., Decatungstate Anion for Photocatalyzed “Window Ledge” Reactions. *Acc. Chem. Res.* **2016**, *49* (10), 2232-2242.
55. Ravelli, D.; Fagnoni, M.; Fukuyama, T.; Nishikawa, T.; Ryu, I., Site-Selective C–H Functionalization by Decatungstate Anion Photocatalysis: Synergistic Control by Polar and Steric Effects Expands the Reaction Scope. *ACS Catal.* **2018**, *8* (1), 701-713.
56. De Waele, V.; Poizat, O.; Fagnoni, M.; Bagno, A.; Ravelli, D., Unraveling the Key Features of the Reactive State of Decatungstate Anion in Hydrogen Atom Transfer (HAT) Photocatalysis. *ACS Catal.* **2016**, *6* (10), 7174-7182.
57. Cheung, K. P. S.; Sarkar, S.; Gevorgyan, V., Visible Light-Induced Transition Metal Catalysis. *Chem. Rev.* **2022**, *122* (2), 1543-1625.
58. Holmberg-Douglas, N.; Nicewicz, D. A., Photoredox-Catalyzed C–H Functionalization Reactions. *Chem. Rev.* **2022**, *122* (2), 1925-2016.

59. Sarver, P. J.; Bacauanu, V.; Schultz, D. M.; DiRocco, D. A.; Lam, Y. H.; Sherer, E. C.; MacMillan, D. W. C., The merger of decatungstate and copper catalysis to enable aliphatic C(sp³)–H trifluoromethylation. *Nat. Chem.* **2020**, *12* (5), 459-467.
60. Schultz, D. M.; Lévesque, F.; DiRocco, D. A.; Reibarkh, M.; Ji, Y.; Joyce, L. A.; Dropinski, J. F.; Sheng, H.; Sherry, B. D.; Davies, I. W., Oxyfunctionalization of the Remote C–H Bonds of Aliphatic Amines by Decatungstate Photocatalysis. *Angew. Chem. Int. Ed.* **2017**, *56* (48), 15274-15278.
61. Wu, W.; Fu, Z.; Tang, S.; Zou, S.; Wen, X.; Meng, Y.; Sun, S.; Deng, J.; Liu, Y.; Yin, D., (*n*Bu₄N)₄W₁₀O₃₂-catalyzed selective oxygenation of cyclohexane by molecular oxygen under visible light irradiation. *Appl. Catal., B* **2015**, *164*, 113-119.
62. Laudadio, G.; Deng, Y.; van der Wal, K.; Ravelli, D.; Nuño, M.; Fagnoni, M.; Guthrie, D.; Sun, Y.; Noël, T., C(sp³)–H functionalizations of light hydrocarbons using decatungstate photocatalysis in flow. *Science* **2020**, *369* (6499), 92-96.
63. Laudadio, G.; Govaerts, S.; Wang, Y.; Ravelli, D.; Koolman, H. F.; Fagnoni, M.; Djuric, S. W.; Noël, T., Selective C(sp³)–H Aerobic Oxidation Enabled by Decatungstate Photocatalysis in Flow. *Angew. Chem. Int. Ed.* **2018**, *57* (15), 4078-4082.

64. Halperin, S. D.; Fan, H.; Chang, S.; Martin, R. E.; Britton, R., A Convenient Photocatalytic Fluorination of Unactivated C–H Bonds. *Angew. Chem. Int. Ed.* **2014**, *53* (18), 4690-4693.
65. Perry, I. B.; Brewer, T. F.; Sarver, P. J.; Schultz, D. M.; DiRocco, D. A.; MacMillan, D. W. C., Direct arylation of strong aliphatic C–H bonds. *Nature* **2018**, *560* (7716), 70-75.
66. Murphy, J. J.; Bastida, D.; Paria, S.; Fagnoni, M.; Melchiorre, P., Asymmetric catalytic formation of quaternary carbons by iminium ion trapping of radicals. *Nature* **2016**, *532* (7598), 218-222.
67. Zeng, J.; Torigoe, T.; Kuninobu, Y., Control of Site-Selectivity in Hydrogen Atom Transfer by Electrostatic Interaction: Proximal-Selective C(sp³)–H Alkylation of 2-Methylanilinium Salts Using a Decatungstate Photocatalyst. *ACS Catal.* **2022**, *12* (5), 3058-3062.
68. Capaldo, L.; Bonciolini, S.; Pulcinella, A.; Nuño, M.; Noël, T., Modular allylation of C(sp³)–H bonds by combining decatungstate photocatalysis and HWE olefination in flow. *Chem. Sci.* **2022**, *13* (24), 7325-7331.
69. Wang, Y.-T.; Shih, Y.-L.; Wu, Y.-K.; Ryu, I., Site-Selective C(sp³)–H Alkenylation Using Decatungstate Anion as Photocatalyst. *Adv. Synth. Catal.* **2022**, *364* (5), 1039-1043.
70. Capaldo, L.; Ravelli, D.; Fagnoni, M., Direct Photocatalyzed Hydrogen Atom Transfer (HAT) for Aliphatic C–H Bonds Elaboration. *Chem. Rev.* **2022**, *122* (2), 1875-1924.

71. Golden, D. L.; Suh, S. E.; Stahl, S. S., Radical C(sp³)–H functionalization and cross-coupling reactions. *Nat. Rev. Chem.* **2022**, *6* (6), 405-427.
72. Pulcinella, A.; Mazzarella, D.; Noël, T., Homogeneous catalytic C(sp³)–H functionalization of gaseous alkanes. *Chem. Commun.* **2021**, *57* (78), 9956-9967.
73. Ye, Z. Q.; Lin, Y. M.; Gong, L., The Merger of Photocatalyzed Hydrogen Atom Transfer with Transition Metal Catalysis for C–H Functionalization of Alkanes and Cycloalkanes. *Eur. J. Org. Chem.* **2021**, *2021* (40), 5545-5556.
74. Laudadio, G.; Deng, Y.; van der Wal, K.; Ravelli, D.; Nuño, M.; Fagnoni, M.; Guthrie, D.; Sun, Y.; Noël, T., C(sp³)–H functionalizations of light hydrocarbons using decatungstate photocatalysis in flow. *Science* **2020**, *369* (6499), 92-96.
75. Wang, Y. H.; Yang, Q. M.; Walsh, P. J.; Schelter, E. J., Light-mediated aerobic oxidation of C(sp³)–H bonds by a Ce(IV) hexachloride complex. *Org. Chem. Front.* **2022**, *9* (10), 2612-2620.
76. Gygi, D.; Gonzalez, M. I.; Hwang, S. J.; Xia, K. T.; Qin, Y. Z.; Johnson, E. J.; Gygi, F.; Chen, Y. S.; Nocera, D. G., Capturing the Complete Reaction Profile of a C–H Bond Activation. *J. Am. Chem. Soc.* **2021**, *143* (16), 6060-6064.
77. Troian-Gautier, L.; Turlington, M. D.; Wehlin, S. A. M.; Maurer, A. B.; Brady, M. D.; Swords, W. B.; Meyer, G. J., Halide Photoredox Chemistry. *Chem. Rev.* **2019**, *119* (7), 4628-4683.

78. Shields, B. J.; Doyle, A. G., Direct C(sp³)-H Cross Coupling Enabled by Catalytic Generation of Chlorine Radicals. *J. Am. Chem. Soc.* **2016**, *138* (39), 12719-12722.
79. Li, P.; Deetz, A. M.; Hu, J.; Meyer, G. J.; Hu, K., Chloride Oxidation by One- or Two-Photon Excitation of N-Phenylphenothiazine. *J. Am. Chem. Soc.* **2022**, *144*, 17604–17610.
80. Rohe, S.; Morris, A. O.; McCallum, T.; Barriault, L., Hydrogen Atom Transfer Reactions via Photoredox Catalyzed Chlorine Atom Generation. *Angew. Chem. Int. Ed.* **2018**, *57* (48), 15664-15669.
81. Zidan, M.; Morris, A. O.; McCallum, T.; Barriault, L., The Alkylation and Reduction of Heteroarenes with Alcohols Using Photoredox Catalyzed Hydrogen Atom Transfer via Chlorine Atom Generation. *Eur. J. Org. Chem.* **2020**, *2020* (10), 1453-1458.
82. Ermolenko, L. P.; Delaire, J. A.; Giannotti, C., Laser flash photolysis study of the mechanism of photooxidation of alkanes catalyzed by decatungstate anion. *J. Chem. Soc., Perkin Trans. 2* **1997**, 25-30.
83. McMillan, G.; Wijnen, M. H. J., Reactions of Alkoxy Radicals v. Photolysis of Di-t-butyl peroxide. *Can. J. Chem.* **1958**, *36*, 1227-1232.
84. Brook, J. H. T., Reaction of Hydrocarbons with Tert.-butoxy Radicals. *Trans. Faraday Soc.* **1957**, *53*, 327-332.
85. Luňák, S.; Sedlák, P., Photoinitiated reactions of hydrogen peroxide in the liquid phase. *J. Photochem. Photobiol., A* **1992**, *68* (1), 1-33.

86. St. John, P. C.; Guan, Y.; Kim, Y.; Kim, S.; Paton, R. S., Prediction of organic homolytic bond dissociation enthalpies at near chemical accuracy with sub-second computational cost. *Nat. Commun.* **2020**, *11* (1), 2328.
87. Texier, I.; Delaire, J. A.; Giannotti, C., Reactivity of the charge transfer excited state of sodium decatungstate at the nanosecond time scale. *Phys. Chem. Chem. Phys.* **2000**, *2* (6), 1205-1212.
88. Lei, Y.; Lei, X.; Westerhoff, P.; Zhang, X.; Yang, X., Reactivity of Chlorine Radicals (Cl^\bullet and $\text{Cl}_2^{\bullet-}$) with Dissolved Organic Matter and the Formation of Chlorinated Byproducts. *Environ. Sci. Technol.* **2021**, *55* (1), 689-699.
89. Capaldo, L.; Ravelli, D., Decatungstate as Direct Hydrogen Atom Transfer Photocatalyst for SOMophilic Alkynylation. *Org. Lett.* **2021**, *23* (6), 2243-2247.
90. Tanielian, C., Decatungstate photocatalysis. *Coord. Chem. Rev.* **1998**, *178-180*, 1165-1181.
91. Hill, C. L., Introduction of functionality into unactivated carbon-hydrogen bonds. Catalytic generation and nonconventional utilization of organic radicals. *Synlett* **1995**, (2), 127.
92. Duncan, D. C.; Netzels, T. L.; Hill, C. L., Early-Time Dynamics and Reactivity of Polyoxometalate Excited States. Identification of a Short-Lived LMCT Excited State and a Reactive Long-Lived Charge-Transfer Intermediate following Picosecond Flash Excitation of $[\text{W}_{10}\text{O}_{32}]^{4+}$ in Acetonitrile. *Inorg. Chem.* **1995**, *34* (18), 4640-4646.

93. Ravelli, D.; Dondi, D.; Fagnoni, M.; Albini, A.; Bagno, A., Electronic and EPR spectra of the species involved in $[\text{W}_{10}\text{O}_{32}]^{4-}$ photocatalysis. A relativistic DFT investigation. *Phys. Chem. Chem. Phys.* **2013**, *15* (8), 2890-2896.
94. Duncan, D. C.; Fox, M. A., Early Events in Decatungstate Photocatalyzed Oxidations: A Nanosecond Laser Transient Absorbance Reinvestigation. *J. Phys. Chem. A* **1998**, *102* (24), 4559-4567.
95. Kothe, T.; Martschke, R.; Fischer, H., Photoreactions of the decatungstate anion $\text{W}_{10}\text{O}_{32}^{4-}$ with organic substrates in solution studied by EPR and kinetic absorption spectroscopy: an example for the persistent radical effect. *J. Chem. Soc., Perkin Trans. 2* **1998**, 503-508.
96. Tanielian, C.; Schweitzer, C.; Seghrouchni, R.; Esch, M.; Mechin, R., Polyoxometalate sensitization in mechanistic studies of photochemical reactions: The decatungstate anion as a reference sensitizer for photoinduced free radical oxygenations of organic compounds. *Photochem. Photobiol. Sci.* **2003**, *2* (3), 297-305.
97. Tanielian, C.; Seghrouchni, R.; Schweitzer, C., Decatungstate Photocatalyzed Electron-Transfer Reactions of Alkenes. Interception of the Geminate Radical Ion Pair by Oxygen. *J. Phys. Chem. A* **2003**, *107* (8), 1102-1111.
98. Tanielian, C.; Lykakis, I. N.; Seghrouchni, R.; Cougnon, F.; Orfanopoulos, M., Mechanism of decatungstate photocatalyzed oxygenation of aromatic alcohols: Part I. Continuous photolysis and laser flash photolysis studies. *J. Mol. Catal. A: Chem.* **2007**, *262* (1), 170-175.

99. Tanielian, C.; Duffy, K.; Jones, A., Kinetic and Mechanistic Aspects of Photocatalysis by Polyoxotungstates: A Laser Flash Photolysis, Pulse Radiolysis, and Continuous Photolysis Study. *J. Phys. Chem. B* **1997**, *101* (21), 4276-4282.
100. Texier, I.; Delouis, J. F.; Delaire, J. A.; Giannotti, C.; Plaza, P.; Martin, M. M., Dynamics of the first excited state of the decatungstate anion studied by subpicosecond laser spectroscopy. *Chem. Phys. Lett.* **1999**, *311*, 139-145.
101. Chemseddine, A.; Sanchez, C.; Livage, J.; Launay, J. P.; Fournier, M., Electrochemical and photochemical reduction of decatungstate: a reinvestigation. *Inorg. Chem.* **1984**, *23* (17), 2609-2613.
102. Armstrong, D. A.; Huie, R. E.; Koppenol, W. H.; Lyman, S. V.; Merényi, G.; Neta, P.; Ruscic, B.; Stanbury, D. M.; Steenken, S.; Wardman, P., Standard electrode potentials involving radicals in aqueous solution: inorganic radicals (IUPAC Technical Report). *Pure Appl. Chem.* **2015**, *87* (11-12), 1139-1150.
103. Ilyin, D. V.; Goddard, W. A.; Oppenheim, J. J.; Cheng, T., First-principles-based reaction kinetics from reactive molecular dynamics simulations: Application to hydrogen peroxide decomposition. *Proc. Natl. Acad. Sci. U.S.A.* **2019**, *116* (37), 18202-18208.
104. Kundu, S.; Zanganeh, J.; Moghtaderi, B., A review on understanding explosions from methane-air mixture. *J. Loss Prev. Process Ind.* **2016**, *40*, 507-523.

105. Protti, S.; Ravelli, D.; Fagnoni, M.; Albini, A., Solar light-driven photocatalyzed alkylations. Chemistry on the window ledge. *Chem. Commun.* **2009**, (47), 7351-7353.

2.6 Chapter Appendix

2.6.1 Photochemical Methane Functionalization: Additional General Information

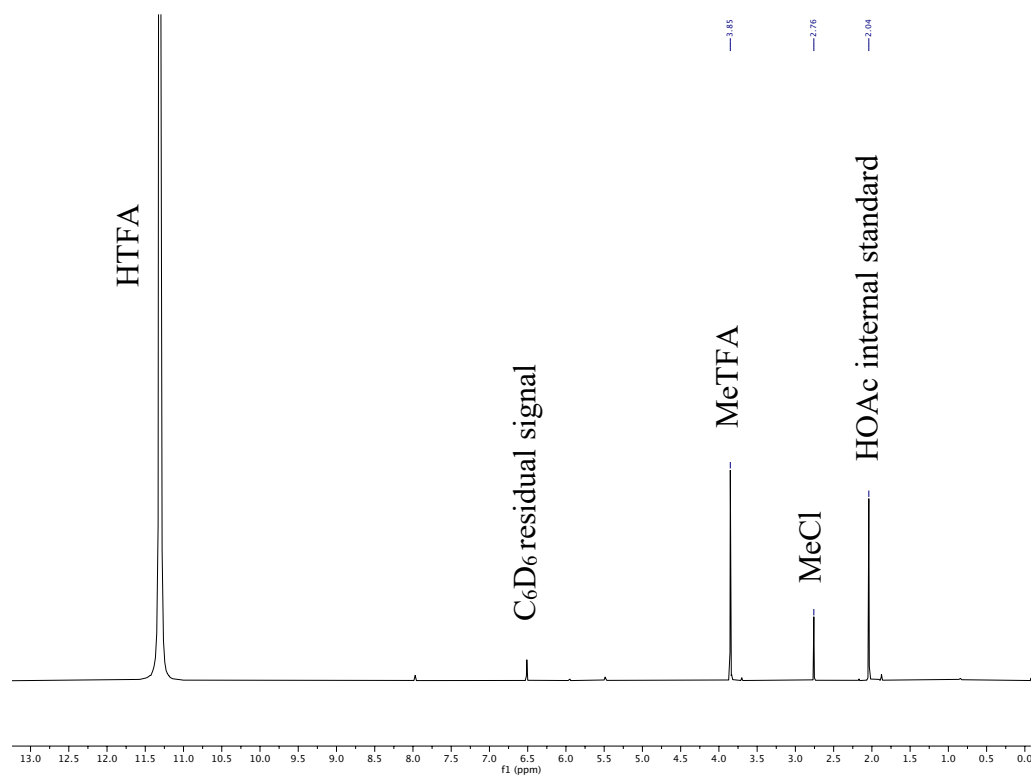


Figure 2.9. Labeled representative ¹H NMR spectrum for photochemical methane functionalization. Either HOAc (shown here) or CH₃NO₂ were used as internal standard, from which product yields were quantified. The small peak at 5.5 ppm may suggest that a small amount of MeCl was further chlorinated.



Figure 2.10. Photograph of a custom-built high pressure reaction vessel used for photolytic reactions.

2.6.2 Re-Oxidation with Dioxygen

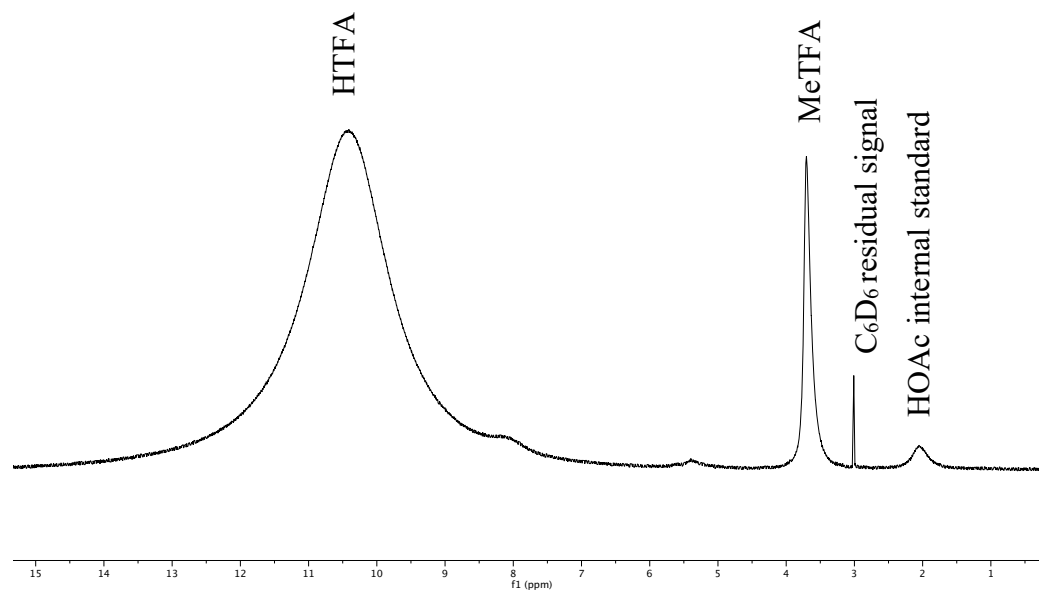


Figure 2.11. Labeled representative ^1H NMR spectrum for re-oxidation experiments with dioxygen in which signal broadening prevents the ability to detect or measure MeCl formation.

2.6.3 Screening of Solids as *In Situ* Co-Oxidants

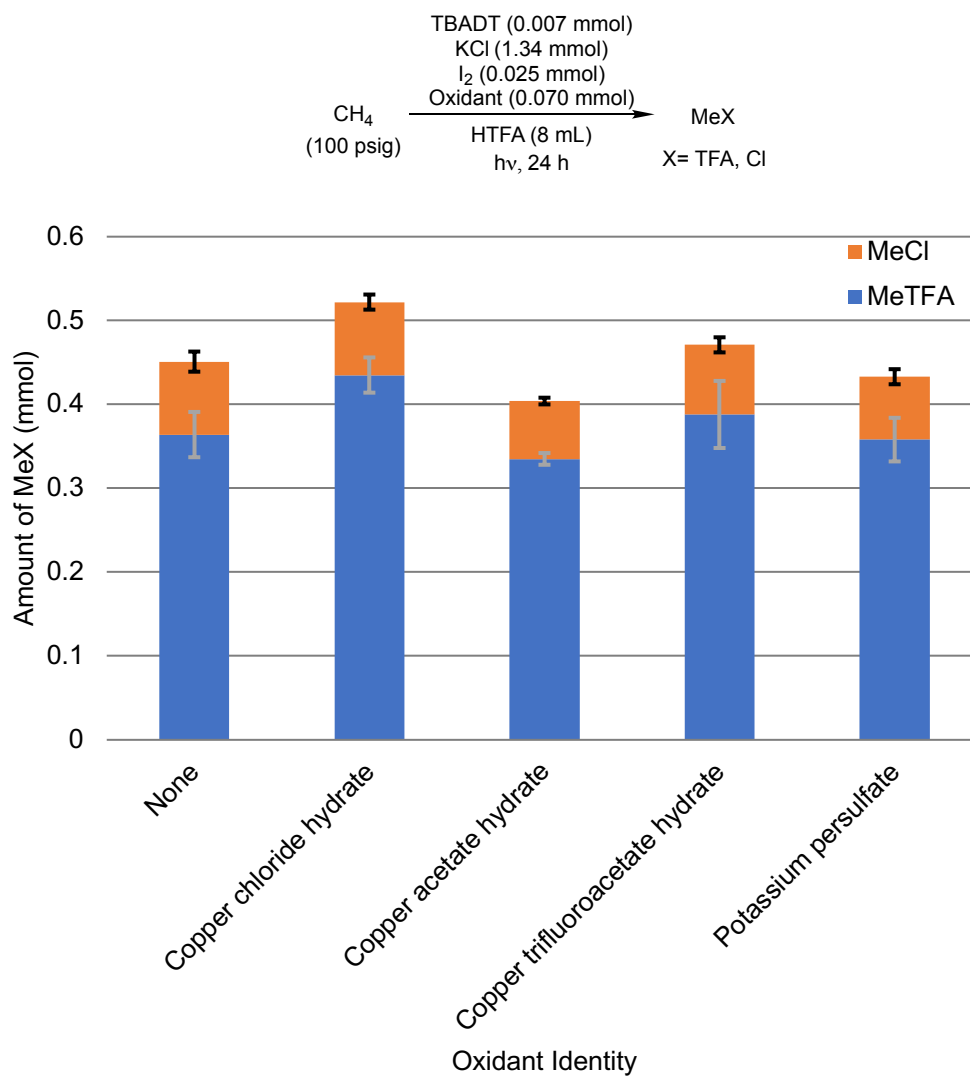


Figure 2.12. Comparison of the amount of MeX (X = TFA, Cl) produced as a method to screen substrates to serve as *in situ* oxidants for the re-oxidation of TBADT under standard aerobic reaction conditions. Each bar graph represents the average of at least three independent experiments with error bars depicting the standard deviations.

2.6.4 Screening of Peroxides as *In Situ* Co-Oxidants

Anaerobic (*i.e.*, dinitrogen-purged), but otherwise standard, reaction conditions were used to probe the ability of alkyl peroxides to serve as *in situ* oxidants for the re-oxidation of TBADT. The addition of ten equivalents of either di-tert-butyl peroxide (DTBP) or tert-butyl hydroperoxide (tBuOOH) relative to TBADT led to a decrease in MeX (X = TFA, Cl) production (Table 2.2, Entries 3 and 4) compared to the reaction without alkyl peroxide addition (Table 2.2, Entry 1).

When the loading of tBuOOH was increased an additional ten-fold, both TBADT TOs and MeX yield increased (Table 2.2, Entry 5). The reaction with 100 equivalents of tBuOOH reflects the highest peroxide loading that can be used while maintaining an environment that falls safely within the pressure limitations of the reaction vessel. This threshold was determined by considering the reaction of each equivalent of added peroxide with one equivalent of HTFA to produce one equivalent of CO₂. Thus, in order to explore reactions with a higher excess of peroxide, the amount of methane was decreased to 15 psig (Table 2.2, Entry 6). The reaction with 15 psig methane and 100 equivalents of tBuOOH resulted in the same TOs, within standard deviation, but MeX yield was increased substantially.

When tBuOOH loading was increased to 1,000 equivalents, > 100% MeX yield was observed (Table 2.2, Entry 7). This > 100% yield alerted us to the likelihood that methyl radical was being formed from a source other than methane under these conditions. The explanation for this additional methyl radical source was located in previous studies in which DTBP was shown to undergo photo-

decomposition to form methyl radical.^{1,2} First, tert-butoxy radical is likely formed from photo-induced O–O bond cleavage of the peroxide. The unstable tert-butoxy radical then decomposes to form acetone and methyl radical. In our case, the data for the reactions with peroxide addition are in agreement with this route of photodecomposition as a resonance in the ¹H NMR spectra at 2.25 ppm is present and was confirmed to be acetone.

When analogous conditions to Entry 6 were used, but with H₂O₂ as the peroxide, which is unable to generate methyl radicals, no improvement of MeX yield (within standard deviation) was observed (Table 2.2, Entry 8) relative to the high methane conversion aerobic reaction (Table 2.2, Entry 2).

Interestingly, all of the reactions with peroxides increased selectivity towards MeTFA. The reactions with peroxide addition, however, all suffered from large standard deviations.

Table 2.2. Screening of peroxides to serve as *in situ* oxidants for the re-oxidation of TBADT.^a

$$\text{CH}_4 \xrightarrow[\text{HTFA (8 mL)}]{\begin{array}{c} \text{TBADT (0.007 mmol)} \\ \text{KCl (1.34 mmol)} \\ \text{I}_2 (0.025 \text{ mmol}) \\ \text{Peroxide} \end{array}} \text{MeX}$$

hv, 24 h X= TFA, Cl

Entry	Peroxide identity	Equivalents of peroxide (relative to TBADT)	Methane pressure (psig)	TOs of MeX (X = TFA, Cl) ^b	% Yield of MeX (X = TFA, Cl) ^c	Molar ratio of MeTFA: MeCl
1	None	N/A	100	64 ± 4.3	1.9 ± 0.078	4.2:1
2	None	N/A	15	50 ± 0.82	8.9 ± 0.58	6.4:1
3	DTBP	10	100	20 ± 8.7	0.60 ± 0.24	35:1
4	tBuOOH	10	100	13 ± 6.2	0.39 ± 0.20	22:1
5	tBuOOH	100	100	160 ± 22	4.7 ± 0.53	280:1
6	tBuOOH	100	15	150 ± 23	39 ± 10	MeTFA exclusively
7	tBuOOH	1,000	15	660 ± 67	120 ± 12	69:1
8	H ₂ O ₂	1,000	15	66 ± 25	13 ± 6.5	22:1

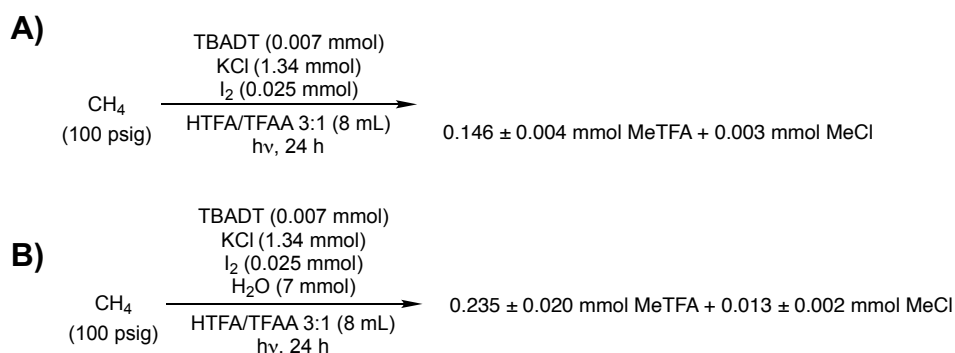
^a Reaction conditions: 0.007 mmol TBADT, 1.34 mmol KCl, and 0.025 mmol I₂, 8 mL HTFA, N₂ purge, pressurized with CH₄, and 24 h of Hg lamp irradiation. Each entry line represents the average of at least three independent experiments reported with their standard deviations; ^b TOs are calculated with respect to TBADT; ^c Percent yields are calculated with respect to methane.

2.6.5 Reactions with Trifluoroacetic Anhydride

In our study of reaction tolerance to water, it was found that water should be considered as a potential detriment in reactions for which TBADT TOs exceed ~1,000. Experiments were performed in which trifluoroacetic anhydride (TFAA) was added at the start of the reaction in an effort to remove *in situ* formed water. When the solvent composition was changed from HTFA to a 3:1 mixture of HTFA to TFAA under otherwise identical standard aerobic reaction conditions, the

production of MeX was hindered (Scheme 2.7A). When standard aerobic reaction conditions were used in a 3:1 solvent mixture of HTFA to TFAA and then charged with 7.0 mmol of water (1,000 equivalents relative to TBADT) before pressurization of methane, the production of MeX was hindered to a lesser extent (Scheme 2.7B). Due to the hinderance on MeX production, the addition of TFAA does not appear to be an effective strategy to remove *in situ* generated water.

Scheme 2.7. Modification of standard aerobic reaction conditions to include a mixture of HTFA and TFAA as reaction solvent, without (A) and with (B) added water, led to decreased MeX (X = TFA, Cl) production. Each reaction scheme represents the average of at least three independent experiments reported with their standard deviations.



2.6.6 Background Reaction of Potassium Chloride and Iodine

Chlorine radicals are known to activate C–H bonds.³ Thus, the reaction of KCl and I₂ in the absence of TBADT was investigated. As noted in the main text, preliminary screening of these reagents (1.34 mmol KCl, 0.050 mmol I₂) in 8 mL HTFA with 100 psig methane led to no MeX (X = TFA, Cl) formation within standard deviation (Table 2.1, Entry 4). However, when the loading of I₂ was halved

but all other conditions remained identical, 0.52 ± 0.06 mmol of MeX (X = TFA, Cl) was produced in $2.1 \pm 0.27\%$ yield with a 3.9:1 ratio of MeTFA to MeCl after 24 h of subjection to a mercury arc lamp. After obtaining these results, we wanted to investigate in more detail the ability of this background reaction to perform methane functionalization.

A kinetic study was performed with 1.34 mmol of KCl and 0.025 mmol of I_2 in order to compare with the kinetic study using standard aerobic reaction conditions. The results from these 94 methane functionalization reactions, plotted as averages with standard deviations for each timepoint, are depicted in Figure 2.13. We observed experiments resulting in substantial MeX formation alongside experiments resulting in little to no MeX formation. Figure 2.14 and Table 2.3 contain the breakdown of each individual reaction, rather than the report of averages with standard deviations. The inconsistent results likely indicate that radical chain processes for MeX formation are possible, but the success of such reactions is highly dependent on factors that we could not identify nor control.

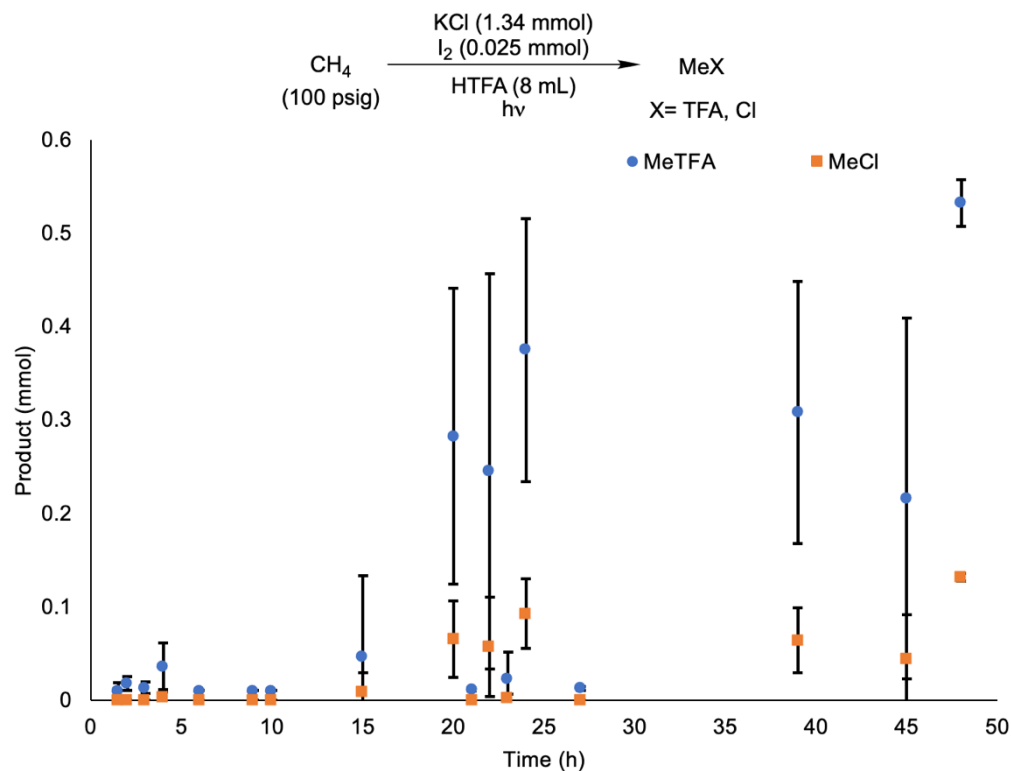


Figure 2.13. Photochemical methane functionalization under standard aerobic reaction conditions in the absence of TBADT as a function of time. Each data point represents the average of at least three independent experiments with error bars depicting the standard deviation of the three experiments.

	0.019	0
3	0.011	0
	0.011	0
	0.011	0
	0.011	0
	0.011	0
	0.026	0
4	0.041	0.004
	0.011	0
	0.011	0
	0.067	0.011
	0.05	0.007
6	0.011	0
	0.01	0
	0.011	0
	0.011	0
	0.011	0
	0.011	0
9	0.011	0
	0.011	0
	0.011	0
10	0.011	0
	0.011	0
	0.011	0
15	0.011	0
	0.224	0.052
	0.015	0
	0.011	0
	0.011	0
	0.011	0
20	0.011	0
	0.172	0.030
	0.381	0.093
	0.351	0.086
	0.411	0.097
	0.374	0.090
	0.011	0
	0.011	0
	0.011	0

21	0.011	0
	0.011	0
	0.015	0
	0.011	0
	0.015	0
	0.011	0
22	0.396	0.101
	0.430	0.105
	0.374	0.082
	0.019	0
	0.011	0
23	0.011	0
	0.011	0
	0.011	0
	0.041	0.004
	0.093	0.015
	0.011	0
	0.011	0
	0.015	0
	0.011	0
24	0.462	0.122
	0.392	0.087
	0.409	0.091
	0.400	0.105
	0.456	0.116
	0.015	0
	0.366	0.097
	0.486	0.123
	0.396	0.097
27	0.011	0
	0.015	0
	0.015	0
	0.011	0
	0.015	0
	0.011	0
39	0.220	0.045
	0.471	0.105
	0.235	0.045
	0.138	0.026

45	0.489	0.123
	0.011	0
	0.284	0.056
	0.019	0
	0.359	0.063
48	0.527	0.134
	0.512	0.127
	0.560	0.134

2.6.7 Additional Calculations: Alternative Pathways

Our mechanism suggests a radical pool containing I•, Cl• and CH₃• species. It is plausible that these radicals react according to our proposed mechanism; however, it is likely that the radicals also react in other undesired paths that could inhibit the desired methane oxidation chemistry. Consequently, we explored other mechanisms that could potentially occur through our radical species.

Given the presence of radical chlorine species, we sought out alternative paths in which Cl• could potentially react to give either the desired products or towards undesired byproducts. When Cl• is present in solution, one plausible reaction step is direct chlorination of methane to produce MeCl and H• according to the following reaction: $\text{CH}_4 + \text{Cl}^* \rightarrow \text{MeCl} + \text{H}^\bullet$. We evaluated direct chlorination and found the reaction to be uphill 21.5 kcal/mol with a transition state energy of 31.9 kcal/mol. Since this reaction step is substantially uphill with a large barrier to surmount, it is not likely to occur in solution.

Another feasible reaction is of Cl• with MeI to afford MeCl and leave I• according to: $\text{MeI} + \text{Cl}^\bullet \rightarrow \text{MeCl} + \text{I}^\bullet$. Chlorination of MeI is downhill -12.7 kcal/mol with a transition state free energy of 32.6 kcal/mol. The C–Cl bond in MeCl is far

stronger than the C–I bond in MeI, and I• makes a much better leaving group than Cl•, so this reaction is exergonic. However, the barrier is quite high, so we consider this step unlikely to occur. We predict that when chlorine and iodine are used simultaneously in catalysis, the two species compete for alkyl radical trapping. Once trapped, the alkyl halides cannot interconvert due to this large barrier (*i.e.*, MeI→MeCl or vice-versa).

Given the overwhelming presence of HTFA, we considered the possibility of HAT between a solvent HTFA and DT•• to form TFA•. DFT predicts that this HAT requires a barrier of 12.5 kcal/mol and is downhill -2.1 kcal/mol. This barrier is relatively large, such that we do not expect this reaction to occur. This agrees with previous experimental observations that claimed HTFA does not undergo HAT due to polarity mismatch with DT.

2.6.8 Chapter Appendix References

1. Brook, J. H. T., Reaction of Hydrocarbons with Tert.-butoxy Radicals. *Trans. Faraday Soc.* **1957**, *53*, 327-332.
2. Garnett McMillan, M. H. J. W., Reactions of Alkoxy Radicals v. Photolysis of Di-t-butyl peroxide. *Can. J. Chem.* **1958**, *36*, 1227-1232.
3. Gonzalez, M. I.; Gygi, D.; Qin, Y.; Zhu, Q.; Johnson, E. J.; Chen, Y.-S.; Nocera, D. G., Taming the Chlorine Radical: Enforcing Steric Control over Chlorine-Radical-Mediated C–H Activation. *J. Am. Chem. Soc.* **2022**, *144* (3), 1464-1472.

3 Extension of the Photo-OxE Process to Oxidants other than Decatungstate

3.1 Introduction

Previous work by our group has shown that the photo-oxyesterification (photo-OxE) process functions using iodine oxides,¹ iron salts,² and high valent manganese complexes³ in addition to use of decatungstate as a photocatalyst (see Chapter 2). With motivation to expand the scope of traditional oxidants capable of facilitating the selective, partial oxidation of light alkanes via the photo-OxE process, several compounds were screened for possible photo-driven methane oxidation.

Copper(II) salts serve as oxidants in Wacker-type olefin oxidation chemistry.⁴ Since the discovery of the Wacker process for the Pd-catalyzed conversion of ethylene to acetaldehyde using copper(II) chloride,⁵ other copper(II) salts, such as copper(II) acetate, have been employed in Wacker-type oxidations.⁴ Through the Wacker process, it was discovered that Cu(II) can be recycled from Cu(I) and acid with unpurified air in addition to pure dioxygen.^{6,7} Our group has used copper(II) salts, namely copper(II) carboxylates, as oxidants for catalytic arene alkenylation chemistry.⁸⁻¹² For these reasons, a series of copper(II) salts was screened for methane oxidation using our photo-OxE reaction conditions.

Our group recently reported manganese oxides and manganese salts in thermal OxE processes for alkane partial oxidation.¹³ We were interested in whether these manganese oxides and manganese salts could be extended for use as oxidants in a photo-OxE process. Previous efforts by our group showed that manganese(IV) dioxide was effective for photo-OxE, leading to interest in whether

this could be extended to manganese oxides in additional oxidation states and/or to manganese salts. This Chapter describes efforts regarding copper(II) and manganese sources as candidates for use in photo-OxE processes.

3.2 Attempted Extension of the Photo-OxE Process to Copper(II) Oxidants

A series of commercial, air-stable copper(II) salts (*i.e.*, $\text{CuCl}_2 \cdot x\text{H}_2\text{O}$, $\text{Cu}(\text{OAc})_2 \cdot x\text{H}_2\text{O}$ ($\text{OAc} = \text{CH}_3\text{CO}_2^-$), $\text{Cu}(\text{TFA})_2 \cdot x\text{H}_2\text{O}$), were investigated with and without additives (*i.e.*, KCl , I_2) for the aerobic photo-oxidation of methane. The abilities of the Cu(II) salts to functionalize methane were compared to the analogous functionalization reactions of KCl and I_2 in the absence of Cu(II) salts.

The screening of copper(II) chloride hydrate ($\text{CuCl}_2 \cdot x\text{H}_2\text{O}$) for methane functionalization is shown in Figure 3.1, wherein MeX ($\text{X} = \text{TFA}, \text{Cl}$) yield is plotted against the combination of additives. The oxidation of methane using $\text{CuCl}_2 \cdot x\text{H}_2\text{O}$ alone and $\text{CuCl}_2 \cdot x\text{H}_2\text{O}$ with KCl and I_2 led to variable MeX production with large standard deviations. The reaction using $\text{CuCl}_2 \cdot x\text{H}_2\text{O}$ with KCl led to higher MeX yield than the corresponding reaction using only KCl (Figure 3.2). The reaction of 0.042 mmol $\text{CuCl}_2 \cdot x\text{H}_2\text{O}$ with 0.67 mmol KCl produced MeX in $0.62 \pm 0.084\%$ yield with respect to methane and 3.7 ± 0.47 TOs of $\text{CuCl}_2 \cdot x\text{H}_2\text{O}$. The control reaction using $\text{CuCl}_2 \cdot x\text{H}_2\text{O}$ with KCl was performed under thermal conditions. Heating 0.042 mmol $\text{CuCl}_2 \cdot x\text{H}_2\text{O}$ and 0.67 mmol KCl in 8 mL HTFA with 100 psig CH_4 at 180 °C for 3 h resulted in the formation of MeTFA in $0.084 \pm 0.032\%$ yield and MeCl in $0.051 \pm 0.051\%$ yield. $\text{CuCl}_2 \cdot x\text{H}_2\text{O}$ suffered from solubility challenges in HTFA both prior to and following irradiation, so our focus was shifted to explore other copper(II) salts.

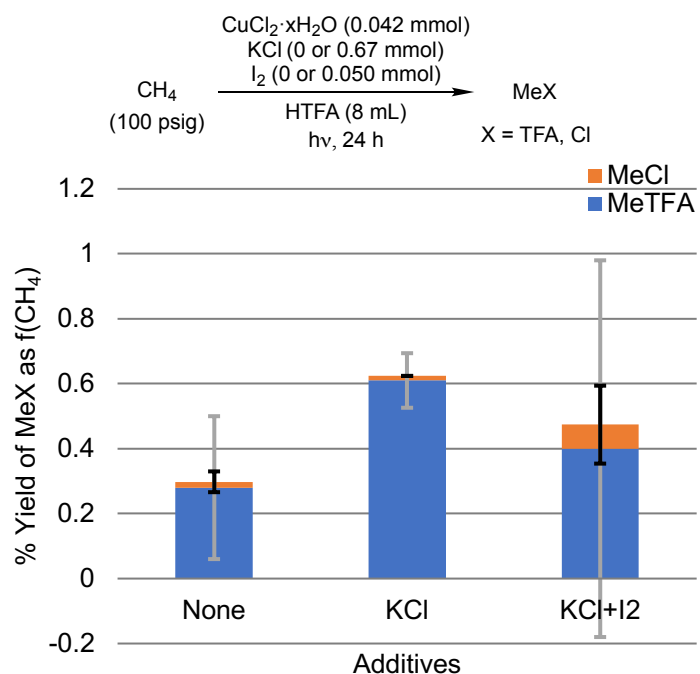


Figure 3.1. Screening of $\text{CuCl}_2 \cdot x\text{H}_2\text{O}$ with and without additives for the photochemical functionalization of methane in HTFA after 24 h of irradiation with a mercury arc lamp. MeX (X = TFA, Cl) production is plotted as yield with respect to methane. Each bar graph represents the average of at least three independent experiments with error bars depicting the standard deviations.

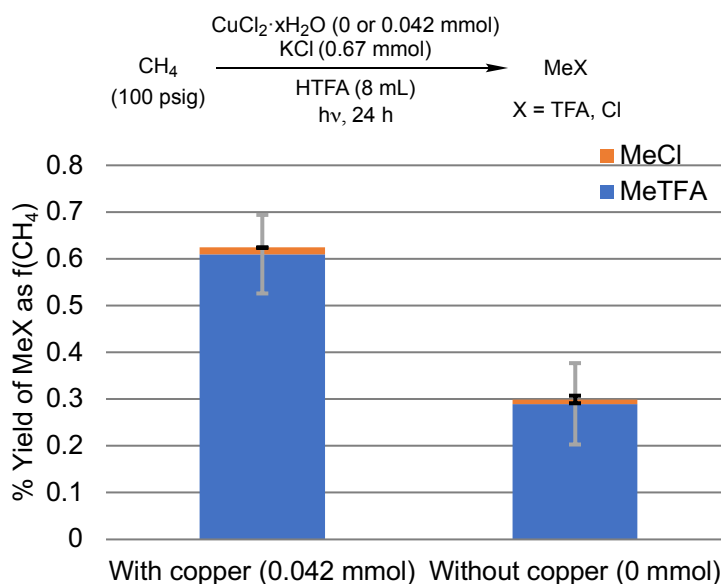


Figure 3.2. Comparison of reactions with and without $\text{CuCl}_2 \cdot x\text{H}_2\text{O}$ for the photochemical functionalization of methane using KCl in HTFA after 24 h of irradiation with a mercury arc lamp. MeX (X = TFA, Cl) production is plotted as

yield with respect to methane. Each bar graph represents the average of at least three independent experiments with error bars depicting the standard deviations.

Copper(II) acetate hydrate ($\text{Cu}(\text{OAc})_2 \cdot x\text{H}_2\text{O}$) was similarly screened for aerobic photo-driven methane functionalization with and without KCl and I_2 additives (Figure 3.3). $\text{Cu}(\text{OAc})_2 \cdot x\text{H}_2\text{O}$ alone was not capable of functionalizing methane. The reaction of $\text{Cu}(\text{OAc})_2 \cdot x\text{H}_2\text{O}$ with KCl showed no improved yield over the analogous reaction in the absence of copper(II) salt (see “Without copper” in Figure 3.2). Here, the addition of both KCl and I_2 led to MeX production with $1.7 \pm 0.27\%$ yield with respect to methane and 9.6 ± 1.6 TOs of $\text{Cu}(\text{OAc})_2 \cdot x\text{H}_2\text{O}$. Excited by these results, further screening was performed to determine the effect of varying the additive loadings relative to $\text{Cu}(\text{OAc})_2 \cdot x\text{H}_2\text{O}$.

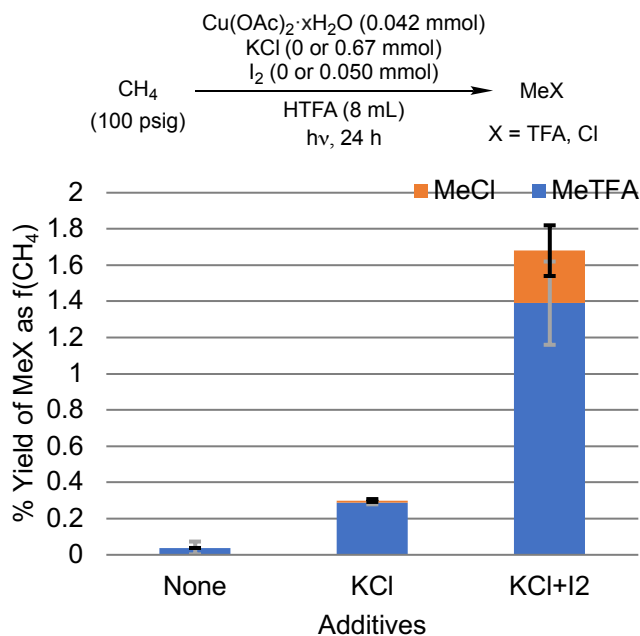


Figure 3.3. Screening of $\text{Cu}(\text{OAc})_2 \cdot x\text{H}_2\text{O}$ with and without additives for the photochemical functionalization of methane in HTFA after 24 h of irradiation with a mercury arc lamp. MeX (X = TFA, Cl) production is plotted as yield with respect

to methane. Each bar graph represents the average of at least three independent experiments with error bars depicting the standard deviations.

When the loading of KCl was doubled to 1.34 mmol for the reaction of $\text{Cu}(\text{OAc})_2 \cdot x\text{H}_2\text{O}$ and KCl, methane was selectively functionalized to MeTFA, albeit with lower yield and higher standard deviation (Figure 3.4). When the loading of KCl was decreased to 0.15 mmol, undesired decarboxylation of the HTFA solvent was observed as indicated by the presence of CF_3H in ^1H NMR spectra. From these experiments, the preferable loading of KCl was identified as 0.67 mmol. Using 0.67 mmol of KCl, the amount of iodine was varied for the reaction using $\text{Cu}(\text{OAc})_2 \cdot x\text{H}_2\text{O}$ with both KCl and I_2 (Figure 3.5). Doubling the loading of I_2 to 0.10 mmol yielded no MeX within standard deviation. Thus, the optimized conditions for methane functionalization using 0.042 mmol $\text{Cu}(\text{OAc})_2 \cdot x\text{H}_2\text{O}$ were determined as 0.67 mmol KCl and 0.05 mmol I_2 .

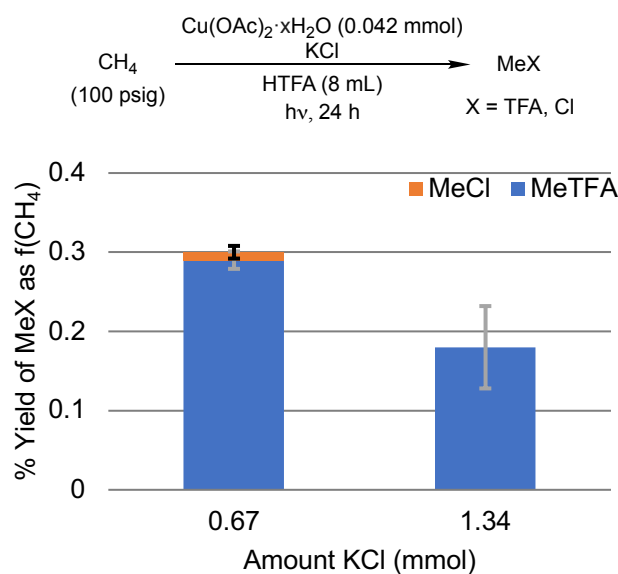


Figure 3.4. Variation of KCl loading for the photochemical functionalization of methane using $\text{Cu}(\text{OAc})_2 \cdot x\text{H}_2\text{O}$ in HTFA after 24 h of irradiation with a mercury

arc lamp. MeX (X = TFA, Cl) production is plotted as yield with respect to methane. Each bar graph represents the average of at least three independent experiments with error bars depicting the standard deviations.

Copper(II) trifluoroacetate hydrate ($\text{Cu}(\text{TFA})_2 \cdot x\text{H}_2\text{O}$) was preliminarily screened for the aerobic photo-oxidation of methane. After 24 h of irradiation of 0.05 mmol $\text{Cu}(\text{TFA})_2 \cdot x\text{H}_2\text{O}$, 0.67 mmol KCl, and 0.05 mmol I_2 in 8 mL HTFA pressurized with 100 psig CH_4 , MeTFA was formed in $0.94 \pm 1.3\%$ yield and MeCl in $0.18 \pm 0.25\%$ yield. Because no MeX was formed within deviation along with the standard deviations being larger than the MeX yields values themselves, the screening of $\text{Cu}(\text{TFA})_2 \cdot x\text{H}_2\text{O}$ was not pursued further.

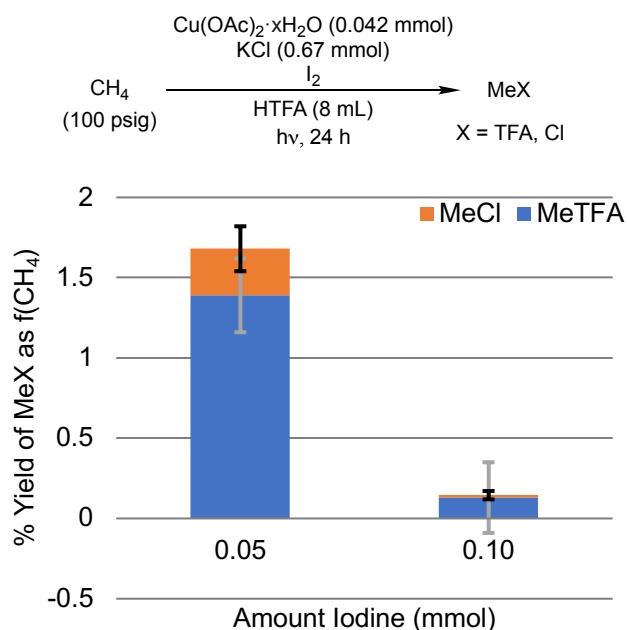


Figure 3.5. Variation of I_2 loading for the photochemical functionalization of methane using $\text{Cu}(\text{OAc})_2 \cdot x\text{H}_2\text{O}$ and KCl in HTFA after 24 h of irradiation with a mercury arc lamp. MeX (X = TFA, Cl) production is plotted as yield with respect to methane. Each bar graph represents the average of at least three independent experiments with error bars depicting the standard deviations.

3.3 Extension of the Photo-OxE Process to Manganese Oxidants

In our investigation of manganese oxides for use in the thermal OxE process, it was found that Mn^{IV} , Mn^{III} , and $\text{Mn}^{\text{II,III}}$ oxides are active for methane oxidation to MeTFA in HTFA, but Mn^{II} oxides are not.¹³ Additive screening with MnO_2 exhibited that neither KCl nor I_2 are required for thermal methane oxidation, but increased yield (~60% based on Mn) occurs in the presence of I_2 . The presence or absence of KCl did not have an effect on thermal methane oxidation using MnO_2 . It is proposed that, in this manganese chemistry, I_2 serves to convert heterogeneous MnO_2 into a soluble form, which is supported by the fact that the initial induction period that occurs for methane functionalization in the presence of MnO_2 in the absence of I_2 in HTFA is not present for the same reaction in the presence of I_2 .

Product analysis via ^1H NMR spectroscopy using manganese oxides for oxidation reactions in HTFA is difficult due to significant resonance broadening from paramagnetic, reduced manganese species. It was found that a work-up procedure involving the addition of NaBiO_3 to the spent product mixtures served to oxidize the reduced manganese species and, therefore, minimized resonance broadening in ^1H NMR spectra.³ This work-up procedure was used for all reactions using manganese oxides (*i.e.*, MnO_2 , MnO) described herein.

MnO_2 was examined under photo-driven conditions and it was found that, unlike under thermal conditions, both KCl and I_2 have an effect on the extent of aerobic methane functionalization. With MnO_2 and either KCl or I_2 , MeTFA is produced in ~10% yield with respect to MnO_2 . When both KCl and I_2 are added,

the yield of MeTFA is increased to $94 \pm 8.8\%$ with respect to MnO_2 , which corresponds to $4.1 \pm 0.48\%$ yield with respect to methane (Figure 3.6).

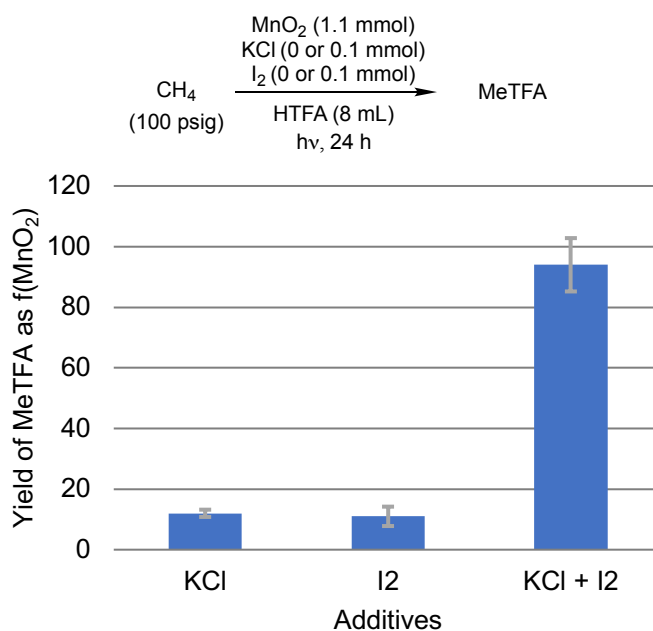


Figure 3.6. Screening of additives for the photochemical functionalization of methane using MnO_2 in HTFA after 24 h of irradiation with a mercury arc lamp. MeTFA is plotted as percent yield with respect to MnO_2 . Each bar graph represents the average of at least three independent experiments with error bars depicting the standard deviations. Adapted from reference.³

A preliminary screening reaction of MnO for aerobic photo-driven methane functionalization was similarly carried out using 1.1 mmol MnO , 0.1 mmol KCl and 0.1 mmol I_2 . After 24 h of photolysis in HTFA, MeTFA was produced in $25 \pm 2.1\%$ yield with respect to MnO and $1.1 \pm 0.064\%$ yield with respect to methane. From there, various loadings of iodine, including the reaction in the absence of iodine, were tested under otherwise identical conditions (Figure 3.7). The presence of iodine was shown to have an important effect on MeX (X = TFA, Cl) production. In the absence of iodine, MeX was produced in $< 5\%$ yield based on MnO . Within deviation, the loading of iodine had little effect on MeX production, both as a

function of MnO and as a function of methane. However, at the loading of 0.10 mmol I₂, MeTFA was produced selectively over MeCl.

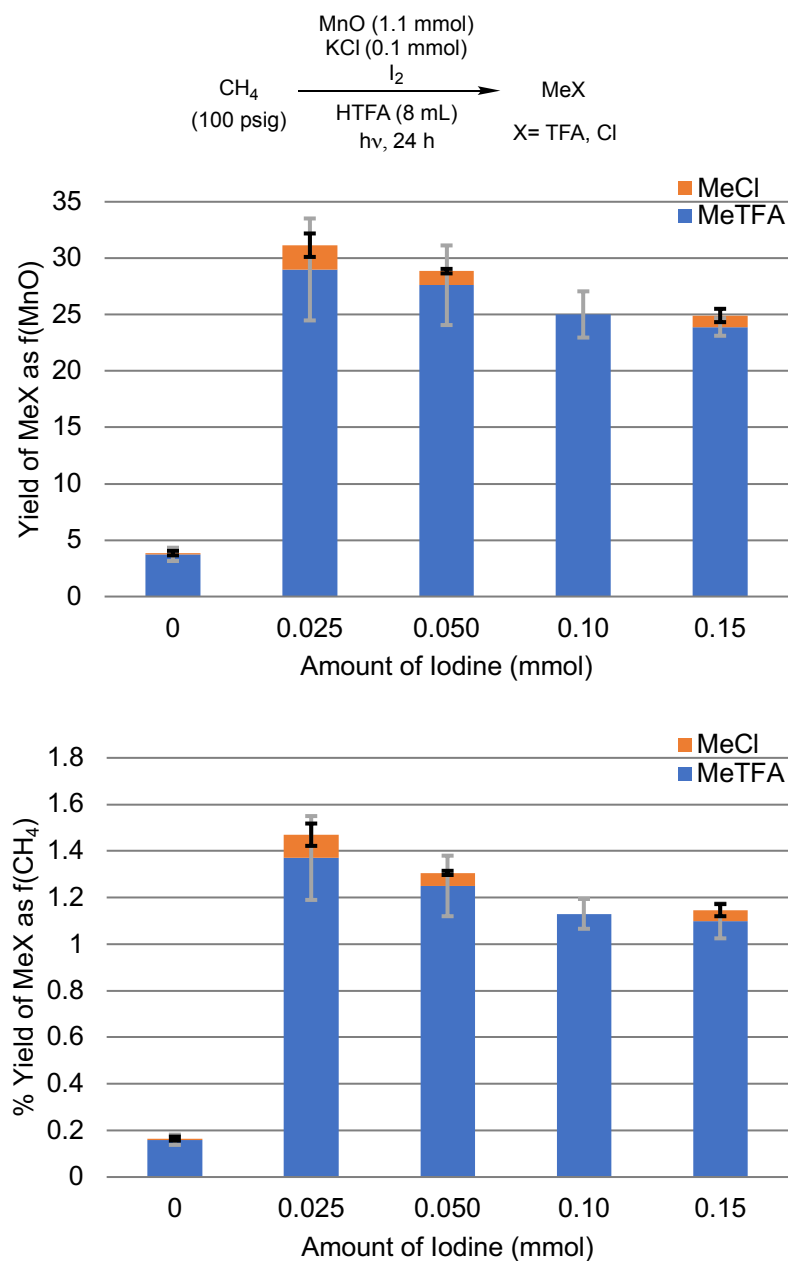


Figure 3.7. Variation of iodine loading for the photochemical functionalization of methane using MnO and KCl in HTFA after 24 h of irradiation with a mercury arc lamp. MeX (X = TFA, Cl) is plotted as percent yield with respect to MnO (top) and as percent yield with respect to methane (bottom). Each bar graph represents the

average of at least three independent experiments with error bars depicting the standard deviations.

In our previous thermal investigation, a bimetallic trifluoroacetate manganese(II) salt, $\text{Mn}_2(\text{HTFA})_4(\mu\text{-TFA})_2(\text{TFA})_2$ was explored for methane oxidation (Figure 3.8).¹³ Catalytic turnover was achieved for methane oxidation using MnO_2 (Scheme 3.1A) and $\text{Mn}_2(\text{HTFA})_4(\mu\text{-TFA})_2(\text{TFA})_2$ (Scheme 3.1B) when a dioxygen atmosphere was used and trifluoroacetic anhydride (TFAA) was present. In an effort to achieve catalytic turnover using $\text{Mn}_2(\text{HTFA})_4(\mu\text{-TFA})_2(\text{TFA})_2$ via our photo-driven process, similar reaction conditions were tested. Photolysis of 0.007 mmol $\text{Mn}_2(\text{HTFA})_4(\mu\text{-TFA})_2(\text{TFA})_2$ under a dioxygen atmosphere in a HTFA/TFAA solvent mixture for 24 h produced MeTFA with ~3 TOs per Mn atom or ~6 TOs per Mn dimer (Scheme 3.2A). In an analogous experiment where the loading of $\text{Mn}_2(\text{HTFA})_4(\mu\text{-TFA})_2(\text{TFA})_2$ was tripled to 0.021 mmol, MeTFA production was reduced to stoichiometric yield (~65%) as a function of Mn atom and ~1.3 TOs as a function of Mn dimer (Scheme 3.2B).

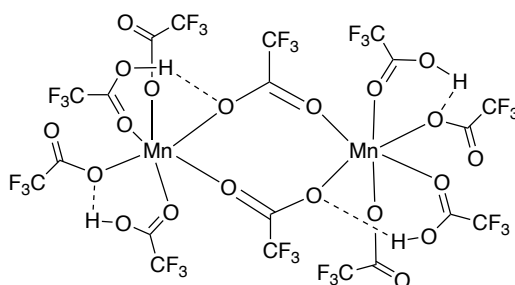
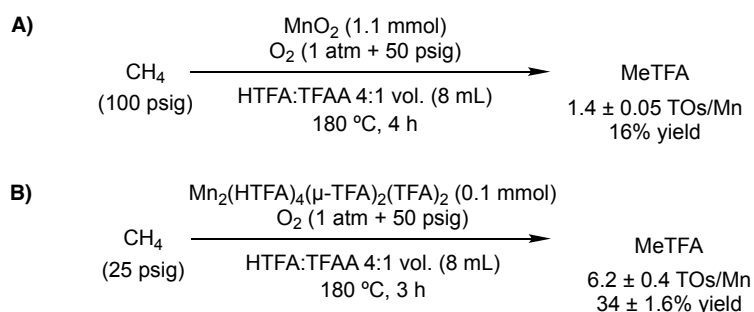


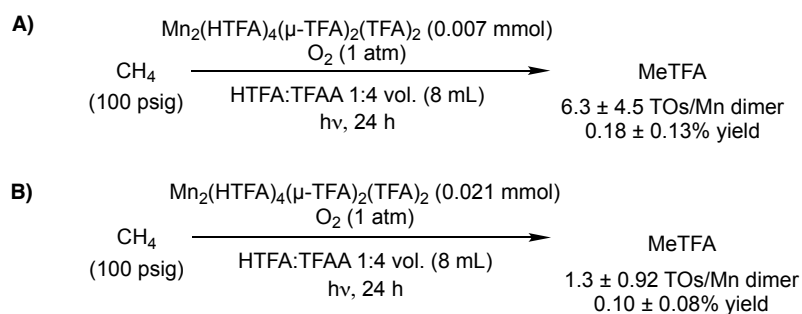
Figure 3.8. Structure of $\text{Mn}_2(\text{HTFA})_4(\mu\text{-TFA})_2(\text{TFA})_2$. Adapted from reference.¹⁴

Scheme 3.1. Reactions for which the addition of TFAA enables catalytic turnover using Mn sources for thermal methane oxidation in the presence of O₂.^a Mn source = MnO₂ (A), Mn₂(HTFA)₄(μ-TFA)₂(TFA)₂ (B). Adapted from reference.¹³



^a MeTFA production is reported as the average of at least three independent experiments with standard deviations.

Scheme 3.2. Reactions for which the addition of TFAA enables catalytic turnover using Mn₂(HTFA)₄(μ-TFA)₂(TFA)₂ for photochemical methane oxidation in the presence of O₂.^a



^a MeTFA production is reported as the average of at least three independent experiments with standard deviations.

3.4 Conclusions and Future Directions

This Chapter presents preliminary studies of Cu(II) and Mn oxidants as candidates for use in our photo-OxE process for methane functionalization. Mn oxidants had previously been studied for our thermal OxE process.¹³ For CuCl₂·xH₂O, the highest MeX (X = TFA, Cl) yield in HTFA was achieved in the presence of KCl. Twenty-four hours of photolysis of a HTFA mixture of 0.042 mmol CuCl₂·xH₂O and 0.67 mmol KCl with 100 psig CH₄ produced MeX in 0.62

$\pm 0.084\%$ yield with respect to methane and 3.7 ± 0.47 TOs of $\text{CuCl}_2 \cdot x\text{H}_2\text{O}$. For $\text{Cu}(\text{OAc})_2 \cdot x\text{H}_2\text{O}$, the highest MeX (X = TFA, Cl) yield in HTFA was achieved in the presence of KCl and I_2 . Twenty-four hours of photolysis of a HTFA mixture of 0.042 mmol $\text{CuCl}_2 \cdot x\text{H}_2\text{O}$, 0.67 mmol KCl, and 0.05 mmol I_2 with 100 psig CH_4 produced MeX in $1.7 \pm 0.27\%$ yield with respect to methane and 9.6 ± 1.6 TOs of $\text{Cu}(\text{OAc})_2 \cdot x\text{H}_2\text{O}$. In a preliminary series of reactions, $\text{Cu}(\text{TFA})_2 \cdot x\text{H}_2\text{O}$ with addition of KCl and I_2 was shown to be an ineffective system for methane functionalization in HTFA.

The ability of MnO_2 to perform photo-driven methane oxidation was extended to MnO; however, lower yields were observed with Mn^{II} compared to Mn^{IV} . Twenty-four hours of photolysis of a HTFA mixture of 1.1 mmol MnO_2 , 0.1 mmol KCl, and 0.1 mmol I_2 with 100 psig CH_4 produced MeX in $94 \pm 8.8\%$ with respect to MnO_2 and $4.1 \pm 0.48\%$ yield with respect to methane. Twenty-four hours of photolysis of a HTFA mixture of 1.1 mmol MnO, 0.1 mmol KCl, and 0.1 mmol I_2 with 100 psig CH_4 produced MeX in $25 \pm 2.1\%$ yield with respect to MnO and $1.1 \pm 0.064\%$ yield with respect to methane.

Unimpressive reactivity of the Cu(II) and Mn oxidants prevented their further study towards application in our photo-OxE process. The copper(II) complexes showed little-to-no improvement over analogous aerobic photo-driven methane oxidation mediated by KCl only. MnO suffered from the challenges of low yields based on methane ($< 1.6\%$) and stoichiometric yields based on Mn oxidant ($< 35\%$). For $\text{Mn}_2(\text{HTFA})_4(\mu\text{-TFA})_2(\text{TFA})_2$, catalytic turnover was

observed upon addition of TFSA and under a dioxygen atmosphere; however, these reactions still suffered from low yields based on methane (< 0.2%).

The goals of the photo-OxE process remain to find effective oxidants for selective, partial oxidation of light alkanes under the milder conditions of photochemistry, compared to thermal chemistry, that can be recycled with pure dioxygen or, ideally, with air. The screening of metal oxides, in particular, has been far from exhaustive to date. KCl and I₂ should continue to be explored as additives for future photo-OxE studies and the roles that they hold should be investigated. Mechanistic studies may elucidate that their roles differ from what was originally observed in our iodate/chloride and periodate/chloride studies,^{15, 16} as is proposed with our thermal manganese chemistry.¹³ As oxidants that function under photochemical conditions for the partial oxidation of light alkanes are identified, future directions should include the extension from use of HTFA as solvent to non-superacidic solvents, such as acetic acid.

3.5 Experimental Section

CAUTION: Many of the reagents and conditions described herein are particularly hazardous. Appropriate safety measures should be taken and appropriate personal protective equipment should be worn (long nitrile gloves up to the elbow) when handling strong acids, especially in large volumes. Broadband mercury arc lamps are dangerous to the skin and eyes, and even a brief exposure can result in permanent damage. The lamps must only be turned on while encased in an enclosure that precludes exposure to the naked eye. Cool to room temperature water must always be recirculated around the lamp to prevent uncontrolled

overheating; this is especially important when conducting reactions containing mixtures of methane and air or dioxygen, which can be explosive.

General Comments and Materials. All reactions were carried out under ambient atmosphere unless indicated otherwise. Potassium chloride, iodine, trifluoroacetic acid (> 99.9%), trifluoroacetic anhydride, glacial acetic acid, nitromethane, copper(II) acetate hydrate, copper(II) chloride hydrate, copper(II) trifluoroacetate hydrate, manganese dioxide, manganese oxide, and sodium bismuth oxide were purchased commercially and used as received. $\text{Mn}_2(\text{HTFA})_4(\mu\text{-TFA})_2(\text{TFA})_2$ was synthesized according to literature procedure.¹⁴ High pressure reaction vessels were constructed from Fisher-Porter tubes, purchased from Andrews Glass, and custom-built reactor tops made with Swagelok stainless steel fittings. These reaction vessels can be safely pressurized to 250 psig at room temperature. The photolysis enclosure was constructed with a power supply feeding a broadband mercury arc lamp. The mercury arc lamp was nested in a quartz immersion well in which cool to room temperature DI water (15-40 °C) was recirculated through at all times the lamp was powered on. The power supply (450 watt, product #7830-60), Hanovia mercury arc lamp (medium pressure, 450 watt, 121.92 mm arc length, 244.35 mm overall length, product #7825-34), and quartz immersion well (product #7854-27) were purchased from Ace Glass. The mercury arc lamp is quoted to irradiate ~ 40-48% in the ultraviolet spectral range, ~ 40-43% in the visible spectral range, and the remainder in the infrared spectral range. Mercury arc lamps were replaced every 1,000 hours. NMR analysis was performed using either a Varian Inova 500 or 600 MHz spectrometer. ¹H NMR data of reaction

mixtures were obtained with a capillary of C_6D_6 as the internal lock reference. Chemical shifts are reported relative to the internal standards of either CH_3NO_2 (δ 4.18) or HOAc (δ 2.04).

General Procedure for Photochemical Methane Functionalization with Copper Salts. Reactions were performed in triplicate. A stir bar was added to each Fisher-Porter reactor and then charged first with solid reagents (copper salt, KCl, I_2) followed by 8 mL HTFA. The reactors were sealed under air and weighed. The reactors were then pressurized with methane and weighed again. The amount of methane added was quantified by the difference in mass before and after methane addition. The reactors were then added to a photolysis enclosure, each positioned 16 cm from the mercury arc lamp with uniform stirring. Reaction time was started 15 minutes following lamp turn on to account for lamp warm up time to reach full intensity. After the reaction, the lamp was turned off and the photolysis chamber was kept closed for at least one minute to ensure the lamp was safely powered off. The reactors were removed, weighed to probe for leaks, and cooled in front of a fan for at least 15 minutes. The reactors were then vented in a fume hood, 20 μ L of internal standard (either CH_3NO_2 or HOAc) were added to each reaction, and the reaction mixtures were thoroughly stirred. An aliquot from each reaction mixture was removed and centrifuged, from which the supernatant of each was added to an NMR tube containing a sealed capillary containing C_6D_6 . The products were analyzed by 1H NMR spectroscopy.

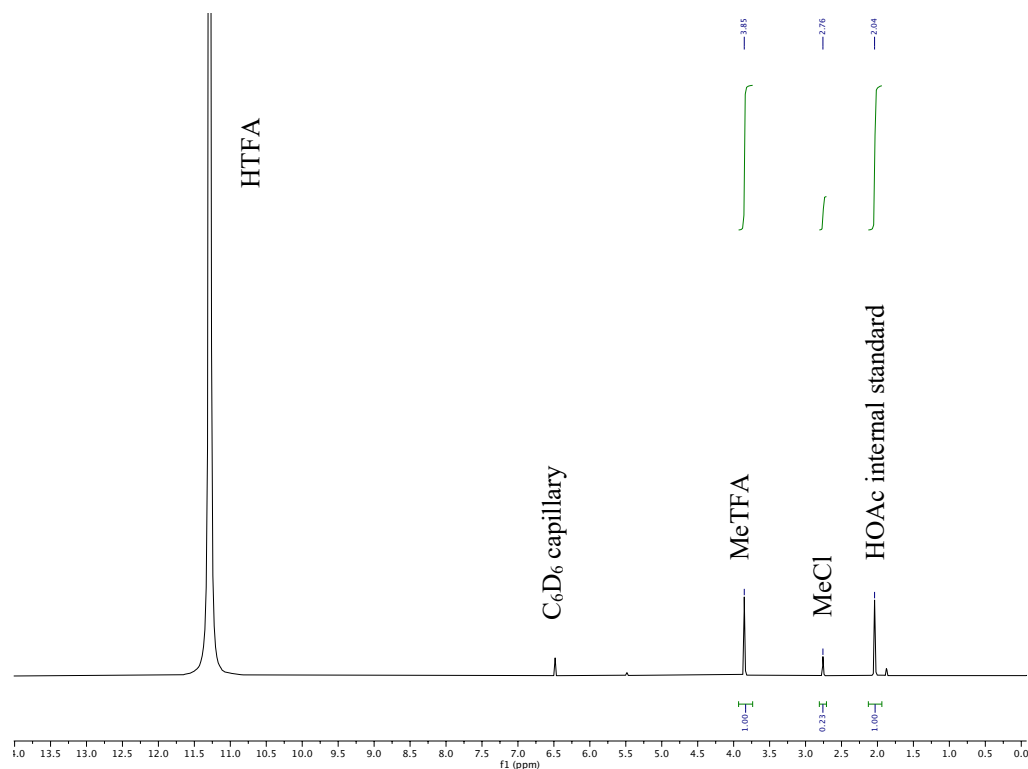


Figure 3.9. Labeled representative ^1H NMR spectrum for photochemical methane functionalization using Cu(II) salts. Either HOAc (shown here) or CH_3NO_2 was used as internal standard, from which product yields were calculated. Conditions: CH_4 (100 psig), $\text{Cu}(\text{OAc})_2 \cdot x\text{H}_2\text{O}$ (0.042 mmol), KCl (0.67 mmol), I_2 (0.05 mmol), HTFA (8 mL), 24 h of photolysis with a mercury arc lamp.

General Procedure for Photochemical Methane Functionalization with Manganese Oxide. Reactions were performed in triplicate. A stir bar was added to each Fisher-Porter reactor and then charged first with solid reagents (MnO , KCl, I_2) followed by 8 mL HTFA. The reactors were sealed under air and weighed. The reactors were then pressurized with methane and weighed again. The amount of methane added was quantified by the difference in mass before and after methane addition. The reactors were then added to a photolysis enclosure, each positioned 16 cm from the mercury arc lamp with uniform stirring. Reaction time was started 15 minutes following lamp turn on to account for lamp warm up time to reach full

intensity. After the reaction, the lamp was turned off and the photolysis chamber was kept closed for at least one minute to ensure the lamp was safely powered off. The reactors were removed, weighed to probe for leaks, and cooled in front of a fan for at least 15 minutes. The reactors were then vented in a fume hood, 20 μL of internal standard (either CH_3NO_2 or HOAc) were added to each reaction, and the reaction mixtures were thoroughly stirred. An aliquot from each reaction mixture was removed and added to a centrifuge tube with NaBiO_3 . The tube was carefully shaken and vented, followed by centrifugation. The supernatant of each centrifuge tube was added to an NMR tube containing a sealed capillary containing C_6D_6 . The products were analyzed by ^1H NMR spectroscopy.

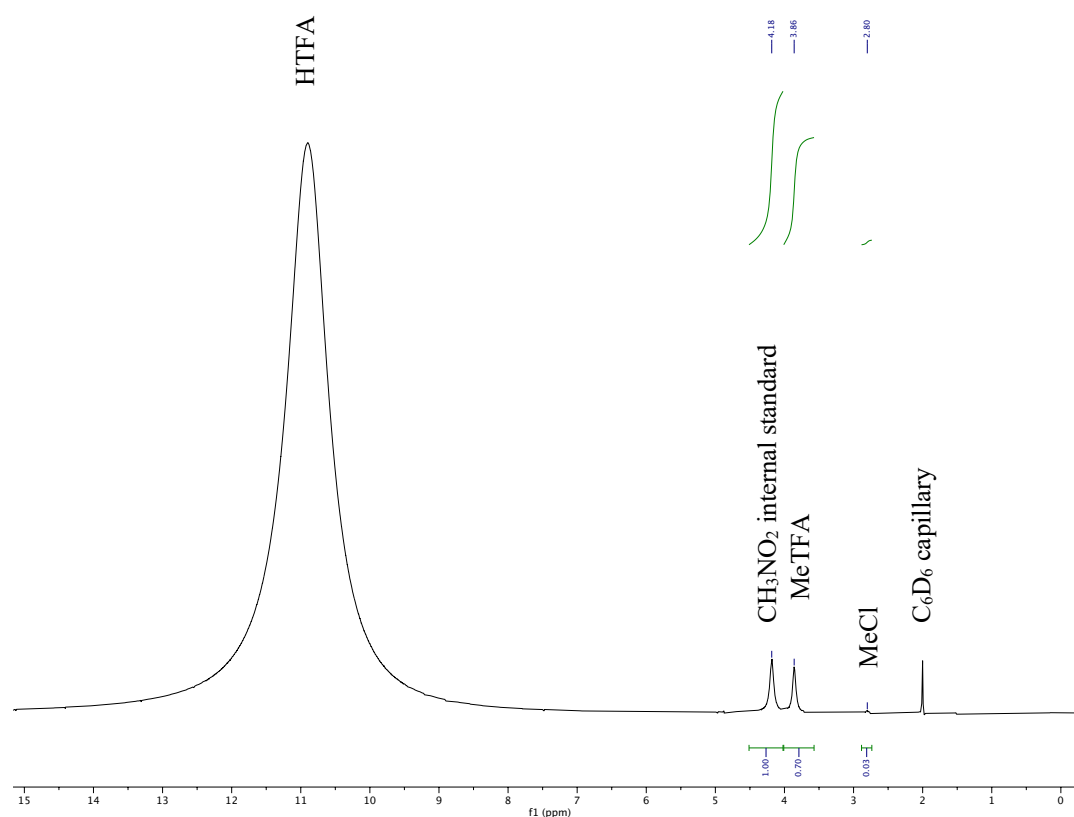


Figure 3.10. Labeled representative ^1H NMR spectrum for photochemical methane functionalization using Mn oxides. Either HOAc or CH_3NO_2 (shown here) was

used as internal standard, from which product yields were calculated. Conditions: CH₄ (100 psig), MnO (1.1 mmol), KCl (0.1 mmol), I₂ (0.025 mmol), HTFA (8 mL), 24 h of photolysis with a mercury arc lamp.

General Procedure for Photochemical Methane Functionalization with Mn₂(HTFA)₄(μ-TFA)₂(TFA)₂. Reactions were performed in triplicate. Synthesized Mn₂(HTFA)₄(μ-TFA)₂(TFA)₂ was stored in a dinitrogen-filled glovebox to protect against degradation over time. The Fisher-Porter reactors were brought into the glovebox, charged with Mn₂(HTFA)₄(μ-TFA)₂(TFA)₂, sealed and removed from the glovebox. Through the needle valve of each reactor top, 8 mL of solvent (HTFA, TFAA) were added and then dioxygen was bubbled through the reaction solution using a long needle. Following one minute of bubbling, the needle was removed and the reactor valve was quickly sealed. The reactors were weighed, pressurized with methane, and weighed again. The amount of methane added was quantified by the difference in mass before and after methane addition. The reactors were then added to a photolysis enclosure, each positioned 16 cm from the mercury arc lamp with uniform stirring. Reaction time was started 15 minutes following lamp turn on to account for lamp warm up time to reach full intensity. After the reaction, the lamp was turned off and the photolysis chamber was kept closed for at least one minute to ensure the lamp was safely powered off. The reactors were removed, weighed to probe for leaks, and cooled in front of a fan for at least 15 minutes. The reactors were then vented in a fume hood, 20 μL of internal standard (either CH₃NO₂ or HOAc) were added to each reaction, and the reaction mixtures were thoroughly stirred. An aliquot from each reaction mixture was removed and centrifuged, from which the supernatant of each was added to an NMR tube

containing a sealed capillary containing C₆D₆. The products were analyzed by ¹H NMR spectroscopy.

3.6 References

1. Liebov, N. S.; Goldberg, J. M.; Boaz, N. C.; Coutard, N.; Kalman, S. E.; Zhuang, T.; Groves, J. T.; Gunnoe, T. B., Selective Photo-Oxygenation of Light Alkanes Using Iodine Oxides and Chloride. *ChemCatChem* **2019**, *11* (20), 5045-5054.
2. Coutard, N.; Goldberg, J. M.; Valle, H. U.; Cao, Y.; Jia, X.; Jeffrey, P. D.; Gunnoe, T. B.; Groves, J. T., Aerobic Partial Oxidation of Alkanes Using Photodriven Iron Catalysis. *Inorg. Chem.* **2022**, *61* (2), 759-766.
3. Liebov, N. S. Hydrocarbon Functionalization. University of Virginia, 2019.
4. Punniyamurthy, T.; Velusamy, S.; Iqbal, J., Recent Advances in Transition Metal Catalyzed Oxidation of Organic Substrates with Molecular Oxygen. *Chem. Rev.* **2005**, *105* (6), 2329-2364.
5. Smidt, J.; Hafner, W.; Jira, R.; Sedlmeier, J.; Sieber, R.; Ruttinger, R.; Kojer, H., Catalytic reactions of olefins on compounds of the platinum group. *Angew. Chem.* **1959**, *71*, 176-182.
6. Smidt, J.; Hafner, W.; Jira, R.; Sieber, R.; Sedlmeier, J.; Sabel, A., The Oxidation of Olefins with Palladium Chloride Catalysts. *Angew. Chem. Int. Ed.* **1962**, *1* (2), 80-88.
7. Jira, R., Acetaldehyde from Ethylene—A Retrospective on the Discovery of the Wacker Process. *Angew. Chem. Int. Ed.* **2009**, *48* (48), 9034-9037.

8. Vaughan, B. A.; Webster-Gardiner, M. S.; Cundari, T. R.; Gunnoe, T. B., A rhodium catalyst for single-step styrene production from benzene and ethylene. *Science* **2015**, *348* (6233), 421-424.
9. Chen, J.; Nielsen, R. J.; Goddard, W. A., III; McKeown, B. A.; Dickie, D. A.; Gunnoe, T. B., Catalytic Synthesis of Superlinear Alkenyl Arenes Using a Rh(I) Catalyst Supported by a “Capping Arene” Ligand: Access to Aerobic Catalysis. *J. Am. Chem. Soc.* **2018**, *140* (49), 17007-17018.
10. Zhu, W.; Luo, Z.; Chen, J.; Liu, C.; Yang, L.; Dickie, D. A.; Liu, N.; Zhang, S.; Davis, R. J.; Gunnoe, T. B., Mechanistic Studies of Single-Step Styrene Production Catalyzed by Rh Complexes with Diimine Ligands: An Evaluation of the Role of Ligands and Induction Period. *ACS Catal.* **2019**, *9* (8), 7457-7475.
11. Jia, X.; Foley, A. M.; Liu, C.; Vaughan, B. A.; McKeown, B. A.; Zhang, S.; Gunnoe, T. B., Styrene Production from Benzene and Ethylene Catalyzed by Palladium(II): Enhancement of Selectivity toward Styrene via Temperature-dependent Vinyl Ester Consumption. *Organometallics* **2019**, *38* (19), 3532-3541.
12. Jia, X.; Frye, L. I.; Zhu, W.; Gu, S.; Gunnoe, T. B., Synthesis of Stilbenes by Rhodium-Catalyzed Aerobic Alkenylation of Arenes via C–H Activation. *J. Am. Chem. Soc.* **2020**, *142* (23), 10534-10543.
13. Coutard, N.; Musgrave, C. B., III; Moon, J.; Liebov, N. S.; Nielsen, R. M.; Goldberg, J. M.; Li, M.; Jia, X.; Lee, S.; Dickie, D. A.; Schinski, W. L.; Wu, Z.; Groves, J. T.; Goddard, W. A., III; Gunnoe, T. B., Manganese

Catalyzed Partial Oxidation of Light Alkanes. *ACS Catal.* **2022**, *12* (9), 5356-5370.

14. Guntlin, C. P.; Zünd, T.; Kravchyk, K. V.; Wörle, M.; Bodnarchuk, M. I.; Kovalenko, M. V., Nanocrystalline FeF₃ and MF₂ (M = Fe, Co, and Mn) from metal trifluoroacetates and their Li(Na)-ion storage properties. *J. Mater. Chem. A* **2017**, *5* (16), 7383-7393.
15. Fortman, G. C.; Boaz, N. C.; Munz, D.; Konnick, M. M.; Periana, R. A.; Groves, J. T.; Gunnoe, T. B., Selective monooxidation of light alkanes using chloride and iodate. *J. Am. Chem. Soc.* **2014**, *136* (23), 8393-8401.
16. Kalman, S. E.; Munz, D.; Fortman, G. C.; Boaz, N. C.; Groves, J. T.; Gunnoe, T. B., Partial oxidation of light alkanes by periodate and chloride salts. *Dalton Trans.* **2015**, *44* (12), 5294-5298.

4 A Tandem Experimental and Computational Study Using Hydrogenation as a Probe Reaction for New Methods of Carbon Dioxide Hydroarylation Using Bifunctional Catalysis

4.1 Introduction

4.1.1 C1 Incorporation Chemistry and Anthropogenic Carbon Dioxide (CO₂)

Catalytic conversion of single-carbon-atom (C1) containing molecules (*e.g.*, CO, CO₂, CH₄) into fuels and value-added chemicals is important to the chemical industry.¹ Not only does the abundance of these molecules make them desirable feedstocks for the chemical industry, but their conversion is also desirable in order to limit environmental pollution. However, there is not one strategy that can be utilized for C1 incorporation chemistry. C1 molecules are often inert (*e.g.*, CO₂, CH₄) or quite reactive (*e.g.*, CO), and each category brings challenges for C1 incorporation chemistry. Examples of C1 incorporation chemistry used in industry include the Fischer-Tropsch process, the water-gas shift reaction, and methane steam reforming. These industrial C1 conversions suffer from high energy requirements, multi-step reactions, and difficult product separations.¹

CO₂ is the greatest anthropogenically emitted greenhouse gas (GHG).² Since the industrial revolution, emissions have largely outweighed the amount required for the Earth's natural carbon-cycle, leading to a continual rise in atmospheric CO₂ concentration ever since.³ In 2018, the U.S. emitted ~6,677 million metric tons of CO₂, a 2.9% increase over 2017 emissions.² Substantial efforts have been dedicated to developing technologies for carbon capture and sequestration (CCS). In CCS, CO₂ is captured from power plants and industrial

processes, transported and compressed (usually in pipelines), and then injected into deep underground rock formations.⁴ In another vision, considering an economically viable method for capture, the anthropogenically released CO₂ could be used by the chemical industry as feedstock for the production of fuels or higher-value chemicals, including carboxylic acids, which will be the focus herein.^{5, 6} It can be argued that implementation of CO₂ fixation processes in synthetic methods will most likely not reduce its atmospheric concentration, and until dihydrogen is produced from a source other than fossil fuels, CO₂ reduction chemistry will remain a curiosity rather than a method to combat atmospheric levels.

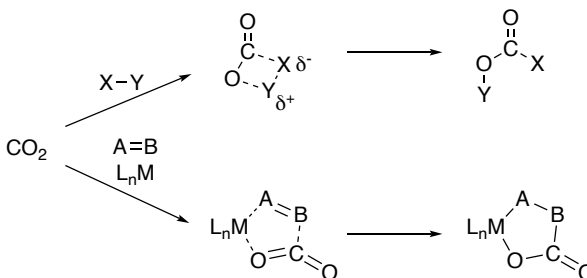
4.1.2 Chemical Properties and Reactivity of CO₂

Although CO₂ is abundant, non-toxic, and inexpensive, its inherent stability, both thermodynamic and kinetic, presents a challenge for its transformation into chemical commodities.^{3, 7} The bond energy of each C=O bond in CO₂ is ~190 kcal/mol.⁸ CO₂ is a linear molecule with $D_{\infty h}$ symmetry. It is a non-polar molecule with two opposing C=O dipole moments. The electronegativity of both oxygen atoms renders them reactive towards electrophilic molecules. At the same time, the electron withdrawing nature of the two oxygen atoms renders the carbon atom electron-deficient, making the carbon atom reactive towards nucleophiles.

Some generic transformations with CO₂ are depicted in Scheme 4.1. Nucleophilic attack of the carbon atom of CO₂ by Grignard reagents can occur at low temperature. Reaction of CO₂ with unsaturated molecules (*e.g.*, alkenes,

alkynes) and low valent transition metal complexes produce five-membered metallalactones.⁷

Scheme 4.1. Common transformations of CO₂: nucleophilic attack (top) and transition-metal mediated oxidative cycloaddition (bottom). X–Y depicts a generic nucleophile. A=B depicts a generic unsaturated molecule. L_nM depicts a generic low valent transition metal-ligated complex. Adapted from reference.⁷



CO₂ binds to transition metals through different modes. Transition metals in low oxidation states typically bind CO₂ through its carbon atom and transition metals in high oxidation states typically bind CO₂ through one or both of its oxygen atoms.⁶ This reactivity with transition metals can be rationalized by considering the molecular orbitals (MOs) of CO₂. The highest occupied molecular orbital (HOMO) of CO₂ is localized on the oxygen atoms, and the lowest unoccupied molecular orbital (LUMO) of CO₂ has more localization on the carbon atom than oxygen atoms. The MOs of CO₂ as well as its binding modes to transition metals are displayed in Figure 4.1.

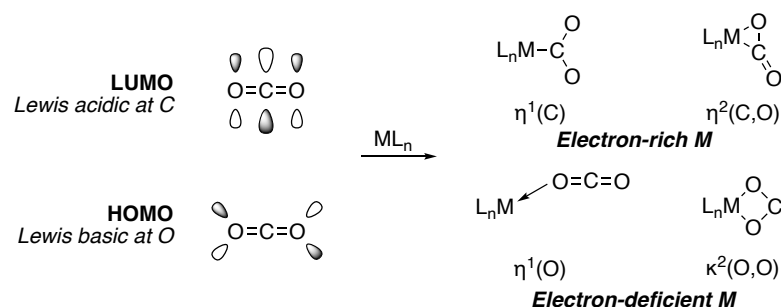
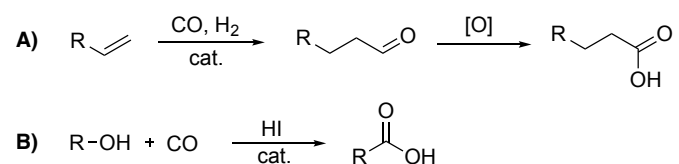


Figure 4.1. Binding modes of CO₂ to transition metal complexes can be understood by the HOMO and LUMO of CO₂. ML_n depicts generic transition metal-ligated complex. Adapted from reference.⁶

4.1.3 Industrial Processes for Synthesis of Carboxylic Acids

Carboxylic acids are used by the chemical, textile, cosmetic, and protective coating industries, among others.⁶ Current industrial production of carboxylic acids uses primarily two methods, one being from alkene starting material and the other being from alcohol starting material. The first method is the cobalt- or rhodium-catalyzed hydroformylation of alkenes with carbon monoxide followed by aldehyde oxidation (Scheme 4.2A).⁹ This two-step process (starting from alkene/CO/H₂) suffers from the fact that it requires separation of the aldehyde following the first step and before the oxidation step. The second method is the rhodium/iodide co-catalyzed carbonylation of alcohols using the Monsanto process, and, similarly, the iridium/iodide co-catalyzed carbonylation of methanol using the Cativa process (Scheme 4.2B).¹⁰ The Monsanto process is limited to small alkyl groups (denoted by R in Scheme 4.2) on the alcohol, which restricts the scope of carboxylic acids that can be produced. The major disadvantage of both processes is that they require the utilization of carbon monoxide, a toxic gas, and therefore suffer from safety concerns.

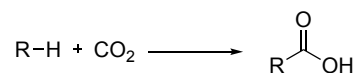
Scheme 4.2. Current industrial methods for the synthesis of carboxylic acids: hydroformylation of alkenes followed by aldehyde oxidation (A) and the Monsanto/Cativa process (B). [O] denotes oxidant. R denotes alkyl group.



4.1.4 Desired Direct Carboxylation of Hydrocarbons and Arenes

The mitigation of problems associated with current industrial processes for the production of carboxylic acids and the utilization of CO₂ as a C1 feedstock source could be combined in an alternate route for carboxylic acid synthesis through the direct carboxylation of hydrocarbons with CO₂. This desirable, one-step process is depicted in Scheme 4.3.

Scheme 4.3. Alternate, desired strategy for synthesis of carboxylic acids through direct carboxylation with CO₂. R denotes alkyl or aryl group.



More specifically, the synthesis of aromatic carboxylic acids from CO₂ is a reaction of interest. Aromatic carboxylic acids are common motifs in biologically active molecules, pharmaceuticals, agrochemicals, polymers, among other fine chemicals.^{11, 12} The Kolbe-Schmitt reaction is an industrial process for the carboxylation of phenol with CO₂ to make salicylic acid, which is the precursor to aspirin.¹³ The Kolbe-Schmitt reaction requires elevated temperature (125 °C) and pressure (100 atm), as well as stoichiometric amounts of strong acid (H₂SO₄).

The direct catalytic carboxylation of arenes was previously limited to use of aryl Grignard compounds, aryl boronic esters, or aryl halides, making the carboxylation a multi-step process.¹¹ However, in recent years, the number of reports of direct carboxylation reactions have increased.¹² CO₂ conversion to aromatic/aryl carboxylic acids have been catalyzed by both homogeneous and heterogeneous processes through approaches such as electrochemical, photocatalytic, enzymatic, and porous materials. Challenges still remain including the requirement of elevated temperatures and pressures as well as the often necessity of a base or Lewis acid.

4.1.5 Metal-Ligand Bifunctional Catalysis

Rapidly developed over the past few decades, metal-ligand bifunctional catalysis has emerged as a highly efficient strategy for organic transformations, namely hydrogenations and dehydrogenations, in both academia and industry.^{14, 15} Industrial companies including Takasago Int. Corp., Merck, Mitsubishi Chemical Corp., and Pfizer utilize bifunctional catalysis for the large-scale hydrogenation of C=O and C=N functionalities.¹⁶⁻¹⁸

A metal-ligand bifunctional catalyst has two active sites with dual reactivities: one nucleophilic site directly bound to the metal center and one electrophilic site located on a ligand (Figure 4.2). Pioneering examples of metal-ligand bifunctional catalysts are depicted in Figure 4.3, for which a hydride ligand occupies the metal-bound nucleophilic site and a proton occupies the ligand-bound electrophilic site.

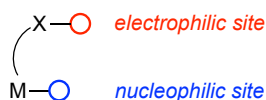


Figure 4.2. General structure of a metal-ligand bifunctional catalyst with a metal-bound nucleophilic site and a ligand-bound electrophilic site.

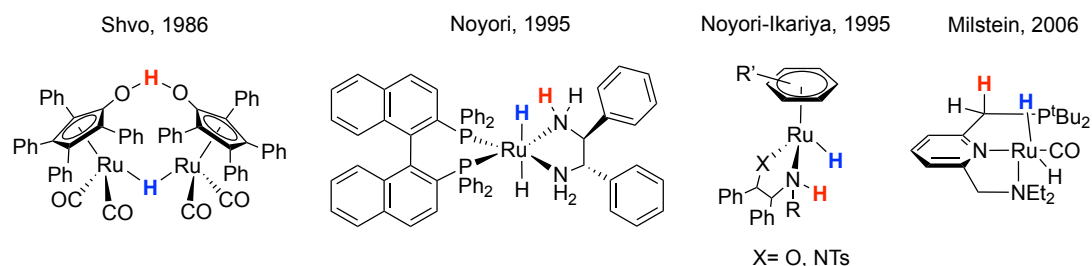


Figure 4.3. Early examples of M/OH, M/NH, and M/CH metal-ligand bifunctional catalysts. Red H denotes $H^{\delta+}$ and blue H denotes $H^{\delta-}$. Adapted from reference.¹⁵

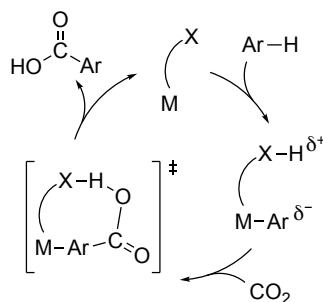
4.1.6 Project Goals

CO_2 fixation chemistry, particularly towards methanol production, has been achieved with zeolites and metal oxides functioning as bifunctional catalysts.¹⁹ In addition to transition metal-ligated complexes, examples of quaternary ammonium and phosphonium salts and metal-organic frameworks can serve as bifunctional catalysts for the reaction of CO_2 and epoxides to form cyclic carbonates.²⁰⁻²³ The project described herein was focused on CO_2 fixation chemistry using molecular, metal-ligand bifunctional catalysts for the production of aromatic carboxylic acids from CO_2 and arenes in a base-free, stoichiometric additive-free system.

A proposed catalytic cycle for this process is shown in Scheme 4.4. An arene (denoted generically as Ar-H) undergoes C-H activation by a metal-ligand bifunctional catalyst (denoted generically as M---X) to form an intermediate containing a nucleophilic metal-bound aryl group and an electrophilic proton bound

to the ligand. CO₂ is then rendered susceptible to reactivity with this intermediate due to its C–O bond dipole, forming a metallocycle transition state that then releases the aromatic carboxylic acid and regenerates the metal-ligand bifunctional catalyst. This project used computational modeling and experimental chemistry for analysis of catalyst design, reactivity studies, and mechanistic studies.

Scheme 4.4. Proposed catalytic cycle for a novel process combining aromatic C–H activation and CO₂ functionalization for the production of aromatic carboxylic acids using metal-ligand bifunctional catalysis. Ar–H denotes generic arene. M---X denotes a simplified catalyst comprised of a transition metal center (M) and ligand (X).



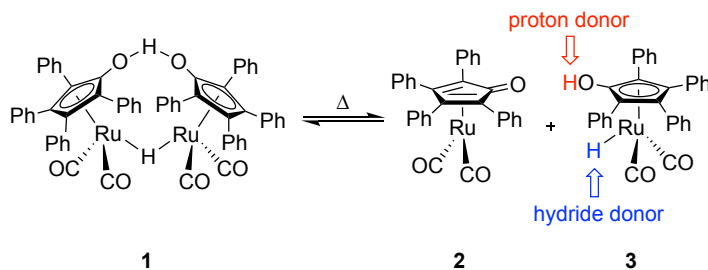
4.1.7 Shvo Catalyst Background and Hydrogenation as Starting Point

Shvo's catalyst, labeled as **1** in Scheme 4.5, was chosen due to its precedent for a wide variety of organic transformations, including oxidations and reductions.²⁴⁻²⁶ It has been studied for the transfer hydrogenation of ketones, aldehydes, imines, alkenes, and alkynes with turnovers exceeding 2,700.^{27, 28}

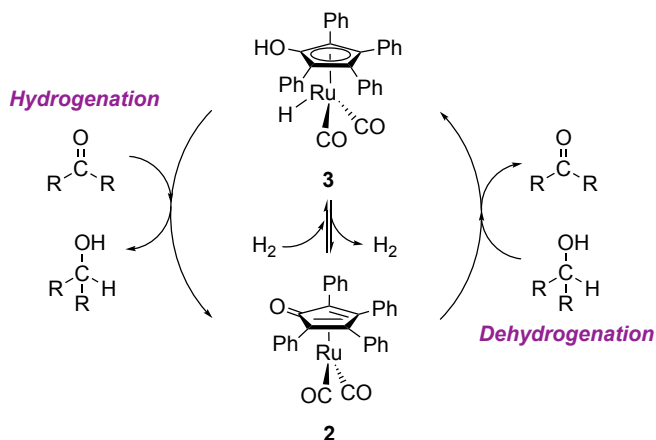
The air- and water-stable tetraphenylcyclopentadienone-ligated diruthenium complex **1** thermally dissociates to form two monomeric and catalytically active species *in situ*: the 16-electron complex **2** and the 18-electron complex **3** (Scheme 4.5).²⁷ The addition or removal of dihydrogen allows for the

conversion between the two catalytically active species (Scheme 4.6). Complex **2** facilitates dehydrogenation chemistry, and complex **3** facilitates hydrogenation chemistry (Scheme 4.6). In one monomer, Ru is in the +2 oxidation state (**3**), and in the other, Ru is in the zero oxidation state (**2**). This creates a situation in which the formally more oxidized monomer (**3**) is the reducing component and the formally more reduced monomer (**2**) is the oxidizing component. Single crystal X-ray structures of **2** and **3** have never been obtained, but solution NMR, mechanistic probes, and trapping experiments have provided evidence for their respective monomeric structures.²⁷

Scheme 4.5. Dimeric and monomeric forms of Shvo's catalyst. The dimeric species **1** thermally dissociates into two active species, **2** and **3**.



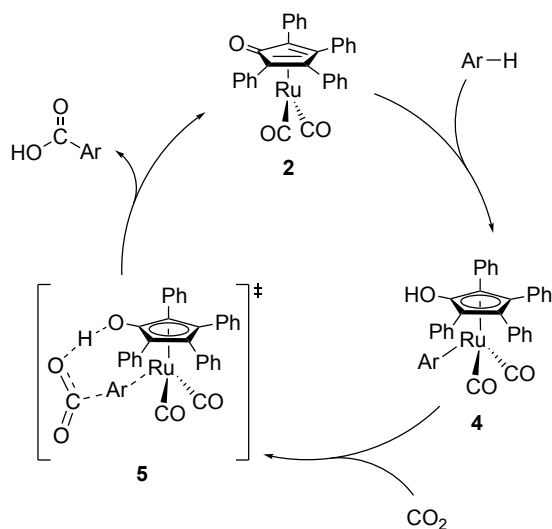
Scheme 4.6. Conversion between the monomeric forms of Shvo's catalyst is achieved through addition or depletion of dihydrogen. Saturated species **3** catalyzes hydrogenation chemistry and saturated species **2** catalyzes dehydrogenation chemistry.



The application of this catalyst to our envisioned use for the direct carboxylation of hydrocarbons and arenes is depicted in Scheme 4.7 (i.e., Scheme 4.7 shows our *proposed* catalytic process). In solution phase in an absence of dihydrogen, Shvo's catalyst will access the form of monomer **2**. To species **2**, an arene undergoes C–H activation to form intermediate **4**, a species **3** analogue with an aryl group in place of the metal-hydride. CO₂ should be rendered susceptible to reaction with the aryl-activated Ru species **4** at each bifunctional site, in a manner analogous to that shown in Scheme 4.4. Through a metallacyclic transition state (**5**), the aromatic carboxylic acid is released and **2** is regenerated.

To our knowledge, there is no precedent for hydroarylation chemistry with Shvo's catalyst. This extension seems feasible because the bond dissociation energy (BDE) of H₂ is 104 kcal/mol and benzene, for example, is 113 kcal/mol.²⁹ Additionally, to our knowledge, there is no precedent for CO₂ chemistry with Shvo's catalyst. Because of the large precedent for hydrogenation chemistry with Shvo's catalyst, hydrogenation of CO₂ was chosen as a starting point. Results from novel hydrogenation of CO₂ with Shvo's catalyst could be benchmarked against previously measured hydrogenation of carbonyl-containing substrates. Following the investigation of CO₂ hydrogenation, CO₂ hydroarylation was to be explored.

Scheme 4.7. Proposed catalytic cycle for Shvo-catalyzed arene carboxylation. Ar-H denotes generic arene.



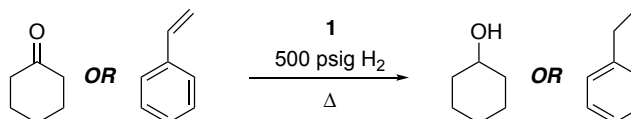
4.2 Experimental Approach to Hydrogenation Chemistry

Before attempting hydrogenation of CO₂, the activity of Shvo-catalyzed ketone and alkene hydrogenation was measured and compared to reported values to ensure that my methodology for hydrogenation reactions was sufficient. Scheme 4.8 contains percent conversion and catalyst turnover (TO) data from these experiments as well as a comparison to the data reported in literature.²⁸ Products were quantified using a gas chromatography-flame ionization detector (GC-FID). These results indicated that the hydrogenation method used could successfully reproduce the results reported in literature, enabling the extension to the exploration of Shvo-catalyzed CO₂ hydrogenation.

Gas chromatography-mass spectrometry (GC-MS) and proton nuclear magnetic resonance spectroscopy (¹H NMR) methods were developed for the quantification of formic acid. Substantial efforts were attempted for CO₂

hydrogenation, but in all cases, no formic acid was detected by GC-MS nor ^1H NMR.

Scheme 4.8. Hydrogenation of cyclohexanone and styrene by Shvo's catalyst. ^aConditions: 50 mmol cyclohexanone, 25 μmol **1**, 500 psig H_2 , 100 $^\circ\text{C}$, 5 h, Average of four independent experiments. ^bConditions: 52 mmol styrene, 20 μmol **1**, 500 psig H_2 , 145 $^\circ\text{C}$, 12 h, Average of five independent experiments. Products were quantified using GC-FID.



Substrate	Experimental Values		Literature Values	
	Conversion (%)	TOs	Conversion (%)	TOs
Cyclohexanone ^a	79(4)	1570(34)	98	1960
Styrene ^b	74(1)	1952(17)	67	2760

4.3 Computational Approach to Hydrogenation Chemistry

4.3.1 Density Functional Theory Details and Model System

In collaboration with the Ess group at Brigham-Young University, I performed Density Functional Theory (DFT) calculations to study mechanistic details of Shvo-catalyzed hydrogenation chemistry *in silico*. Calculations on Shvo's catalyst were performed using a simplified model wherein the phenyl groups of the cyclopentadienyl ring were substituted with hydrogen atoms (Figure 4.4). No significant differences were found between the simplified and full systems, with calculated energies differing by, at most, 4 kcal/mol. Reaction solvent was modeled using an implicit solvent model.

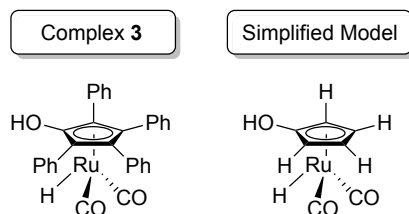


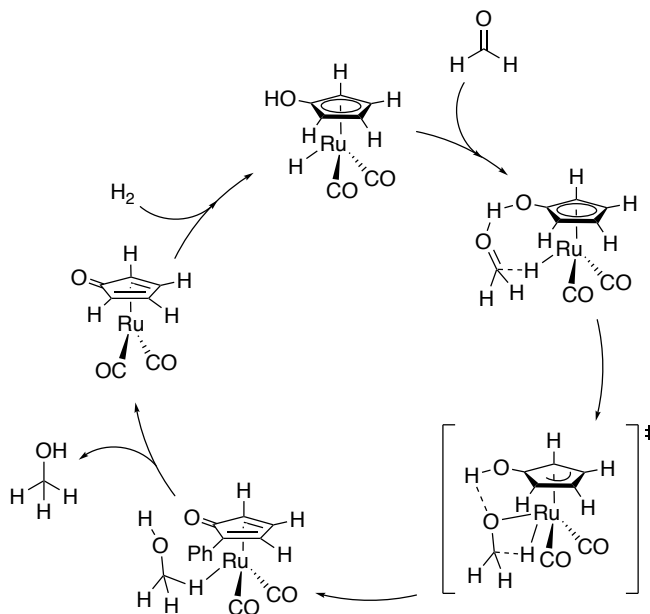
Figure 4.4. Comparison of complex **3** to simplified model system used in DFT calculations. Complex **2** is analogously modeled in which ligand phenyl groups are replaced with protons.

Calculations were performed separately using two functionals: the hybrid generalized gradient-approximation functional B3LYP³⁰⁻³² and the hybrid meta-generalized gradient-approximation functional M06.³³ The difference between the two functionals lies in the tradeoff between accuracy and computational cost. Both functionals include local spin-density and the gradient of the local spin-density in order to approximate the exchange-correlation energy.³⁴ However, the added dependence of the exchange-correlation energy on kinetic energy density in the M06 functional is considered advantageous for the accuracy in transition metal-containing calculations. With presently-available functionals, DFT calculations are considered to be accurate within 2-3 kcal/mol.³⁵

4.3.2 Mechanisms of Shvo-Catalyzed Hydrogenation

Precedent exists for the elucidation of the mechanisms for Shvo-catalyzed hydrogenation, both experimentally and computationally.²⁷ It has been proposed that for ketones, aldehydes, and alcohols the proton and hydride are transferred from the catalyst to the substrate in a concerted manner, but for amines and imines they are transferred in a sequential manner with protonation occurring first.³⁶

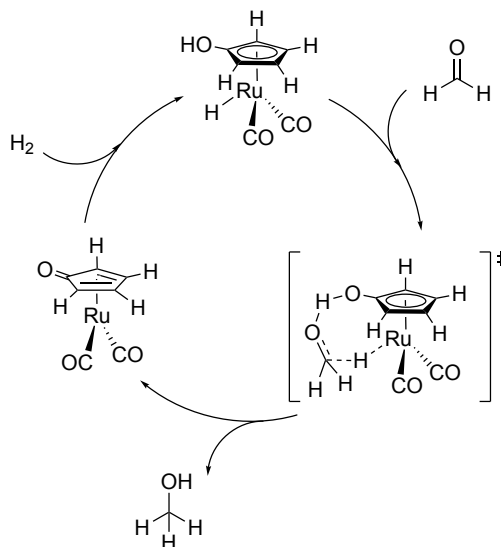
Scheme 4.9. Proposed inner sphere concerted mechanism for Shvo-catalyzed ketone hydrogenation using formaldehyde as a model substrate. Adapted from reference.²⁷



There has been debate regarding whether the hydrogenation reactions of ketones, aldehydes, and alcohols using Shvo's catalyst occur through an inner sphere mechanism, for which the substrate coordinates to the metal center (Scheme 4.9), or an outer sphere mechanism, for which there is no coordination of the substrate (Scheme 4.10). Casey and coworkers measured KIE values for the Shvo-catalyzed hydrogenation of benzaldehyde as $k_H/k_D = 3.6(3)$.³⁷ This value is most consistent with a mechanism in which the proton and hydride are transferred in a single, rate-determining step.²⁷ DFT calculations were used to compare the reaction barriers of the inner and outer sphere mechanisms. For Shvo-catalyzed formaldehyde hydrogenation, the transition state was calculated to be ~ 25 kcal/mol higher for the inner sphere mechanism than the outer sphere mechanism.³⁶ The DFT calculations are more consistent with an outer sphere concerted mechanism and,

thus, the outer sphere concerted mechanism was the primary mechanism explored for the computational mechanistic investigation herein.

Scheme 4.10. Proposed outer sphere concerted mechanism for Shvo-catalyzed ketone hydrogenation using formaldehyde as a model substrate. Adapted from reference.²⁷



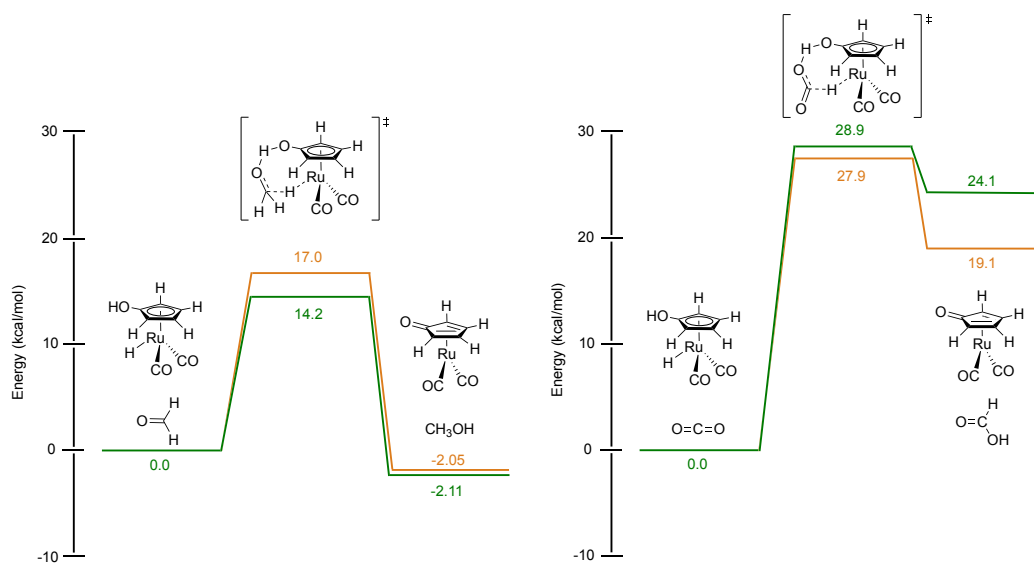
4.3.3 Mechanistic Investigation of Formaldehyde and Carbon Dioxide Hydrogenation via Outer Sphere Concerted Mechanism

First, the outer sphere concerted mechanism depicted in Scheme 4.10 was investigated via DFT calculations. Shvo-catalyzed hydrogenation of ketones was calculated to serve as a point of comparison to CO₂. Formaldehyde was chosen as the substrate for the ability to compare to previous computational reports wherein formaldehyde is commonly chosen as the carbonyl-containing substrate.^{36, 38}

The energy profile diagrams for Shvo-catalyzed hydrogenation of formaldehyde and CO₂ are shown in Scheme 4.11. In order to make a comprehensive comparison between substrates, and to determine if one functional

led to different results than the other, both B3LYP and M06 functionals were used in separate series of calculations. It was found that the hydrogenation of formaldehyde is calculated to be a slightly exergonic reaction ($\Delta G < 0$) with a moderate kinetic barrier ($\Delta G^\ddagger \cong 14\text{-}17$ kcal/mol). The hydrogenation of CO_2 is calculated to be an endergonic reaction ($\Delta G > 0$) with a larger kinetic barrier ($\Delta G^\ddagger \cong 28\text{-}29$ kcal/mol). Within the accuracy of DFT mentioned above, both functionals yielded similar results with respect to one another. Thus, for many subsequent calculations, B3LYP was utilized due to its lower computational cost.

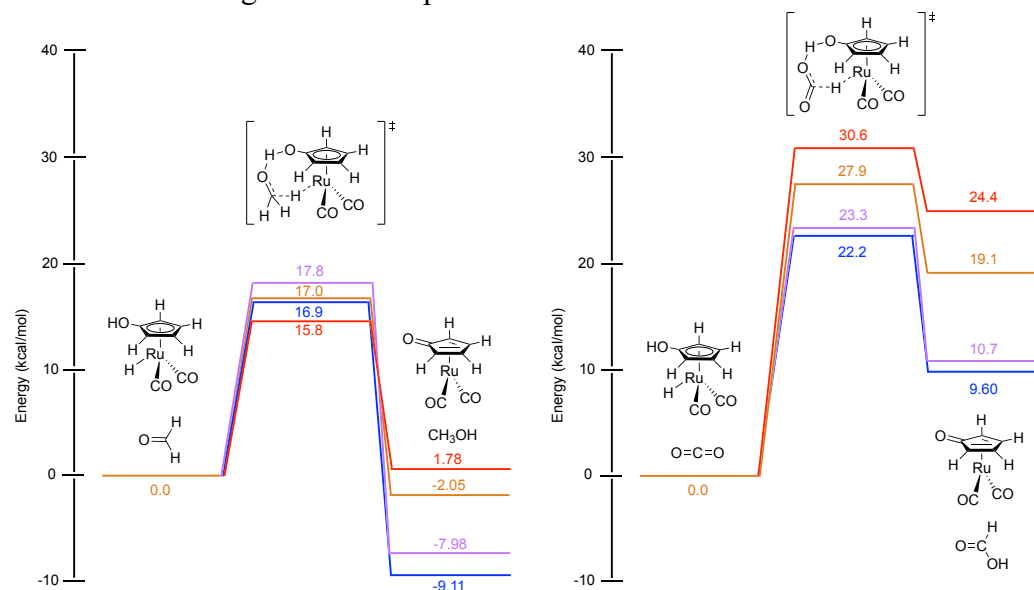
Scheme 4.11. DFT calculated free energy profile diagrams for hydrogenation of formaldehyde (left) and CO_2 (right) using outer sphere concerted mechanism. Calculations were performed using the B3LYP functional (orange) and the M06 functional (green). Tetrahydrofuran solvent was modeled using the SMD implicit model.



4.3.4 Solvent Effects on Formaldehyde and Carbon Dioxide Hydrogenation via Outer Sphere Concerted Mechanism

Because of the ionic nature of metal-ligand bifunctional catalysis, it is hypothesized that polarity and proticity of the reaction solvent may play an important role in the feasibility and/or rate of hydrogenation. Thus, the effects of solvent on the energetics of the reaction were explored using a series of four implicit solvents: toluene, tetrahydrofuran, methanol, and water. These calculations were performed using the B3LYP functional. Scheme 4.12 contains the energy profile diagrams for the hydrogenation of formaldehyde and CO₂ via the outer sphere concerted mechanism. These results depict several trends. Regarding formaldehyde hydrogenation, ΔG^\ddagger values show little variation. On the contrary, ΔG^\ddagger values decrease with an increase in solvent polarity for CO₂ hydrogenation. In both cases of hydrogenation, ΔG^\ddagger values are dependent on solvent polarity. For formaldehyde hydrogenation, the reaction moves from energy-neutral to exergonic with increasing solvent polarity. For CO₂ hydrogenation, the reaction becomes less endergonic with increasing solvent polarity.

Scheme 4.12. DFT calculated free energy profile diagrams for hydrogenation of formaldehyde (left) and CO₂ (right) using outer sphere concerted mechanism as a function of solvent (red = toluene, orange = tetrahydrofuran, purple = methanol, blue = water). Calculations were performed using the B3LYP functional. Solvent was modeled using the SMD implicit model.



From ΔG^\ddagger values, rates of reaction (k) can be predicted using the Eyring equation, for which h is Planck's constant, k_b is the Boltzmann constant, and R is the ideal gas constant. The ΔG^\ddagger values of 17.0 and 27.9 kcal/mol obtained for the hydrogenation of formaldehyde and CO₂ in tetrahydrofuran, a slightly polar, aprotic solvent, can be used to calculate the predicted rate constants of 430 and $9.15 \times 10^{-6} \text{ s}^{-1}$ at 100 °C, respectively. Considering instead the ΔG^\ddagger values of 16.9 and 22.2 kcal/mol obtained for the hydrogenation of formaldehyde and CO₂ in water, the most polar, protic solvent, the predicted rate constants are calculated as 974 and 0.764 s^{-1} , respectively. The increase in approximately five orders of magnitude for the rate of CO₂ hydrogenation in water compared to the rate in tetrahydrofuran

supports the prediction that polarity and/or proticity of the reaction solvent plays a role in the rate of hydrogenation for CO₂.

A more thorough investigation of solvent effects would be achieved through utilization of explicit solvent models.³⁹ Explicit solvent models can more realistically model the specific interactions of solvent molecules with the catalyst and substrate. Inclusion of these specific interactions are important when solvent molecules actively participate in the chemistry. Here, hydrogen bonding is an intermolecular interaction that would be important to consider for realistic modeling.

4.4 Exploration of Ligand Modifications

4.4.1 Selection of Shvo Analogues

Analogues to Shvo's catalyst containing modifications to the tetraphenylcyclopentadienone ligand have been documented in previous reports.⁴⁰ In an effort to investigate the effect of electronic modifications to the tetraphenylcyclopentadienone ligand on hydrogenation chemistry, two analogues were chosen to compare to Shvo's catalyst (Figure 4.5). The first analogue, **18e-Br**, contains para-substitution of bromine atoms on the two ligand phenyl rings furthest from the OH functionality. The second analogue, **18e-OMe**, contains para-substitution of methoxy groups on the two ligand phenyl rings furthest from the OH functionality. We were curious to what extent the electron-withdrawing and electron-donating natures of **18e-Br** and **18e-OMe**, respectively, might affect hydrogenation chemistry, both computationally and experimentally, relative to Shvo's catalyst, which will be referred to as 18e in the following sections for clarity.

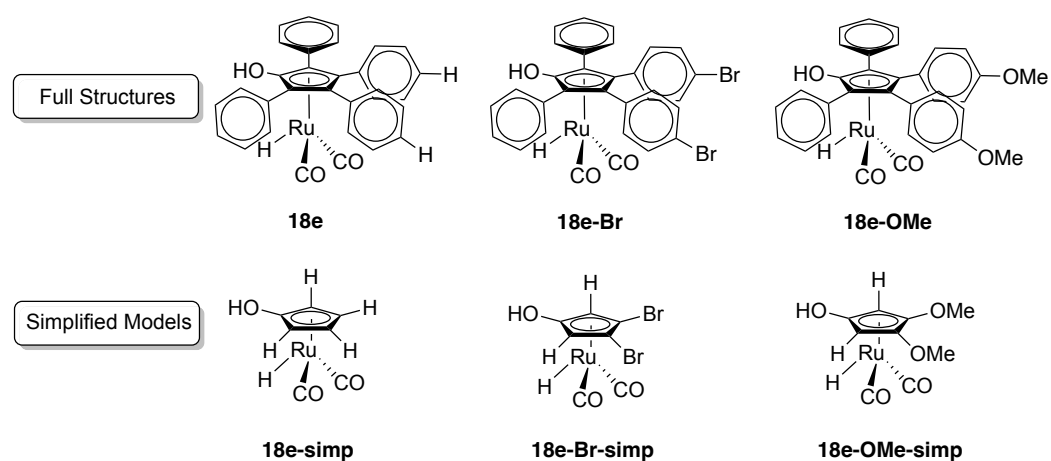
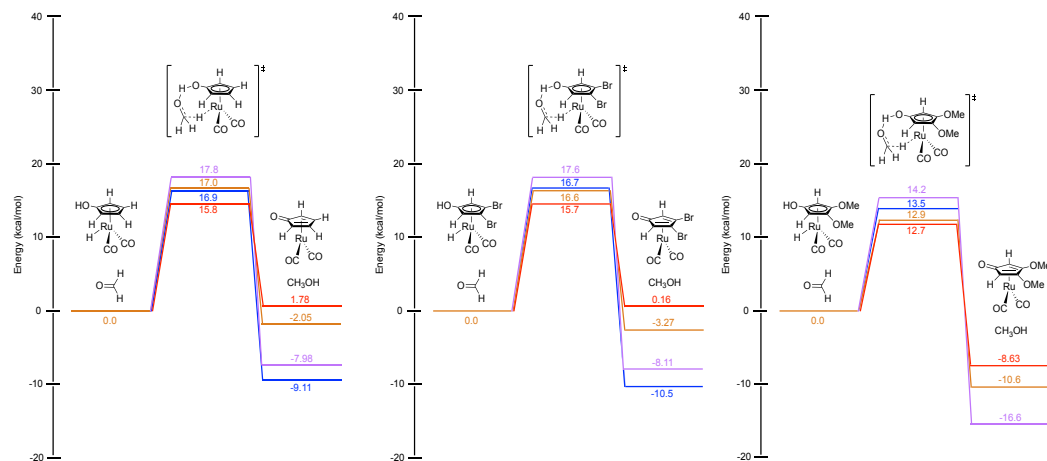


Figure 4.5. Shvo's catalyst and analogues depicted in their full chemical structures and in their simplified models utilized in DFT calculations.

4.4.2 Mechanistic Investigation of Formaldehyde and Carbon Dioxide Hydrogenation with Shvo Analogues via Outer Sphere Concerted Mechanism

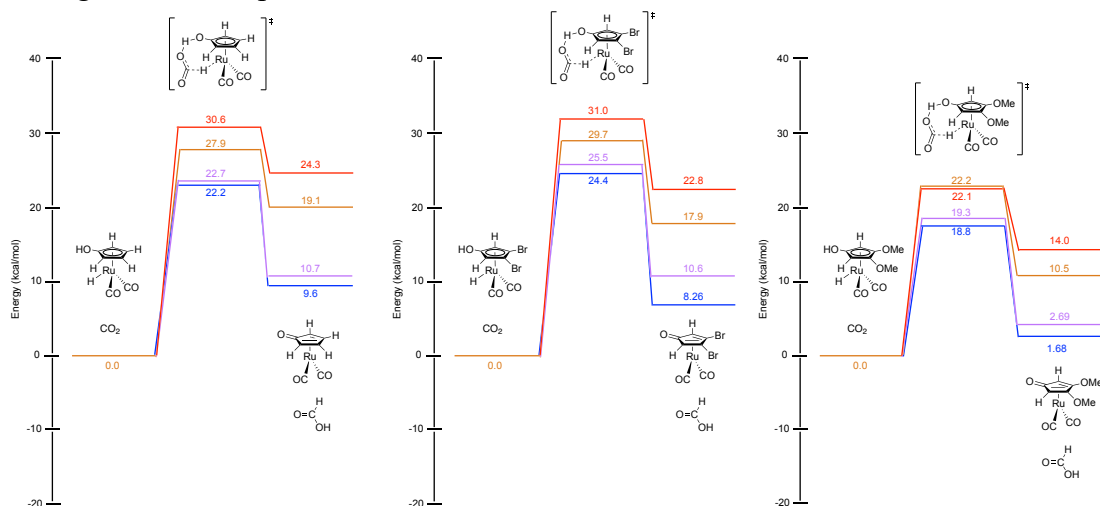
We were interested in investigating how the electronic modifications of the Shvo analogues would affect the reaction barriers for formaldehyde and CO₂ hydrogenation. DFT calculations using the simplified models of these analogues were performed for formaldehyde (Scheme 4.13) and CO₂ (Scheme 4.14) hydrogenation via the outer sphere concerted mechanism using the B3LYP functional. Calculations with each of the aforementioned four solvents (toluene, tetrahydrofuran, methanol, water) were performed using an implicit solvent model.

Scheme 4.13. DFT calculated free energy profile diagrams for hydrogenation of formaldehyde using Shvo analogues via outer sphere concerted mechanism as a function of solvent (red = toluene, orange = tetrahydrofuran, purple = methanol, blue = water). Calculations were performed using the B3LYP functional. Solvent was modeled using the SMD implicit model.



For formaldehyde hydrogenation, there is little change between **18e** and **18e-Br** regarding the values of ΔG and ΔG^\ddagger . For **18e-OMe-simp**, both ΔG and ΔG^\ddagger values are decreased relative to **18e-simp** and **18e-Br-simp**. Here, the 16-electron species could not be properly located using water as solvent (*i.e.*, the geometry optimization calculation failed to converge). The same general trend exists for CO₂ hydrogenation, for which there is little difference in the energetics of the reaction and of the transition state for **18e-simp** and **18e-Br-simp**, but both values are decreased, relatively, for **18e-OMe-simp**. In fact, using water, the most polar solvent, the ΔG value for the hydrogenation of CO₂ becomes just slightly positive.

Scheme 4.14. DFT calculated free energy profile diagrams for hydrogenation of CO₂ using Shvo analogues via outer sphere concerted mechanism as a function of solvent (red = toluene, orange = tetrahydrofuran, purple = methanol, blue = water). Calculations were performed using the B3LYP functional. Solvent was modeled using the SMD implicit model.



4.4.3 Experimental Investigation of Carbon Dioxide Hydrogenation with Shvo Analogues

From the predictions made by DFT, we were particularly interested in whether experimental reactivity of **18e-OMe** would afford formic acid from CO₂. I synthesized both **18e-Br** and **18e-OMe** using analogous procedures to **18e** (see Experimental Section). Similar to **18e**, the hydrogenation of cyclohexanone was tested first as a benchmark. Six independent reactions of 25 μ mol **18e-Br** and 50 mmol cyclohexanone pressurized with 500 psig H₂ at 100 °C for 5 h yielded cyclohexanol with 1348 ± 75 TOs and $78 \pm 5\%$ conversion. The percent conversion for **18e-Br** is identical, within deviation, to the analogous reaction with **18e** (see Scheme 4.8). The TOs of cyclohexanol are slightly lower with **18e-Br** compared with **18e**. After many attempts of CO₂ hydrogenation with **18e-Br** and **18e-OMe**, no formic acid was detected via GC-MS nor via ¹H NMR spectroscopy.

4.5 Conclusions and Future Directions

The development of a process that utilizes CO₂ instead of CO as chemical feedstock could lay the groundwork for future, renewable methods of C1 incorporation chemistry. Metal-ligand bifunctional catalysis offers a strategy for homogeneous, base-free functionalization of carbon dioxide. Utilization of Shvo's catalyst was a desirable starting point due to its effectiveness in a wide variety of transformations, specifically in transfer hydrogenation. Hydrogenation of CO₂ was chosen as a starting point to this project with hydroarylation being the overall reactivity we aimed to achieve.

Following the synthesis of Shvo's catalyst, ketone and alkene hydrogenations were performed, for which the results were compared to literature, in order to determine that the experimental methods used for hydrogenation were adequate. Quantification methods for formic acid were developed using GC-MS and ¹H NMR spectroscopy. However, CO₂ hydrogenation experiments with Shvo's catalyst were unsuccessful.

Mechanistic studies using DFT calculations allowed Shvo-catalyzed CO₂ hydrogenation to be compared to previously reported formaldehyde hydrogenation.^{36, 38} Separate calculations were performed with two functionals of differing levels of approximations, B3LYP and M06, and it was found that both produced similar results. Further mechanistic studies compared hydrogenations of formaldehyde and CO₂ in four solvents of differing polarities using an implicit solvent model and it was found that more polar solvents led to more favorable energetics, both of the reaction and of the transition state. Analogues to Shvo's

catalyst, for which experimental methods for their syntheses have been previously reported, were compared computationally for the hydrogenation of formaldehyde and of CO₂ in the aforementioned four solvents. These mechanistic studies identified an analogue containing a methoxy-derivatized ligand as more favorable for formaldehyde and CO₂ hydrogenation. However, neither of the analogues showed experimental success for CO₂ hydrogenation.

Because Shvo's catalyst was shown to be unsuccessful for CO₂ hydrogenation, CO₂ hydroarylation was not pursued. However, the strategy outlined in this chapter could be extended to the investigation of alternate metal-ligand bifunctional catalysts. In fact, the tandem experimental and computational nature of this project allows for *in silico* prediction of likely candidates for arene carboxylation chemistry before time and resources are expended for the synthesis of catalysts and execution of reactivity studies.

4.6 Experimental Section

General Comments and Materials. Unless otherwise noted, all reactions were performed under ambient atmosphere. All chemicals and gases were purchased from commercial sources and used as received. Carbon dioxide and dihydrogen pressure were monitored by a Span pressure gauge (0-3000 psig, with 50 psig markings). ¹H NMR data were collected on a Varian 600 MHz spectrometer and referenced to either CDCl₃ or CD₂Cl₂ solvent residual signals. Chemical shifts are reported in ppm (δ). Infrared spectroscopy (IR) data were collected on a Shimadzu IRAffinity-1 spectrometer with KBr film/pellet holder. GC-MS data were collected on a GCMS-QP2010 Plus spectrometer with a DB-FFAP capillary

column (60 m x 0.250 mm x 0.25 μm). GC-FID data were collected on a Shimadzu GC-2014 spectrometer with a DB-5MS UI capillary column (30 m x 0.320 mm x 0.25 μm). X-ray diffraction (XRD) data were collected on a Bruker Kappa APEXII Duo system equipped with a fine-focus sealed tube and a graphite monochromator. Crystals were mounted on a MiTeGen MicroLoop coated with Paratone oil. All high-pressure reactions were performed in custom-built Swagelok stainless-steel high-pressure reactors containing a custom-built stainless-steel reaction vessel and Teflon liner. The reactors were sealed using a polytetrafluoroethylene (PTFE) O-ring.

Synthesis of Tetraphenylcyclopentadienone. The procedure is adapted from a published procedure.⁴¹ A round-bottom flask was charged with 40 mL of 200 proof ethanol and a stir bar and heated to 60 °C. Benzil (10 mmol) and dibenzyl ketone (10 mmol) were added to the flask. Potassium hydroxide (5 mmol) was dissolved in 5 mL of 200 proof ethanol. A reflux apparatus was assembled, and the temperature was increased to 72 °C. The potassium hydroxide solution was added dropwise. The solution was refluxed for 25 min and then submerged in an ice bath. Tetraphenylcyclopentadienone (9.4 mmol, 94%) was isolated via vacuum filtration and washed with 200 proof ethanol. The solid was stored in a glovebox. Tetraphenylcyclopentadienone was characterized by IR and ¹H NMR spectroscopy. IR: 1709, 1701 cm^{-1} . ¹H NMR (CDCl_3): 6.9-7.3 (m).

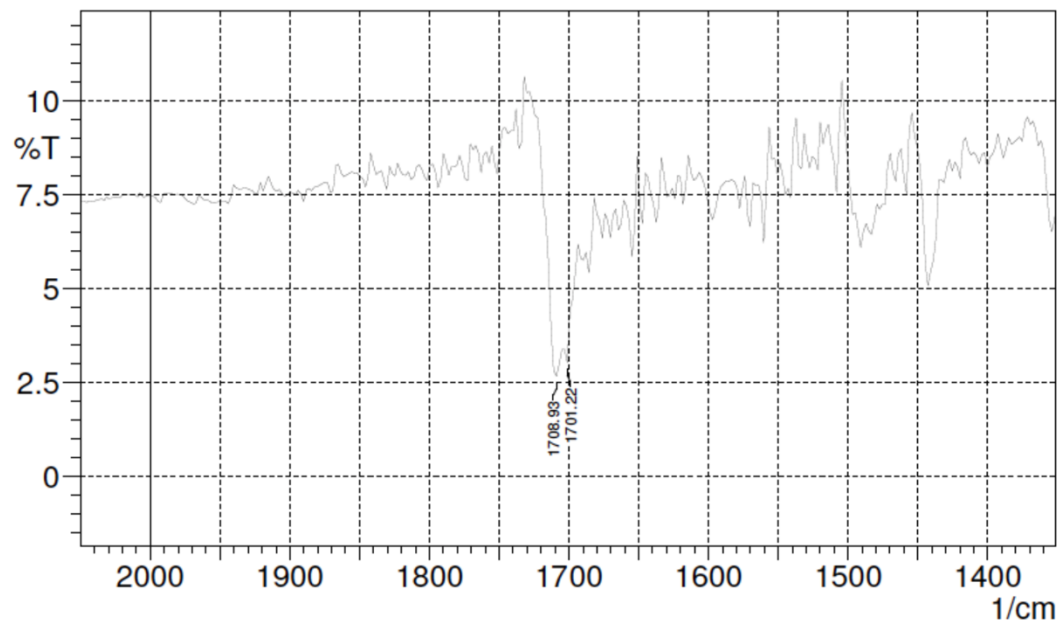


Figure 4.6. IR spectrum of tetraphenylcyclopentadienone.

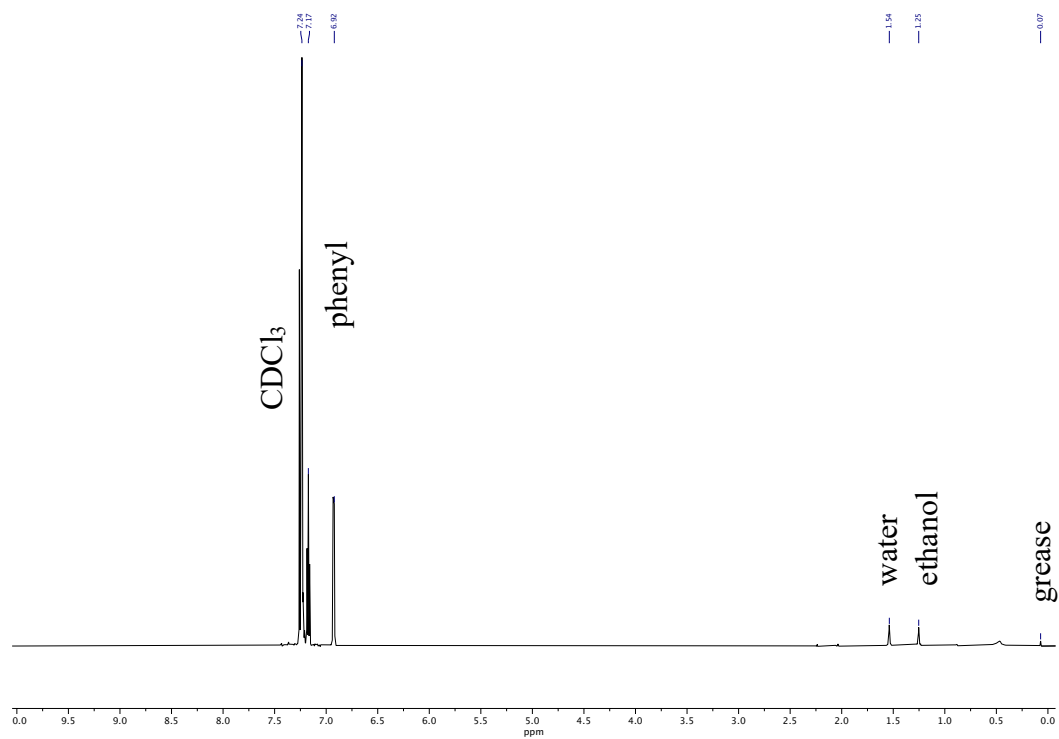


Figure 4.7. ¹H NMR spectrum of tetraphenylcyclopentadienone.

Synthesis of 3,4-Bis(4-bromophenyl)-2,5-diphenyl-2,4-cyclopentadienone. A round-bottom flask was charged with 40 mL of 200 proof ethanol and a stir bar and heated to 60 °C. 4,4'-Dibromobenzil (5 mmol) and dibenzyl ketone (5 mmol) were added to the flask. Potassium hydroxide (5 mmol) was dissolved in 8 mL of 200 proof ethanol. A reflux apparatus was assembled, and the temperature was increased to 72 °C. The potassium hydroxide solution was added dropwise. The solution was refluxed for 2 h and then submerged in an ice bath. 3,4-Bis(4-bromophenyl)-2,5-diphenyl-2,4-cyclopentadienone (2.7 mmol, 54%) was isolated via vacuum filtration and washed with 200 proof ethanol. The solid was stored in a glovebox. 3,4-Bis(4-bromophenyl)-2,5-diphenyl-2,4-cyclopentadienone was characterized by ¹H NMR spectroscopy. ¹H NMR (CD₂Cl₂): 6.8-7.4 (m).

Synthesis of 3,4-Bis(4-methoxyphenyl)-2,5-diphenyl-2,4-cyclopentadienone. A round-bottom flask was charged with 40 mL of 200 proof ethanol and a stir bar and heated to 60 °C. 4,4'-Dimethoxybenzil (5 mmol) and dibenzyl ketone (5 mmol) were added to the flask. Potassium hydroxide (5 mmol) was dissolved in 8 mL of 200 proof ethanol. A reflux apparatus was assembled, and the temperature was increased to 72 °C. The potassium hydroxide solution was added dropwise. The solution was refluxed for 30 mins and then submerged in an ice bath. 3,4-Bis(methoxyphenyl)-2,5-diphenyl-2,4-cyclopentadienone was isolated via vacuum filtration and washed with 200 proof ethanol. The solid was stored in a glovebox. 3,4-Bis(methoxyphenyl)-2,5-diphenyl-2,4-

cyclopentadienone was characterized by ^1H NMR spectroscopy. ^1H NMR (CD_2Cl_2): 3.8 (s, 6H), 6.7-7.2 (m, 18H).

Synthesis of Shvo's Catalyst (1). The procedure is adapted from a published procedure.⁴² A round-bottom flask was charged with triruthenium dodecacarbonyl (0.49 mmol), tetraphenylcyclopentadienone (1.5 mmol), 80 mL methanol, and a stir bar. Standard Schlenk techniques were used to reflux the mixture under a dinitrogen atmosphere for 40 h. The yellow-orange solid (0.33 mmol, 45%) was isolated via vacuum filtration and washed with methanol. The solid was stored in a glovebox. Shvo's catalyst ($\text{Ru}_2\text{C}_6\text{H}_4\text{O}_6$) was characterized by IR spectroscopy, ^1H NMR spectroscopy, and X-ray crystallography. IR: 3057, 2033, 2006, 1975, 1962 cm^{-1} . ^1H NMR (CD_2Cl_2): -18.4 (s, 1H), 7.0 (m, 40H).

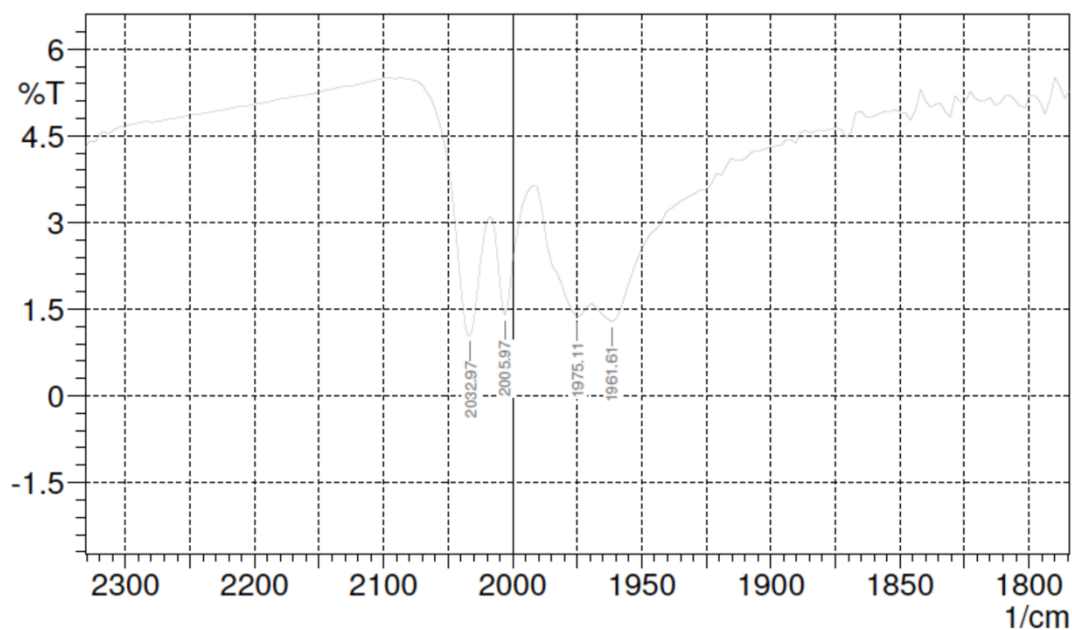


Figure 4.8. IR spectrum of **1**.

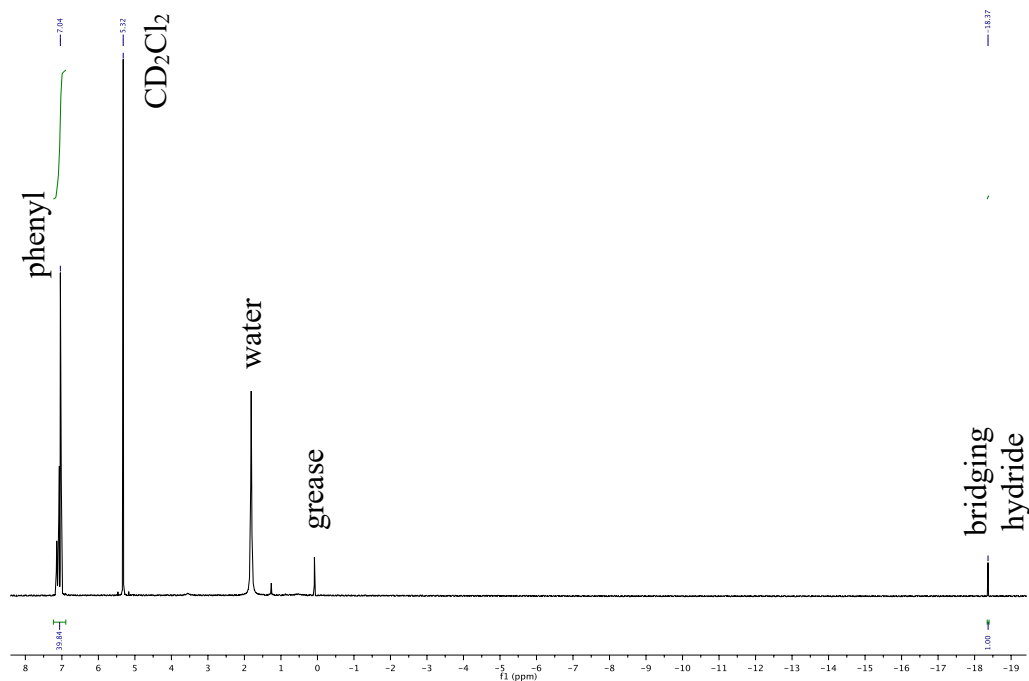


Figure 4.9. ^1H NMR spectrum of **1**.

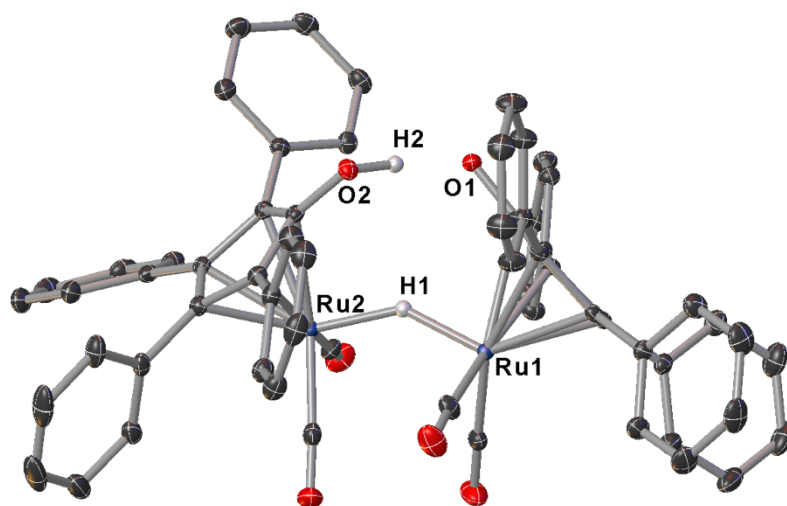


Figure 4.10. ORTEP plot of **1** as determined by single crystal X-ray crystallography. Ellipsoids are drawn at 50% probability level. Hydrogen atoms, with the exception of the bridging hydride and hydroxyl proton, are omitted for clarity. A molecule of tetrahydrofuran that co-crystallized with the catalyst is also omitted for clarity. The crystal structure of **1** has been previously reported and can be located in the Cambridge Structural Database by CCDC number 953038.⁴³

Table 4.1. Crystallographic data for **1**.^a

Chemical formula	C ₆₆ H ₅₀ O ₇ Ru ₂
FW (g/mol)	1157.20
T (K)	100(2)
λ (Å)	0.71073
Crystal size (mm)	0.199 x 0.227 x 0.247
Crystal habit	yellow block
Crystal system	triclinic
Space group	P -1
a (Å)	12.8846(11)
b (Å)	14.5125(12)
c (Å)	14.5549(13)
α (°)	74.998(2)
β (°)	89.665(2)
γ (°)	86.969(2)
V (Å³)	2625.1(4)
Z	2
ρ_{calc} (g/cm³)	1.464
μ (mm⁻¹)	0.632
F(000)	1180
θ range (°)	1.45 to 29.62
Index ranges	-17 ≤ h ≤ 16, -20 ≤ k ≤ 20, -20 ≤ l ≤ 20
Reflections collected	62411
Independent reflections	14764 [R(int) = 0.0288]
Data / restraints / parameters	14764 / 0 / 684
Goodness-of-fit on F²	1.017
R₁ [I > 2σ(I)]	0.0239
wR₂ [all data]	0.0603

^a Data reported here correspond to the crystal structure I obtained, depicted in Figure 4.10.

Table 4.2. Select bond lengths for **1**.^a

Bond	Length (Å)
Ru1–H1	1.72(2)
Ru2–H1	1.68(2)
O1–H2	1.53(3)
O2–H2	0.97(3)

^a Data reported here correspond to the crystal structure I obtained, depicted in Figure 4.10.

Synthesis of Shvo's Catalyst Analogues. A round-bottom flask was charged with triruthenium dodecacarbonyl and either 3,4-bis(bromophenyl)-2,5-

diphenyl-2,4-cyclopentadienone or 3,4-bis(methoxyphenyl)-2,5-diphenyl-2,4-cyclopentadienone in a 1:3 molar ratio, 80 mL methanol, and a stir bar. Standard Schlenk techniques were used to reflux the mixture under a dinitrogen atmosphere for 40 h. The solid was isolated via vacuum filtration and washed with methanol. The solid was stored in a glovebox and was characterized by ^1H NMR spectroscopy. For bromine analogue: ^1H NMR (CD_2Cl_2): -18.5 (s, 1H), 6.8-7.4 (m, 36H). For methoxy analogue: ^1H NMR (CD_2Cl_2): -18.5 (s, 1H), 3.7 (s, 12H), 7.2-6.5 (m, 36H).

General Ketone/Alkene Hydrogenation Procedure. A Teflon liner was charged with Shvo's catalyst, substrate, and a stir bar. The Teflon liner was added to a stainless-steel reaction vessel, the reactor was assembled, and then sealed with a vise. The high-pressure line was used to pressurize the reactor with 500 psig H_2 . The reactor was added to an aluminum block, heated to the desired temperature and stirred at 800 rpm. Following the reaction, the reactors were allowed to cool to room temperature and then were slowly vented in a fume hood. Biphenyl (for cyclohexanone hydrogenation) or hexamethylbenzene (for styrene hydrogenation) was added to the reaction mixture as internal standard. GC-FID was used for product quantification using linear regression analysis. A plot of peak area ratios versus molar ratios gave a regression line. For cyclohexanone hydrogenation, the slope and correlation coefficient of the regression lines were 2.42 and 0.994 (cyclohexanone) and 2.31 and 0.999 (cyclohexanol). For styrene hydrogenation, the slope and correlation coefficient of the regression lines were 1.78 and 0.999 (styrene) and 1.81 and 0.999 (ethylbenzene).

General CO₂ Hydrogenation Procedure. A Teflon liner was charged with Shvo's catalyst, 5 mL solvent, and a stir bar. The Teflon liner was added to a stainless-steel reaction vessel, the reactor was assembled, and then sealed with a vise. The high-pressure line was used to pressurize the reactor with 250 psig CO₂ followed by 250 psig H₂. The reactor was added to an aluminum block, heated at the desired temperature and stirred at 800 rpm. Following the reaction, the reactors were allowed to cool to room temperature and then were slowly vented in a fume hood. Cyclohexane was added to the reaction mixture as internal standard. GC-MS was used for formic acid quantification using linear regression analysis. A plot of peak area ratios versus molar ratios gave a regression line. The slope and correlation coefficient of the regression line were 0.0720 and 0.999 (formic acid).

Computational Details. Calculations were carried out using Gaussian09⁴⁴ at DFT level by means of the hybrid B3LYP functional and analogously by means of the M06 functional. Shvo's catalyst was modeled by $[(\eta^5\text{-C}_4\text{H}_4\text{COH})\text{Ru}(\text{CO})_2\text{H}]$, where the phenyl substituents on the cyclopentadienyl ring were replaced by hydrogen atoms. Optimization calculations were performed using the 6-31G(d,p) basis set for carbon, oxygen, and hydrogen atoms and the lanl2dz basis set⁴⁵ for ruthenium. Single point energy calculations were performed using the def2-tzvpd basis set⁴⁶ for all atoms. All calculations were performed without any geometrical constraints. For optimized structures, analytical frequency calculations were performed to characterize the structures as minima or transition states. IRC calculations were performed to confirm the connection between transition states and their relevant minima. Solvent effects were included using the SMD continuum

model.⁴⁷ Calculations were submitted to the Fulton Supercomputing Lab at Brigham Young University and the Rivanna Supercomputing Lab at the University of Virginia. Optimized coordinates can be found on the Gunnoe Group Hard Drive.

4.7 References

1. Liu, Y.; Deng, D.; Bao, X., Catalysis for Selected C1 Chemistry. *Chem* **2020**, *6* (10), 2497-2514.
2. Agency, U. S. E. P., Inventory of U.S. Greenhouse Gas Emissions and Sinks. 2020.
3. Aresta, M.; Dibenedetto, A., Utilisation of CO₂ as a chemical feedstock: opportunities and challenges. *Dalton Trans.* **2007**, (28), 2975-2992.
4. Agency, U. S. E. P. Carbon Dioxide Capture and Sequestration: Overview.
5. Mikkelsen, M.; Jørgensen, M.; Krebs, F. C., The teraton challenge. A review of fixation and transformation of carbon dioxide. *Energy Environ. Sci.* **2010**, *3* (1), 43-81.
6. Tortajada, A.; Juliá-Hernández, F.; Börjesson, M.; Moragas, T.; Martin, R., Transition-Metal-Catalyzed Carboxylation Reactions with Carbon Dioxide. *Angew. Chem. Int. Ed.* **2018**, *57* (49), 15948-15982.
7. Sakakura, T.; Choi, J.-C.; Yasuda, H., Transformation of Carbon Dioxide. *Chem. Rev.* **2007**, *107* (6), 2365-2387.
8. Glockler, G., Carbon–Oxygen Bond Energies and Bond Distances. *J. Phys. Chem.* **1958**, *62* (9), 1049-1054.
9. Witcoff, H. R., B. G.; Plotkin, J. S., *Industrial Organic Chemicals*. 2nd ed.; John Wiley & Sons, Inc.: Hoboken, 2004.

10. Cheung, H. T., R. S.; Torrence, G. P. , *Ullmann's Encyclopedia of Industrial Chemistry*. Wiley-VCH Verlag GmbH & Co. KGaA: 2000.
11. Hölsher, M. G., C.; Keim, W.; Müller, T. E.; Peters, M.; Leitner, W., Carbon Dioxide as a Carbon Resource – Recent Trends and Perspectives. *Z. Naturforsch* **2012**, *67b*, 961-975.
12. Rawat, A.; Dhakla, S.; Lama, P.; Pal, T. K., Fixation of carbon dioxide to aryl/aromatic carboxylic acids. *Journal of CO₂ Utilization* **2022**, *59*, 101939.
13. Lindsey, A. S.; Jeskey, H., The Kolbe-Schmitt Reaction. *Chem. Rev.* **1957**, *57* (4), 583-620.
14. Ikariya, T. S., M., *Topics in Organometallic Chemistry: Bifunctional Molecular Catalysis*. Springer: Berlin, 2011.
15. Dub, P. A.; Gordon, J. C., Metal–Ligand Bifunctional Catalysis: The “Accepted” Mechanism, the Issue of Concertedness, and the Function of the Ligand in Catalytic Cycles Involving Hydrogen Atoms. *ACS Catal.* **2017**, *7* (10), 6635-6655.
16. Magano, J.; Dunetz, J. R., Large-Scale Carbonyl Reductions in the Pharmaceutical Industry. *Org. Process Res. Dev.* **2012**, *16* (6), 1156-1184.
17. Blaser, H.-U.; Pugin, B.; Spindler, F., Asymmetric Hydrogenation. In *Organometallics as Catalysts in the Fine Chemical Industry*, Beller, M.; Blaser, H.-U., Eds. Springer Berlin Heidelberg: Berlin, Heidelberg, 2012; pp 65-102.

18. Blaser, H.-U.; Malan, C.; Pugin, B.; Spindler, F.; Steiner, H.; Studer, M., Selective Hydrogenation for Fine Chemicals: Recent Trends and New Developments. *Adv. Synth. Catal.* **2003**, *345* (1-2), 103-151.
19. Dokania, A.; Ramirez, A.; Bavykina, A.; Gascon, J., Heterogeneous Catalysis for the Valorization of CO₂: Role of Bifunctional Processes in the Production of Chemicals. *ACS Energy Lett.* **2019**, *4* (1), 167-176.
20. Kumatabara, Y.; Okada, M.; Shirakawa, S., Triethylamine Hydroiodide as a Simple Yet Effective Bifunctional Catalyst for CO₂ Fixation Reactions with Epoxides under Mild Conditions. *ACS Sustain. Chem. Eng.* **2017**, *5* (8), 7295-7301.
21. Toda, Y.; Komiyama, Y.; Kikuchi, A.; Suga, H., Tetraarylphosphonium Salt-Catalyzed Carbon Dioxide Fixation at Atmospheric Pressure for the Synthesis of Cyclic Carbonates. *ACS Catal.* **2016**, *6* (10), 6906-6910.
22. Liang, J.; Huang, Y.-B.; Cao, R., Metal-organic frameworks and porous organic polymers for sustainable fixation of carbon dioxide into cyclic carbonates. *Coord. Chem. Rev.* **2019**, *378*, 32-65.
23. North, M.; Pasquale, R.; Young, C., Synthesis of cyclic carbonates from epoxides and CO₂. *Green Chem.* **2010**, *12* (9), 1514-1539.
24. Blum, Y.; Shvo, Y., Catalytically Reactive Ruthenium Intermediates in the Homogeneous Oxidation of Alcohols to Esters. *Isr. J. Chem.* **1984**, *24* (2), 144-148.

25. Shvo, Y.; Czarkie, D.; Rahamim, Y.; Chodosh, D. F., A new group of ruthenium complexes: structure and catalysis. *J. Am. Chem. Soc.* **1986**, *108* (23), 7400-7402.
26. Karvembu, R.; Prabhakaran, R.; Natarajan, K., Shvo's diruthenium complex: a robust catalyst. *Coord. Chem. Rev.* **2005**, *249* (9), 911-918.
27. Conley, B. L.; Pennington-Boggio, M. K.; Boz, E.; Williams, T. J., Discovery, Applications, and Catalytic Mechanisms of Shvo's Catalyst. *Chem. Rev.* **2010**, *110* (4), 2294-2312.
28. Blum, Y.; Czarkie, D.; Rahamim, Y.; Shvo, Y., (Cyclopentadienone)ruthenium carbonyl complexes - a new class of homogeneous hydrogenation catalysts. *Organometallics* **1985**, *4* (8), 1459-1461.
29. Blanksby, S. J.; Ellison, G. B., Bond Dissociation Energies of Organic Molecules. *Acc. Chem. Res.* **2003**, *36* (4), 255-263.
30. Becke, A. D., Density-Functional Thermochemistry. III. The Role of Exact Exchange. *J. Chem. Phys.* **1993**, *98*, 5648-5652.
31. Lee, C.; Yang, W.; Parr, R. G., Development of the Colle-Salvetti correlation-energy formula into a functional of the electron density. *Phys. Rev. B: Condens. Matter* **1988**, *37* (2), 785-789.
32. Stephens, P. J.; Devlin, F. J.; Chabalowski, C. F.; Frisch, M. J., Ab Initio Calculation of Vibrational Absorption and Circular Dichroism Spectra Using Density Functional Force Fields. *J. Phys. Chem.* **1994**, *98* (45), 11623-11627.

33. Zhao, Y.; Truhlar, D. G., The M06 suite of density functionals for main group thermochemistry, thermochemical kinetics, noncovalent interactions, excited states, and transition elements: two new functionals and systematic testing of four M06-class functionals and 12 other functionals. *Theor. Chem. Acc.* **2008**, *120* (1), 215-241.
34. Cramer, C. J., *Essentials of Computational Chemistry: Theories and Models*. 2nd ed.; John Wiley & Sons, Inc.: Hoboken, 2004.
35. Bogojeski, M.; Vogt-Maranto, L.; Tuckerman, M. E.; Müller, K.-R.; Burke, K., Quantum chemical accuracy from density functional approximations via machine learning. *Nat. Commun.* **2020**, *11* (1), 5223.
36. Comas-Vives, A.; Ujaque, G.; Lledós, A., Hydrogen Transfer to Ketones Catalyzed by Shvo's Ruthenium Hydride Complex: A Mechanistic Insight. *Organometallics* **2007**, *26* (17), 4135-4144.
37. Casey, C. P.; Singer, S. W.; Powell, D. R.; Hayashi, R. K.; Kavana, M., Hydrogen Transfer to Carbonyls and Imines from a Hydroxycyclopentadienyl Ruthenium Hydride: Evidence for Concerted Hydride and Proton Transfer. *J. Am. Chem. Soc.* **2001**, *123* (6), 1090-1100.
38. Yamakawa, M.; Ito, H.; Noyori, R., The Metal–Ligand Bifunctional Catalysis: A Theoretical Study on the Ruthenium(II)-Catalyzed Hydrogen Transfer between Alcohols and Carbonyl Compounds. *J. Am. Chem. Soc.* **2000**, *122* (7), 1466-1478.
39. Foresman, J. B.; Frisch, Æ., *Exploring Chemistry with Electronic Structure Methods*. 3rd ed.; Gaussian, Inc.: Wallingford, CT.

40. Cesari, C.; Sambri, L.; Zacchini, S.; Zanotti, V.; Mazzoni, R., Microwave-Assisted Synthesis of Functionalized Shvo-Type Complexes. *Organometallics* **2014**, *33*, 2814-2819.
41. Johnson, J. R.; Grummitt, O., Tetraphenylcyclopentadienone. *Org. Syn.* **1943**, *23*, 92-93.
42. Casey, C. P.; Singer, S. W.; Powell, D. R.; Hayashi, R. K.; Kavana, M., Hydrogen Transfer to Carbonyls and Imines from a Hydroxycyclopentadienyl Ruthenium Hydride: Evidence for Concerted Hydride and Proton Transfer. *J. Am. Chem. Soc.* **2001**, *123*, 1090-1100.
43. Pasini, T.; Solinas, G.; Zanotti, V.; Albonetti, S.; Cavani, F.; Vaccari, A.; Mazzanti, A.; Ranieri, S.; Mazzoni, R., Substrate and product role in the Shvo's catalyzed selective hydrogenation of the platform bio-based chemical 5-hydroxymethylfurfural. *Dalton Trans.* **2014**, *43*, 10224-10234.
44. Frisch, M. J. G., *Gaussian 09, Revision D.01*. Gaussian, Inc.: Wallingford, CT, 2009.
45. Hay, P. J.; Wadt, W. R., Ab initio effective core potentials for molecular calculations. Potentials for the transition metal atoms Sc to Hg. *J. Chem. Phys.* **1985**, *82* (1), 270-283.
46. Weigend, F.; Ahlrichs, R., Balanced basis sets of split valence, triple zeta valence and quadruple zeta valence quality for H to Rn: Design and assessment of accuracy. *Phys. Chem. Chem. Phys.* **2005**, *7* (18), 3297-3305.

47. Marenich, A. V.; Cramer, C. J.; Truhlar, D. G., Performance of SM6, SM8, and SMD on the SAMPL1 Test Set for the Prediction of Small-Molecule Solvation Free Energies. *J. Phys. Chem. B* **2009**, *113* (14), 4538-4543.